Control of Hysteretic Systems with Preisach Representations

by

Robert Benjamin Gorbet

A thesis
presented to the University of Waterloo
in fulfilment of the
thesis requirement for the degree of
Doctor of Philosophy
in
Electrical Engineering

Waterloo, Ontario, Canada, 1997

©Robert Benjamin Gorbet 1997

National Library of Canada
Acquisitions and Bibliographic Services
395 Wellington Street
Ottawa ON K1A 0N4
Canada

Bibliothèque nationale du Canada
Acquisitions et services bibliographiques
395, rue Wellington
Ottawa ON K1A 0N4
Canada

Your file Votre référence

Our file Notre référence

The author has granted a non-exclusive licence allowing the National Library of Canada to reproduce, loan, distribute or sell copies of this thesis in microform, paper or electronic formats.

The author retains ownership of the copyright in this thesis. Neither the thesis nor substantial extracts from it may be printed or otherwise reproduced without the author's permission.

L'auteur a accordé une licence non exclusive permettant à la Bibliothèque nationale du Canada de reproduire, prêter, distribuer ou vendre des copies de cette thèse sous la forme de microfiche/film, de reproduction sur papier ou sur format électronique.

L'auteur conserve la propriété du droit d'auteur qui protège cette thèse. Ni la thèse ni des extraits substantiels de celle-ci ne doivent être imprimés ou autrement reproduits sans son autorisation.

0-612-22209-8

Canada

The University of Waterloo requires the signatures of all persons using or photocopying this thesis. Please sign below, and give address and date.

Control of Hysteretic Systems with Preisach Representations

The last decade has seen a growing interest in the application of so-called "smart materials" as sensors and actuators. Transducers made from these materials are self-contained and scalable, and are well-adapted for use in distributed sensing and actuation. However, many of these smart materials display a highly non-linear input-output behaviour known as hysteresis, which can introduce delays and cause errors in position control tasks.

This thesis examines some of the properties of the Preisach hysteresis model, as they pertain to controller design. The Preisach model is general in nature, and has been successful in modelling the hysteresis in several smart materials: magnetostrictives, piezoelectrics, and shape memory alloys. A novel state-space framework for the model is introduced, and a class of Preisach model is shown to be dissipative. This allows the application of energy-based controller design techniques to these non-linear systems. The Passivity Theorem is applied to determine a set of stabilizing controllers for velocity feedback of this dissipative class of Preisach models.

Experimentally, Preisach model identification is carried out for two shape memory alloy actuator configurations, including a differential actuator. For each actuator, models which are in the dissipativity class are identified. Applying the aforementioned theoretical results, this immediately provides a stability result for velocity feedback control of these actuators. While simulations using these models provide a good qualitative match with experimental data, other models were identified for which the match was better. However, these better models were not in the dissipativity class, suggesting that this class is likely somewhat conservative.

Acknowledgements

In the three years during which this research was undertaken, I have had the pleasure and privilege of working with some wonderful people, each of whom deserves more thanks than this page allows.

My supervisors, Professors Kirsten Morris and David Wang, provided support, guidance, and friendship over the years, and I would particularly like to thank them for their diligent critique of this work. They remained calm and maintained perspective despite a seemingly impossible schedule which I imposed on myself, and hence upon them. I would also like to thank Professor Dan Miller for the many consultations and for his ability to instantly generate creative counterexamples.

I have spent nearly every day of the last five years with my office mate and friend, Milind Ghanekar. Many little details of the thesis work were resolved in conversation with Milind as well as Mauro Rossi and Dan Madill. More importantly though, Milind's constant smile and wacky sense of humour were welcome distractions from research.

I would also like to thank my family. Their constant love and encouragement has been a source of strength for as long as I can remember. In particular, my wife Maud took care of me and kept me sane during the incredibly stressful period during which I was writing this document. Without her support, I don't think I would have made it.

Finally, I owe thanks to the taxpayers of Canada. Each of you, through your tax dollars and the Natural Sciences and Engineering Research Council, contributed nearly $0.01 to my education.

for Maud, of course...

Contents

List of Tables

List of Figures

Chapter 1

Introduction

The last decade has seen a growing interest in the field of "smart materials" and "smart structures". The definition of the latter is generally agreed upon: a *smart structure* is one which monitors itself and/or its environment in order to respond to changes in its condition[9]. A smart bridge might be able to detect high wind conditions and reduce posted speed limits accordingly, or detect degradation in footings or piers and alert maintenance crews. A smart building may sense the presence of high winds or the onset of an earthquake, and adjust its dynamic properties automatically to minimize damage or occupant discomfort. In order to perform these tasks efficiently, the smart structure requires a large number of distributed control sites, each responsible for local sensing, decision and actuation functions. It is here that so-called smart materials enter the picture.

Just what constitutes "intelligence" in a material is the subject of much debate. Some argue that there is no *one* material which satisfies the dictionary definition of "intelligent", although hybrid materials can come close[9]. However, there are a number of materials which might be termed "self-adapting" or "responsive", and the

ability to adapt is certainly a part of "intelligence". These materials are able to alter one or more of their physical properties, such as stiffness or viscosity, in response to external stimuli such as temperature, stress, or electric fields. Transducers made of these materials are self-contained and often completely scalable, making them well-suited for the task of distributed sensing and actuation.

Two of the most popular classes of these materials are piezoceramics and shape memory alloys. Although they can also be used as sensors, particularly piezoceramics, this work concentrates on their function as actuators. Piezoceramics are capable of generating very small strains, at high stress, in response to high electric fields. The focus of piezoceramic actuator applications has been in active vibration and noise control[e.g. 22, 15]. Shape memory alloys (SMA) generate significant strains (up to 8%) in response to a temperature change. The stresses achievable are lower than those for piezoceramics. Although SMA actuators have also been proposed as actuators for vibration and noise control[e.g. 27, 22], their relatively low bandwidth limits their usefulness in these applications. However, their ability to generate large strains has promoted their use as an "artificial muscle". They have one of the highest force/mass ratios of any actuator system[31], and have been applied in numerous research robots as a replacement for joint motors[e.g. 17, 23, 46]. The fact that the material properties are maintained when the actuator is scaled has resulted in the development of mini-actuators for fine positioning[4, 21] and micro-valves for flow control[66].

The adaptive abilities of these "smart materials" are the result of physical changes occurring within the material. These changes occur in a highly non-linear fashion, introducing significant hysteresis in the actuator response. This is true of piezoceramics and SMA, and also of other smart actuators such as magnetostrictives and electrorheological fluids. This hysteretic behaviour introduces delays, and

can lead to significant error in positioning tasks.

Controller design, simulation and stability analysis of systems incorporating hysteretic elements requires accurate modelling of their behaviour. Modelling based on physical properties of specific hystereses has been carried out for decades and, in the case of ferromagnetics, over a century. It is only recently, however, that work has been done on general hysteresis modelling schemes. The most popular of these is the Preisach hysteresis model. Since physical mechanisms of hysteresis vary amongst different materials, this generality is preferred if one wishes to develop results which would benefit more than one type of hysteretic actuator.

1.1 Thesis Goals

The goals of this research are twofold. First, to investigate the properties of the Preisach hysteresis model as they pertain to feedback controller design. This general hysteresis model has recently been successfully applied in modelling both piezoceramic and shape memory alloy hystereses[27], and has been proposed for magnetostrictive modelling as well[38, 56]. In the course of this investigation, a novel state-space representation for the Preisach model is set out, allowing the application of dissipativity theory in controller design. Dissipativity theory is but one example of state-space based controller design techniques which are made accessible by the introduction of this framework.

The second aspect of the work is concerned with Preisach modelling of two configurations of shape memory alloy actuator. A novel approach is taken with respect to a constant-load, single-wire actuator, which results in an analytical form of the associated Preisach model. Although Preisach modelling of this type of actuator has been carried out in the past[27], the lack of an analytical model form has limited

the ability to analyze systems incorporating these actuators. A Preisach model for a two-wire differential actuator is also derived, resulting in what is believed to be the first stability results for such an actuator.

1.2 Outline

The thesis is organized in the following manner. Chapter 2 provides background on hysteresis. A working definition is presented, along with assumptions limiting the types of hysteresis nonlinearities being considered. A brief history of hysteresis modelling is given and the reasons for retaining the Preisach model for this study are outlined. The Preisach model is described in Chapter 3. After introducing the model structure, representation conditions are given and the model identification procedure is detailed. Extensions to the Preisach model are also briefly described.

Chapter 4 examines some mathematical properties of the model which arise in the case of specific types of hystereses. Chapter 5 is concerned with the modelling of two shape memory alloy actuators. The hysteresis is described, and some history of SMA modelling presented. Two actuator configurations are tested to verify the suitability of the Preisach model, and several models are identified for each.

In Chapter 6, the Preisach model is cast in a non-linear state-space framework. A state space is identified, along with the state transition and output operators. Some properties of the state space are also investigated. Chapter 7 examines the energy storage properties of the Preisach model. This study leads to a proof of the dissipativity of the Preisach model. Chapter 8 investigates the design of feedback controllers for systems with Preisach model representations. The final chapter describes the contributions of this work, along with some potential areas for future study.

Chapter 2

Hysteresis

This chapter provides background on hysteresis. The first section gives a definition of hysteresis as it is understood in this work, as well as some of the terminology associated with hysteresis graphs. The second section describes one of the more popular analogies used to explain the physical causes of hysteresis in magnetic materials: the "domain wall analogy". In the third section, a brief summary of developments in modelling of hysteresis is given. In order to motivate the choice of the Preisach model in this work, the hysteresis present in two smart materials is described in Section 4. Similarities in physical behaviour between these materials and domain walls are pointed out. The final section summarizes the reasons for using the Preisach model in this study.

2.1 Definitions and Terminology

The word hysteresis comes from the Greek *hustereia*, "to arrive late", and in its most basic form hysteresis is simply a lag of the output behind the input. While there

have been attempts to provide a more rigorous mathematical definition[e.g. 64], these usually include some systems which one would not consider to be hysteretic at all. As such, they are not entirely satisfactory. Here, we will limit ourselves to a graphical definition, along with a set of assumptions (Assumption 2.1), which form an "operational" definition which suits the scope of this work.

Hysteresis can be represented graphically as a relation in the u-y plane. Figure 2.1 shows an example of an hysteretic relation, along with a sample path. The loop which bounds the region where $y(t)$ is multivalued is called the *major (hysteresis) loop*. The domain of input values u corresponding to this region is denoted $[u_-, u_+]$; the range of outputs, $[y_-, y_+]$. Each new segment of the output path in the u-y plane is called a *branch* (labeled 1 to 5 in Figure 2.1), and branching results from a local extremum in the input. *Ascending branches* are followed for increasing inputs (1,3,5), *descending branches* if the input is decreasing (2,4). Successive branches which cross inside the major loop form *minor (hysteresis) loops*. In Figure 2.1, minor loops are formed by branches 2 and 3, 4 and 5, but not by 2 and 5 since they are not successive.

The above paragraph on terminology contains several statements, made as facts, which imply certain assumptions about the hystereses being considered in this work. Although these are so common that they are often assumed implicitly, it is worthwhile re-stating them clearly.

Assumption 2.1 (Hysteresis Forms)
It will be assumed in this work that hystereses satisfy the following assumptions.

1. *The major loop is bounded. In other words, u_-, u_+, y_- and y_+ are all finite.*
2. *Branching occurs as a result of, and only as a result of, an input reversal. In other words, the sign of the input and output derivatives are always the same.*

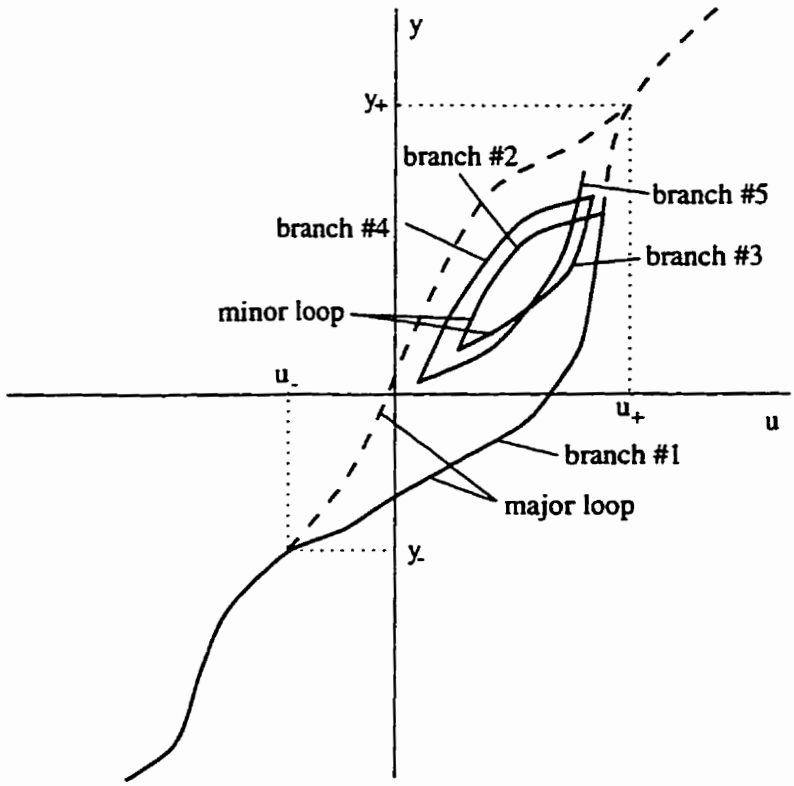

Figure 2.1: Hysteresis Terminology

Hystereses are further categorized by the type of memory they exhibit[43]. In systems with *local* memory, the future output depends only on the current output and current and future inputs. The "memory" of a local hysteresis is entirely captured in the current output. In hystereses with *non-local* memory, the future output depends not only on the current output, but also on the past history of input extrema.

2.2 The Domain Wall Analogy

In attempting to understand the physical mechanisms of hysteresis in any material, it is instructive to look to magnetic hysteresis, where there has been over a century of study. The hysteresis in magnetic materials is often described using what is called a *domain wall* analogy. The material is composed of elementary dipoles: tiny polarized particles which orient themselves according to the applied field. Regions of similarly-oriented dipoles form *domains* of polarization, and the overall magnetization depends on the relative extent of the positive and negative domains. The *domain walls* are the imaginary boundaries which separate these regions. As an applied field is varied, these regions grow or shrink in size, depending on polarity: the domain walls are said to *move*. This behaviour is illustrated in Figure 2.2.

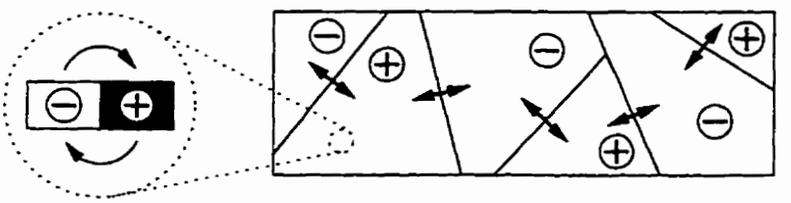

Figure 2.2: Sketch of the Domain Wall Analogy

An elementary dipole which is isolated in a field would not display hysteresis: it would simply re-orient itself instantaneously if the field changed polarity. Hysteresis is said to arise due to material defects and internal friction between dipoles, which can be thought of as "inertial forces" causing the dipoles to exhibit a preference for their current orientation. The applied field must overcome these inertial forces if it is to change the dipole orientation. It is these inertial forces which give rise to hysteretic behaviour.

While the domain wall idea originated in ferromagnetics, we will see that the

analogy is equally applicable to other hysteretic systems composed of elementary particles having binary state.

2.3 Modelling History

Some of the first recorded scientific observations of hysteresis were made by Lord Raleigh[ref. 1], in connection with the behaviour of magnetic materials exposed to a time-varying electric field. Since those initial observations, the ubiquity of this phenomenon has become apparent. Hysteresis has been identified in many different areas of study, including physics, engineering, chemistry, biology, and economics[ref. 64].

For nearly a century, engineers and scientists have been developing hysteresis models based principally on an understanding of physical or chemical properties in a specific system of interest. In more recent decades, mathematicians have also come to contribute to the field.

Mathematical models are well adapted to analysis, but often suffer from complications in implementation, since they generally require the use of numerical approximation techniques. Because they are removed from the underlying cause of the hysteresis, the parameters in mathematical models are often difficult to associate with the physical system, and they often lack the intuition of physical models. Unfortunately, in the absence of standard controller design techniques for strong non-linearities such as hysteresis, intuition is often the most powerful tool available to the designer. An excellent, albeit very mathematical, treatment of the available mathematical models (and some physical models as well) can be found in [64].

A major drawback of physical models, especially in the context of this work,

is that they are specific to a particular type of system. Physical models of smart material hysteresis would have to be developed separately for each different material. and may in fact have entirely different structures. This implies separate controller design techniques and analyses. and precludes any general results which might benefit the broad spectrum of smart materials.

In the 1930s. F. Preisach developed a model for hysteresis in magnetic materials which straddles the boundary between physical and mathematical[51]. Originally based on the physical notion of magnetic domains described in the previous section. the model retains much of the intuition associated with physical models. However. in recent decades it has been abstracted and successfully applied in other areas. thus demonstrating its generality, a property usually associated with purely mathematical models.

When investigating mathematical models of hysteresis, several researchers' names appear quite often. The foremost is that of Visintin. who has written and edited substantial review works on hysteresis models of all types[61, 62, 63. 64]. Other review papers include [24, 50]. Krasnosel'skiĭ and Pokrovskii were probably the first to extend Preisach-type models to more general elementary hysteresis operators. They have written what appears to be the most complete mathematical work on hysteresis models to date[34].

Since the work by Krasnosel'skiĭ on the abstraction of the Preisach model, the mathematical properties of the model have been investigated by Brokate and Visintin[6], and many extensions and variations have been proposed. These extensions are often associated with the names Della Torre[33, 59] and Mayergoyz[e.g. 44]. Mayergoyz has compiled a number of his own publications, as well as those of others in the field, into a monograph[43] which is an excellent reference on the Preisach model and its extensions. The text addresses many of the problems gen-

erally associated with mathematical models: identification techniques, a simple implementation form, as well as necessary and sufficient conditions for Preisach model representation.

2.4 Hysteresis in Smart Materials

This section describes the hystereses present in piezoceramics and shape memory alloys. These are some of the most commonly used smart materials, and those for which the hysteresis mechanism is best understood. For a comprehensive source on smart actuators, sensors, structures and their applications, the reader is referred to [9].

2.4.1 Shape Memory Alloys

Many different metal alloys have been found to display shape memory properties[67]. The most commonly used in electrical actuator applications is a near-binary mixture of nickel and titanium, commonly called *Ni-Ti-NOL* since it was first developed at the US Naval Ordinance Laboratory[7]. The large strain recovery in SMA is made possible by the existence of two distinct, temperature-dependent crystalline phases within the alloy. At low temperatures, the alloy is in the *martensite* phase, while at higher temperatures, the structure changes to *austenite.*[1] As the wire undergoes heating from the fully martensite phase, the percentage of martensite diminishes, while that of austenite increases, until the alloy is 100% austenite.

[1]For the purposes of this study, the terms austenite and martensite are best defined by linking them to their respective crystalline lattice structures. Austenite has a rigid, cubic structure, while martensite is characterized by a softer, rhombic lattice.

The transformation from martensite to austenite, and back again, is characterized by a large hysteresis loop, as depicted in Figure 2.3. The temperatures associated with the transformation are A_s, A_f and M_s, M_f: the austenite and martensite start and finish temperatures. Between A_s and A_f, and from M_s to M_f, the structure of the alloy is a mix of martensite and austenite. Typical transformation temperatures in degrees Celsius, for NiTi which is 49.5% nickel, are $M_f = 19$, $M_s = 47$, $A_s = 53$, $A_f = 80$[14]. However, these parameters are highly dependent on alloy composition and processing: variations on the order of 2-3% in alloy composition can cause shifts of over 100 degrees in transformation temperatures.

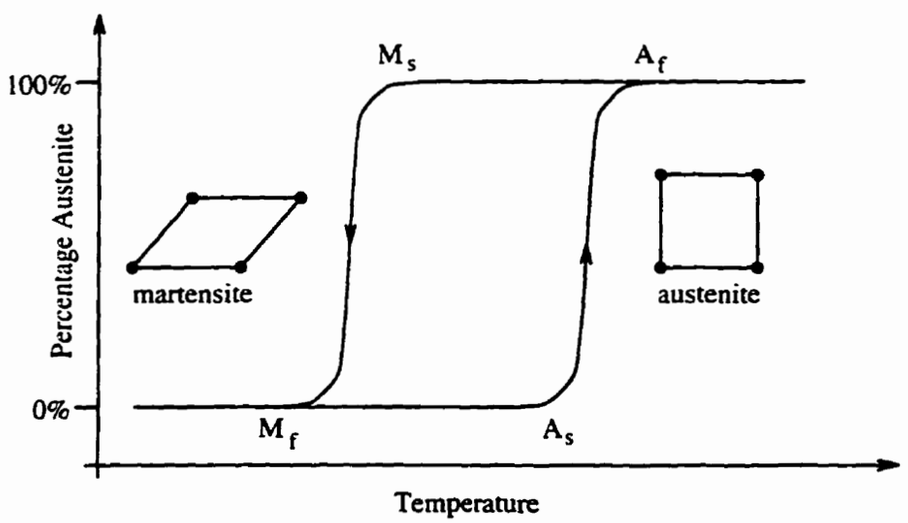

Figure 2.3: Hysteresis Curve and Transition Temperatures for SMA

The most efficient use of NiTi as an actuator is in wire form[54]. A sketch of the stress-strain characteristics of austenite NiTi and martensite NiTi is shown in Figure 2.4. The utility of SMA wire as an actuator comes from the change in this characteristic as the alloy undergoes a phase change between austenite and martensite. The strain resulting from a particular stress will be different in each

phase. This allows work to be done on a load by heating the wire. A wire subject to a stress of σ_1 MPa (cf. Figure 2.4) can recover substantial strain, on the order of 5%, when heated from martensite to austenite. If only a few cycles are required, strains of up to 8% can be recovered.

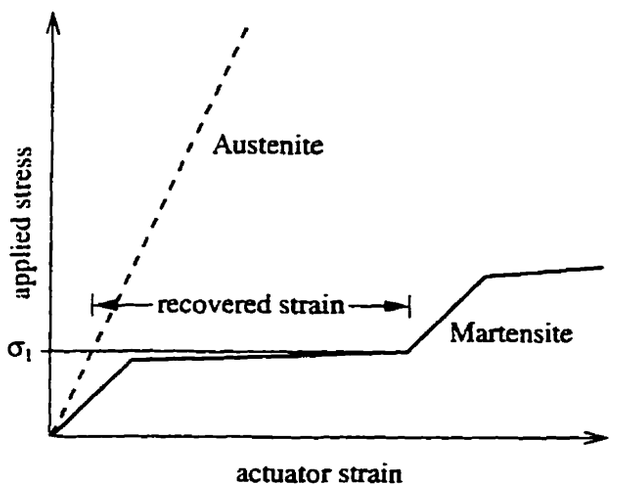

Figure 2.4: Stress-Strain Curves of Austenite and Martensite for SMA

The phase transformation process is similar in nature to the description of the domain wall analogy. The individual crystals of NiTi are thought of as dipoles, and their "polarization" is their current phase state. Domains of martensite and austenite are in fact visible at the microscopic level during the transformation. During cooling, the martensite can be seen to be growing, "taking over" the austenite; upon cooling, it recedes[16]. The domain walls, separating regions of martensite and austenite, "move". Hysteresis arises in part due to internal friction associated with the phase transformation[70].

In an unconstrained alloy, several variants of martensite form during cooling, suggesting the need for a "multi-state" dipole analogy. However, in wire actuators the material is never unconstrained. In this case only one variant of martensite is

formed[16], and the binary state dipole analogy remains appropriate.

2.4.2 Piezoceramics

The "piezoelectric effect" refers to the ability of certain materials to generate electric charge in response to mechanical stress[9]. The inverse transformation is also possible, and it is this property which is the basis for the use of piezoelectric materials as actuators.

Piezoceramics are ferroceramic materials which have been treated in order that they exhibit the piezoelectric effect. Ferroceramics contain many elementary electric dipoles, similar to the magnetic dipoles of magnetic materials. These respond to an applied electric field by orienting themselves with the field direction. A change in material dimension, the extent of which is dependent on dipole geometry, occurs during this re-alignment. In order to create a piezoceramic actuator, the ferroceramic material is exposed to a strong electric field as it is heated to the Curie point and slowly cooled. This process, known as *poling*, leaves all dipoles aligned in one direction. It is only after this poling process that ferromagnetics become useful as actuators.

When the poling field is removed, a residual electric field E_r remains within the material, effectively introducing a "pre-strain". Subsequent applied fields of the same polarity as the poling field will cause an increase in strain, while the opposite polarity produces a strain reduction. When the applied field is removed, the dipoles will attempt to realign themselves with the residual field E_r. Material defects prevent this realignment from being total, introducing the hysteresis characteristic sketched in Figure 2.5. The hysteresis is not as pronounced as that displayed by shape memory alloys, and has a more regular shape.

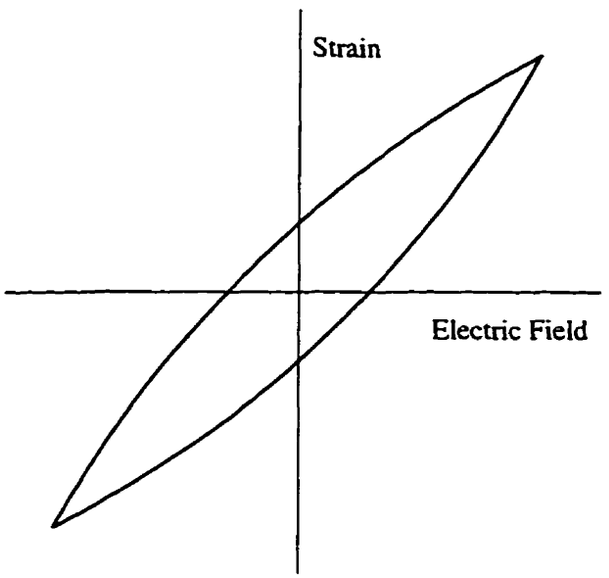

Figure 2.5: Sketch of Piezoceramic Hysteresis Characteristic

Typical poling fields for piezoceramics are 1V/μm, and strains are generally limited to 0.1%[9]. Due to the large electric fields required for actuation, material thicknesses in control applications are usually on the order of 0.1-0.3mm. It is suggested in [9] that the control field be limited to 75% of the poling field, in order to avoid re-poling the material. This results in control voltages on the order of 75-225V.

A classical application of piezoceramic actuators is in vibration control[e.g. 15], where squares of piezoelectric sheet are bonded to either the side of a cantilevered flexible beam, near the clamp. By controlling the electric field across the piezoceramic, the strain, and hence bending moment in the beam, can be controlled. This can be used to damp out unwanted beam vibration.

2.5 Model Selection

The Preisach model has been chosen for this work for two main reasons. One of the goals of the research was to develop results pertaining to the control of smart materials. Piezoceramics and shape memory alloys are referred to as examples, but other smart materials also display hysteretic behaviour. The generality of the Preisach model is therefore appealing, since results may potentially be applied to any system for which a Preisach model exists. Despite its generality, however, the Preisach model has inherited a physically based structure from its roots in magnetic hysteresis modelling. This structure is often absent in purely mathematical models, and leads in this case to an intuitive interpretation of model behaviour.

Aside from these compelling reasons, the Preisach model has further advantages of a more practical nature:

- The model is able to represent the non-local memory which has been shown to exist in shape memory alloys[49].
- It has been shown that the model is suited to piezoceramic and shape memory alloy representation[27].
- The significant problems of identification and implementation have been addressed by Mayergoyz[43].
- Several mathematical properties of the model have been investigated[6, 34].

In the past few years, as a testament to its generality and practicality, the Preisach model seems to have emerged as the preferred model for engineering applications. This corroborates the opinion of Brokate and Visintin[6], that the Preisach model "may be the most satisfactory mathematical model of hysteresis available."

2.6 Summary

This chapter provided a working definition of hysteresis, outlined the types of hysteresis being considered, and discussed the history of modelling. The popular domain wall analogy from ferromagnetics was described, and parallels drawn with the hysteresis mechanisms in shape memory alloys and piezoceramics. Given these parallels, it is expected that the Preisach model of ferromagnetic hysteresis may be successfully applied to these newer materials. This, and several other compelling reasons, motivate the choice of the Preisach model for this study. In the next chapter, the Preisach model will be described in detail.

Chapter 3

The Preisach Model

This chapter intends to familiarize the reader with the Preisach hysteresis model. The first section describes the input-output form of the model. Section 2 discusses the Preisach plane, the source of much of the intuition associated with the model. Section 3 presents the necessary and sufficient conditions for representation by a Preisach model. In Section 4, the model identification procedure is described.

Since its invention in the 1930s, several extensions and variations of the Preisach model have been proposed. The form described in this chapter, and applied in the research, is that which has come to be known as the "classical" Preisach model. The final section of this chapter briefly describes, for the benefit of the reader, some of the more important extensions of the classical model form. The information in this chapter is mainly compiled from Mayergoyz' monograph[43].

3.1 Model Description

The main assumption made in the Preisach model is that the system can be thought of as a parallel summation of a continuum of weighted relay hystereses $\gamma_{\alpha\beta}$. This is illustrated in Figure 3.1, where the value $\mu(\alpha,\beta)$ represents the weighting of the relay $\gamma_{\alpha\beta}$. Each relay is characterized by the pair of switching values (α,β), with $\alpha \geq \beta$, so that there is a unique representation of the collection of relays as points in the half-plane $\mathcal{P} = \{(\alpha,\beta) | \alpha \geq \beta\}$ (cf. Figure 3.2). The vertical portions of the

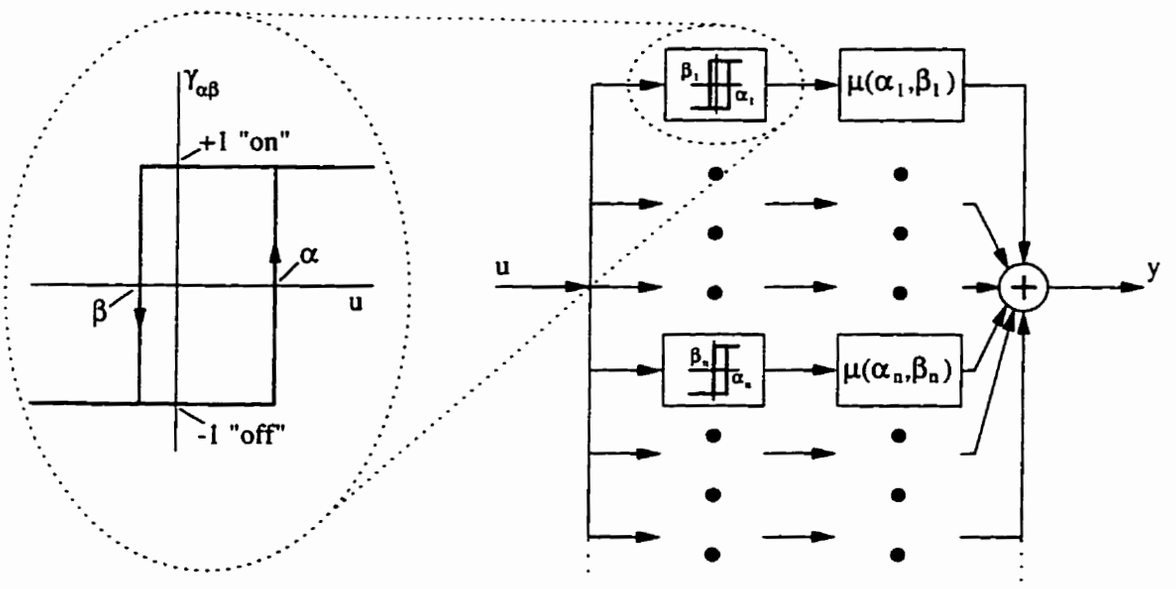

Figure 3.1: Schematic of the Preisach Model

relays are irreversible: they can only be traversed in one direction. The horizontal sections are reversible. Degenerate relays, those with $\alpha = \beta$, are fully reversible.

Mathematically, each of these relays can be represented as a relation in $\mathbf{R}^2$

$$\gamma_{\alpha\beta} \triangleq \{(\zeta,-1);\ \zeta \leq \alpha\} \cup \{(\zeta,+1);\ \zeta \geq \beta\},$$

with the output at any particular time dependent on the input history up to that

time. The behaviour of these relays, and hence the Preisach model, is only defined for continuous inputs u. As this input varies with time, each individual relay adjusts its output according to the current input value, and the weighted sum of all the relay outputs provides the overall system output (cf. Figure 3.1)

$$y(t) = \iint_{\mathcal{P}} \mu(\alpha, \beta)[\gamma_{\alpha\beta} u](t) d\alpha d\beta. \tag{3.1}$$

The collection of weights $\mu(\alpha, \beta)$ forms a weighting function $\mu : \mathcal{P} \mapsto \mathbf{R}$, which describes the relative contribution of each relay to the overall hysteresis.

In magnetics, the relays γ represent the magnetic dipoles which make up the material. When modelling SMA actuators, the relays may represent individual crystals, which are assumed to be in one of two distinct phases.

3.2 The Preisach Plane

The region $\mathcal{P}$ is often referred to as the Preisach plane, and it is seen that it plays a central role in the Preisach model. Every point in $\mathcal{P}$ represents a unique relay, and $\mathcal{P}$ is the support for the weighting function μ, as illustrated in Figure 3.2. It will be demonstrated in this section that the Preisach plane also provides an alternative way of looking at the model behaviour. This leads to a clearer understanding of some of its properties.

3.2.1 The Preisach Plane Boundary

This section introduces the Preisach plane boundary, a unique mechanism for keeping track of the state of individual relays.

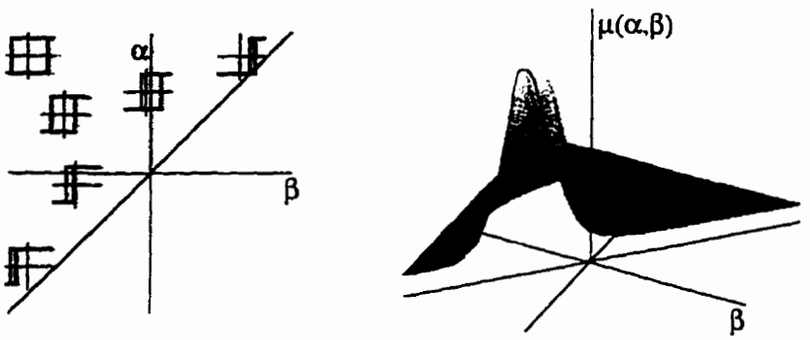

Figure 3.2: Utility of the Preisach Plane

First, divide the relays in $\mathcal{P}$ into two time-varying regions, $\mathcal{P}_-$ and $\mathcal{P}_+$, defined as follows:

$$\mathcal{P}_-(t) \triangleq \{(\alpha,\beta) \in \mathcal{P} \mid \text{output of } \gamma_{\alpha\beta} \text{ at } t \text{ is } -1\}$$
$$\mathcal{P}_+(t) \triangleq \{(\alpha,\beta) \in \mathcal{P} \mid \text{output of } \gamma_{\alpha\beta} \text{ at } t \text{ is } +1\},$$

so that $\mathcal{P}_-(t) \cup \mathcal{P}_+(t) = \mathcal{P}$ at all times. It will become clear that each set is connected. The time-dependence will often be implicit, with $\mathcal{P}_-$ and $\mathcal{P}_+$ used to denote these regions.

Now, consider an hysteretic system exposed to a monotonically increasing input, taking it from negative saturation to positive saturation along the major loop. In negative saturation, all relays are in the "-1" state and $\mathcal{P}_- = \mathcal{P}$, $\mathcal{P}_+ = \emptyset$ (Figure 3.3a). As the input increases, it switches a relay $\gamma_{\alpha\beta}$ to "+1" as it passes $u = \alpha$, moving it from $\mathcal{P}_-$ to $\mathcal{P}_+$. The boundary between $\mathcal{P}_-$ and $\mathcal{P}_+$ can be represented as a horizontal line in the Preisach plane, which moves up as the input increases (Figure 3.3b), switching relays from $\mathcal{P}_-$ to $\mathcal{P}_+$ until the system is in positive saturation (Figure 3.3c). Similarly, if the input now reverses and begins to decrease monotonically, a vertical boundary is generated sweeping from right to left, switching relays $\gamma_{\alpha\beta}$ from $\mathcal{P}_+$ to $\mathcal{P}_-$ as it passes $u = \beta$ (Figure 3.3d).

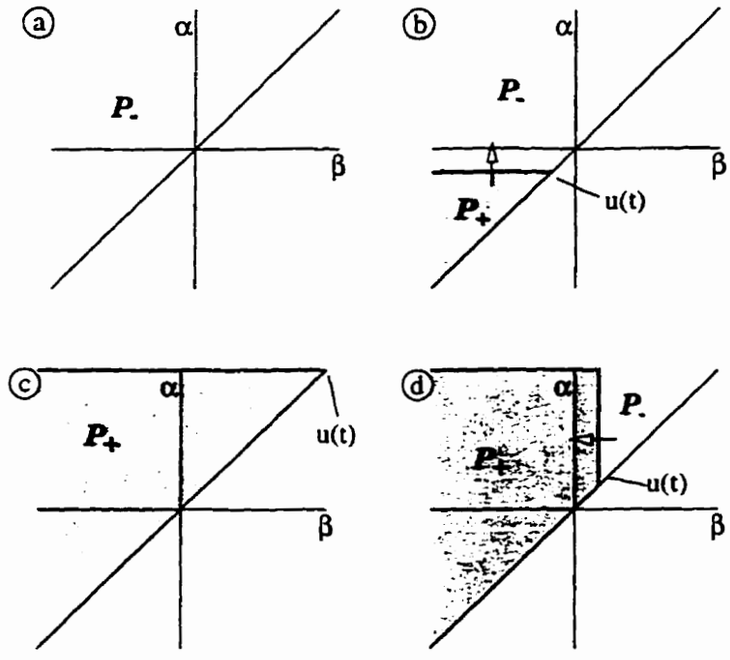

Figure 3.3: Preisach Boundary Behaviour

The similarity between the Preisach plane boundary and the domain wall described in Section 2.2 is clear. As the input evolves over time, the boundary "moves" in $\mathcal{P}$, always separating relays into two groups of "like polarization".

The Preisach plane boundary also represents, in a sense, the memory of the Preisach model. When an arbitrary input is applied to the hysteresis, monotonically increasing segments generate horizontal branches on the boundary, while monotonically decreasing segments generate vertical branches. Input reversals cause corners in the boundary. The history of past input reversals—and hence of branching behaviour—is stored in the corners of the boundary.

Observation 3.1 (Key Boundary Facts)

The boundary plays a very important role in the analysis of the Preisach model. The

reader will find subsequent discussion involving the boundary easier if the following facts are clear at this point.

- *The area below and to the left of the boundary represents those relays whose outputs are positive, and is denoted* $\mathcal{P}_+$.
- *The area above and to the right of the boundary represents those relays whose outputs are negative, and is denoted* $\mathcal{P}_-$.
- *The boundary always intersects the line* $\alpha = \beta$ *at* (u, u)*;* u *is the current input value.*

The astute reader will recognize at this point that inputs can be constructed so that boundary corners are generated, but later removed. For example, if an input maximum is followed by a minimum, and then by a larger maximum, the memory of the first reversal will be "erased". This "wiping out" property has been identified as one of two conditions which are necessary and sufficient for existence of a Preisach representation for an hysteresis[43]. These representation conditions will be discussed in greater detail in Section 3.3.

3.2.2 Restricting the Domain of μ

In hystereses with closed major loops, the domain of hysteretic behaviour is bounded by $[u_-, u_+]$ (cf. Figure 2.1). The behaviour outside $[u_-, u_+]$ is fully reversible, indicating that only degenerate relays, with $\alpha = \beta$, contribute to the output for inputs outside $[u_-, u_+]$. Hence, we have $\mu(\alpha, \beta) = 0$ for points in $\mathcal{P}$ satisfying $\alpha > \beta$ and either $\alpha > u_+$ or $\beta < u_-$. Note that if the hysteresis has zero slope outside the major loop, μ will also be zero on $\alpha = \beta$ outside $[u_-, u_+]$.

In any physical setup, there are limitations which impose a further constraint which can effectively be interpreted as a restriction on the domain of μ. Saturation of the control input, say at u_+^{sat} and u_-^{sat}, means that some relays in $\mathcal{P}$ can never be exercised, and cannot contribute to a change in output. This effectively restricts the domain of μ to a triangle in $\mathcal{P}$ defined by

$$\mathcal{P}_r \triangleq \{(\alpha,\beta) \in \mathcal{P} | u_-^{sat} \leq \beta \leq \alpha \leq u_+^{sat}\}.$$

These two restrictions are illustrated in Figure 3.4, where $\mu = 0$ outside the shaded area. It will be assumed that, in the design of the overall system, the equipment used to generate control signals has been suitably chosen so that it is capable of exercising the entire hysteresis loop (ie. $[u_-, u_+] \subset [u_-^{sat}, u_+^{sat}]$).

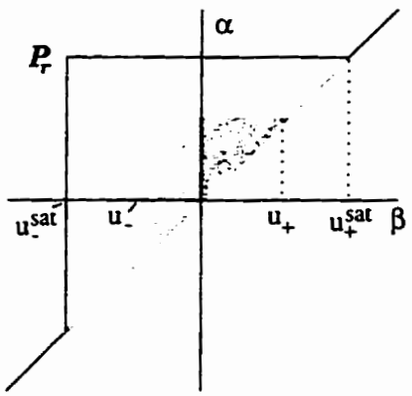

Figure 3.4: Restriction of the Preisach Plane

3.2.3 From Boundary to Output

Using the definitions of $\mathcal{P}_+$ and $\mathcal{P}_-$, the output equation (3.1) can be written as

$$y(t) = \iint_{\mathcal{P}_r} \mu(\alpha,\beta)[\gamma_{\alpha\beta}u](t)d\alpha d\beta$$

$$
\begin{aligned}
&= \iint_{\mathcal{P}_+(t)} \mu(\alpha,\beta)d\alpha d\beta - \iint_{\mathcal{P}_-(t)} \mu(\alpha,\beta)d\alpha d\beta \\
&= \iint_{\mathcal{P}_+(t)} \mu(\alpha,\beta)d\alpha d\beta - \left[\iint_{\mathcal{P}_r} \mu(\alpha,\beta)d\alpha d\beta - \iint_{\mathcal{P}_+(t)} \mu(\alpha,\beta)d\alpha d\beta\right] \\
&= 2\iint_{\mathcal{P}_+(t)} \mu(\alpha,\beta)d\alpha d\beta - \iint_{\mathcal{P}_r} \mu(\alpha,\beta)d\alpha d\beta. \qquad (3.2)
\end{aligned}
$$

Since the boundary defines the region $\mathcal{P}_+$, knowledge of the boundary configuration at time t, along with the weighting function μ, is sufficient to determine $y(t)$. Note that this does not preclude non-local memory, since the boundary stores the effects of past input extrema in its corners.

That the Preisach model represents static hystereses is now easily verified. The output is determined by the boundary, and the boundary itself is defined by past values of input extrema, as well as the current input value. Neither the *time* at which input extrema occur, nor the *shape* of the input between extrema influence the boundary. Hence, the output depends only on the current input value, and on past input extrema and the order in which they occur.

The area swept out by the boundary during a monotonic change in input determines the resulting change in output. This is made more precise by the following proposition.

Proposition 3.2 (Output Variation)
A monotonic change in input which causes the boundary to sweep out an area Ω from time t_1 to time t_2 results in an output variation

$$y(t_2) - y(t_1) = 2sgn\left[u(t_2) - u(t_1)\right] \iint_{\Omega} \mu(\alpha,\beta)d\alpha d\beta. \qquad (3.3)$$

Proof

Consider the example of Figure 3.5. The input decreases from $u(t_1)$ to $u(t_2)$, removing the region Ω from $\mathcal{P}_+$ and adding it to $\mathcal{P}_-$.

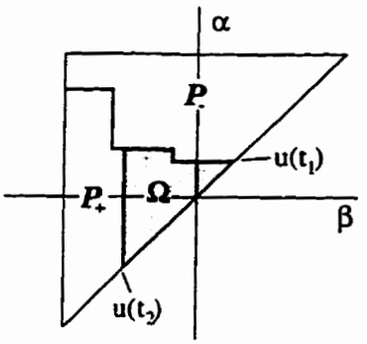

Figure 3.5: Preisach Plane: Monotonic Input Decrease

From equation (3.2), the difference in output is given by

$$\begin{aligned} y(t_2) - y(t_1) &= \left[2 \iint_{\mathcal{P}_+(t_2)} \mu(\alpha,\beta) d\alpha d\beta - \iint_{\mathcal{P}_r} \mu(\alpha,\beta) d\alpha d\beta \right] - \\ &\quad \left[2 \iint_{\mathcal{P}_+(t_1)} \mu(\alpha,\beta) d\alpha d\beta - \iint_{\mathcal{P}_r} \mu(\alpha,\beta) d\alpha d\beta \right] \\ &= 2 \iint_{\mathcal{P}_+(t_2)} \mu(\alpha,\beta) d\alpha d\beta - 2 \iint_{\mathcal{P}_+(t_1)} \mu(\alpha,\beta) d\alpha d\beta \\ &= -2 \iint_{\Omega} \mu(\alpha,\beta) d\alpha d\beta. \end{aligned}$$

Similarly, if u is increasing, it shifts the points of Ω from $\mathcal{P}_-$ to $\mathcal{P}_+$, and the sign of the output variation is reversed. ■

Corollary 3.3

For any region Ω swept out by the boundary in response to a monotonic change in input, the Preisach model weighting function μ satisfies

$$\iint_{\Omega} \mu(\alpha, \beta) d\alpha d\beta \geq 0$$

if, and only if, the sign of the input and output increments are the same.

Proof

The result follows directly from equation (3.3). ∎

3.2.4 Anhysteretic State

A magnetic system in which no remnant magnetization is present is said to be in the *anhysteretic state*[1]. One recognized method for removing remnant magnetization from a magnetic material is to apply a sinusoidal input whose amplitude decays from a value greater than $\max\{|u_+|, |u_-|\}$. This technique has also been successfully applied to "initialize" a differential SMA actuator in order to remove residual hysteresis and obtain repeatable experimental results[20]. The effect of this decaying sinusoid on the Preisach boundary is that it will approximate the line $\alpha = -\beta$. As the decay rate decreases, the change from one maximum (minimum) to the next decreases, the length of the horizontal (vertical) boundary segments decreases, and the closeness of the approximation increases. This prompts the following definition.

Definition 3.1 (Anhysteretic State)

A Preisach model will be said to be in the anhysteretic state whenever its boundary corresponds to the line $\alpha = -\beta$.

If the hysteresis is symmetric about the origin, as in the case of magnetics, then the Preisach weighting function will be symmetric about $\alpha = -\beta$, leading to an output of zero in the anhysteretic state. Furthermore, it will be seen in Chapter 7 that this is a state of minimum stored energy for the Preisach model.

In subsequent analysis, it is important to have a well-defined initial state. Although the choice of this initial condition is somewhat arbitrary, the above discussion suggests the anhysteretic state as a good choice, based on energy arguments as well as the analogy to magnetic materials.

Assumption 3.1 (Initial Condition)
It will be assumed throughout this work that the initial boundary, at time $t = -\infty$, is the line $\alpha = -\beta$.

Because the initial boundary intersects the origin of the Preisach plane, and the model is only defined for continuous signals, this assumption means that valid inputs must satisfy $\lim_{t \to -\infty} u(t) = 0$.

Since inputs can only generate horizontal or vertical boundary segments, it is not possible to return a system to the anhysteretic state. It is, however, possible to approximate this state arbitrarily closely, by applying an oscillatory, slowly decaying input such as a lightly-damped sinusoid.

3.2.5 The Preisach Plane Origin

The Preisach weighting function results from an identification process, detailed in Section 3.4, which must be carried out on the system to be modeled. Identification data is collected by varying the input to the system in a pre-determined fashion

and measuring the resulting output. The reference value for the input during this identification is arbitrary: for a temperature-based actuator such as SMA, one may choose any value such as absolute zero, zero centigrade, or ambient temperature. The "zero" of the Preisach plane represents an input value corresponding to this reference. It will be assumed in this work that models are identified with respect to ambient conditions. For the SMA example, the Preisach temperature input would be $(T - T_{ambient})$.

3.2.6 Model Symmetry

While magnetic hysteresis usually has symmetric output saturation values, some hystereses, such as that present in an SMA actuator, are "shifted" (cf. Figure 2.3). It is clear from the discussion of the boundary behaviour that the Preisach model as described thus far is unable to reproduce this output shift. In negative saturation, $u < u_-^{sat}$ and all relay outputs are -1, so that $\mathcal{P}_+ = \emptyset$. The output is given from equation (3.2) as

$$2\iint_{\mathcal{P}_+} \mu(\alpha,\beta)d\alpha d\beta - \iint_{\mathcal{P}_r} \mu(\alpha,\beta)d\alpha d\beta \;=\; -\iint_{\mathcal{P}_r} \mu(\alpha,\beta)d\alpha d\beta.$$

In positive saturation, relay outputs are $+1$, $\mathcal{P}_+ = \mathcal{P}_r$, and the output is given by

$$\begin{aligned} 2\iint_{\mathcal{P}_+} \mu(\alpha,\beta)d\alpha d\beta - \iint_{\mathcal{P}_r} \mu(\alpha,\beta)d\alpha d\beta &= 2\iint_{\mathcal{P}_r} \mu(\alpha,\beta)d\alpha d\beta - \iint_{\mathcal{P}_r} \mu(\alpha,\beta)d\alpha d\beta \\ &= \iint_{\mathcal{P}_r} \mu(\alpha,\beta)d\alpha d\beta. \end{aligned}$$

In other words, the saturation values of the Preisach model are symmetric about zero. In order to model "output-shifted" hystereses, an offset is added so that the

output is given by

$$y(t) = \iint_{\mathcal{P}} \mu(\alpha, \beta)[\gamma_{\alpha\beta} u](t) d\alpha d\beta + \frac{y_+^{sat} + y_-^{sat}}{2},$$

where y_-^{sat} and y_+^{sat} are the output values obtained when the input is saturated. Since it is assumed that $[u_-, u_+] \subset [u_-^{sat}, u_+^{sat}]$, these values are unique.

3.3 Preisach Model Representation Conditions

The previous section introduced the Preisach plane and the boundary which separates relays in different states within the plane. The definition of the plane and the boundary behaviour imply that the Preisach model displays certain properties, known as the *wiping out property* and *congruent minor loop property.* It has been shown by Mayergoyz that a necessary and sufficient condition for existence of a Preisach representation for a particular system is that the system display these two properties[43]. The final subsection discusses the inability of the classical Preisach model to reproduce a specific type of behaviour, known as accommodation, which appears in some hysteretic systems. The behaviour will be defined in that section.

3.3.1 Wiping Out Property

In [43], Mayergoyz defines two system characteristics known as the *wiping out property* and the *congruent minor loop property*, and shows that they are necessary and sufficient conditions for existence of a Preisach model. The first of these properties is described here; the second is the subject of the next section.

We have seen that input extrema generate the corners of the Preisach boundary, and that this boundary represents the memory of the Preisach model. The wiping

out property states that certain input extrema can remove the effects of previous extrema, essentially "wiping out" the memory of the model. This behaviour is sketched in Figure 3.6.

Suppose the boundary at some time t_1 is as depicted in Figure 3.6a, with the input constant at u_1. If the input increases, a new horizontal branch is generated on the boundary, sweeping upwards through $\mathcal{P}_r$ (Figure 3.6b). As $u(t)$ reaches and passes the previous input maximum, the corner previously generated is "wiped out" (Figure 3.6c) and as the input continues to increase, the memory of that previous extremum has been removed (Figure 3.6d). At any particular time, the previous extrema which are retained by the boundary are referred to by Mayergoyz as the *dominant input extrema.* These will be discussed in greater detail in Chapter 6.

Proposition 3.4

Preisach plane boundaries are always non-increasing with respect to β in $\mathcal{P}$.

Proof

Since inputs can only generate horizontal and vertical boundary segments, an increasing boundary implies that there is a horizontal segment, say at $\alpha = u_1$, followed by a vertical segment with points $\alpha > u_1$ (cf. Figure 3.7). But at any time t the boundary always intersects the line $\alpha = \beta$ at $(u(t), u(t))$. Since the vertical segment just described cannot intersect this line at all, there must be another horizontal segment, say at $\alpha = u_2 > u_1$, to complete the boundary. But this is not possible because of the wiping out property: the input maximum $u = u_2$ would have removed the memory of the previous maximum $u = u_1$, preventing the formation of an increasing boundary section. ∎

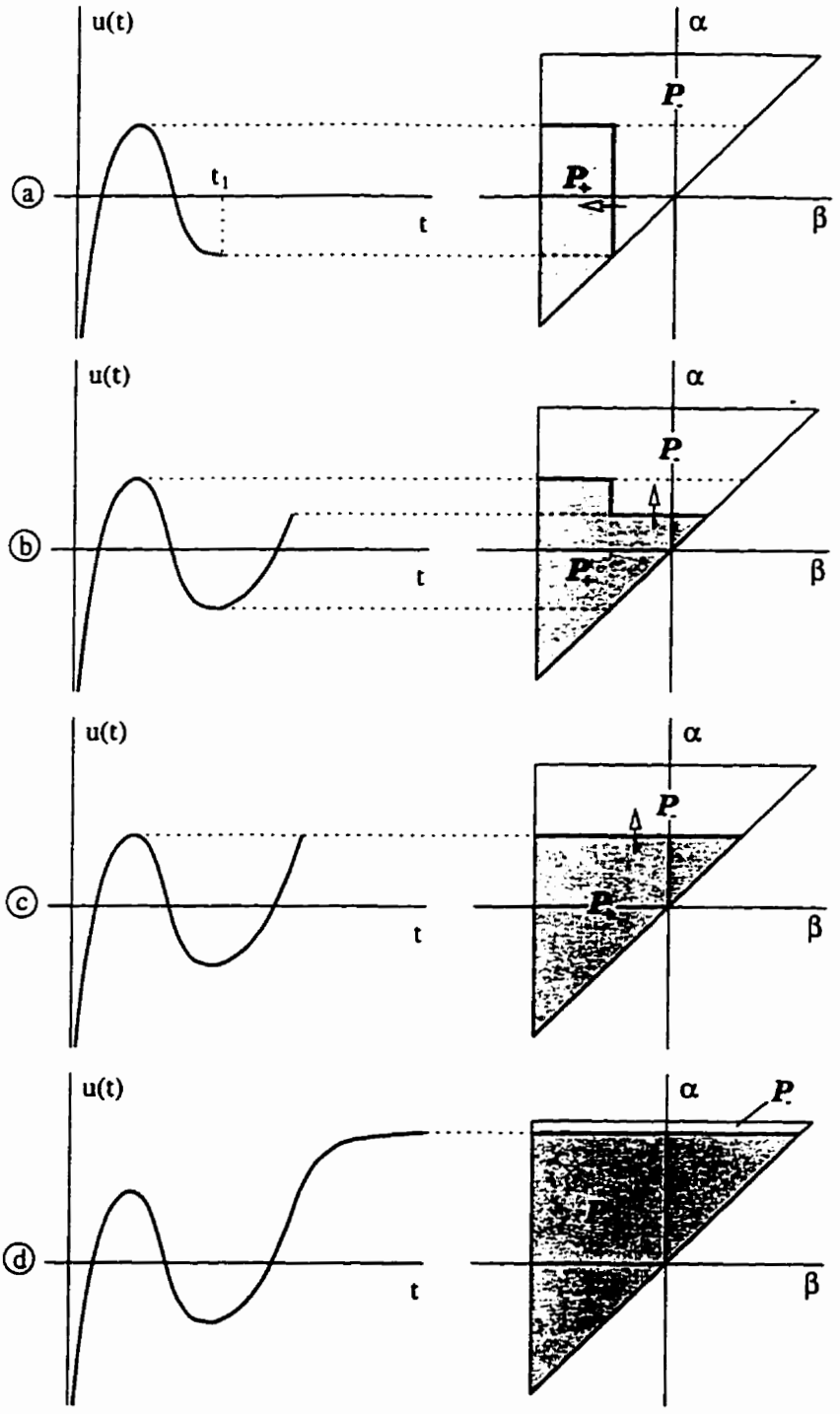

Figure 3.6: Wiping Out Property

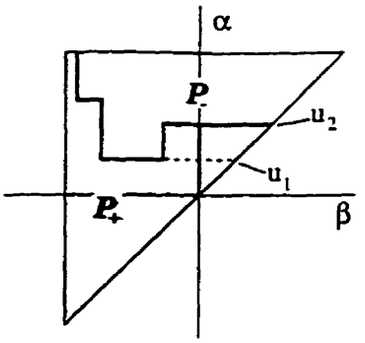

Figure 3.7: Boundary Violating the Wiping Out Property

3.3.2 Congruent Minor Loop Property

The congruent minor loop property requires that any two *comparable* minor loops have the same shape. That this is a property of the Preisach model is once again evident from a discussion of behaviour in the Preisach plane.

Definition 3.2 (Comparable Minor Loops)
Two minor loops are comparable if they are generated by input variation between the same two distinct values, regardless of past input history.

Consider two different input signals which generate comparable minor loops through variation between u_2 and $u_3 > u_2$, but have different input histories. Before reaching u_2, the first input has a peak at $u_1 > u_3$, while the second has a smaller peak before u_2 of magnitude u_1' satisfying $u_3 < u_1' < u_1$. The different input histories ($u_1 \neq u_1'$) mean that these minor loops will be displaced from one another in the input-output plane. This is illustrated, along with the Preisach plane diagrams for each input, in Figure 3.8.

The change in output, Δy, due to input variation between u_2 and u_3 will be entirely determined by the region Ω, regardless of past input history. At any time

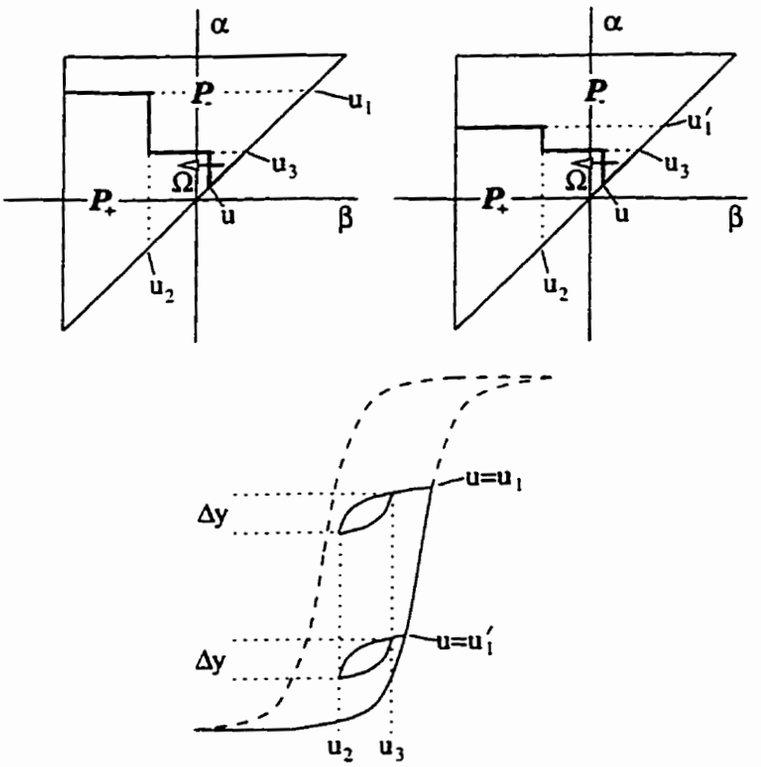

Figure 3.8: Congruent Minor Loop Property

when $u_2 < u < u_3$, the same triangle (shaded in Figure 3.8) has been swept in both cases. As a result, at any point on the minor loop the output variation from the previous extremum will be identical for both inputs, and the minor loops should have exactly the same shape.

3.3.3 Minor Loop Accommodation

Some physical hystereses display a behaviour known as *accommodation*, which the classical Preisach model is unable to represent. This is because this behaviour violates the wiping out property. When a Preisach hysteresis is subjected to an input which oscillates between two distinct input values, the wiping out property

implies that minor loops which are generated by this oscillation should be identical. The term "accommodation", or sometimes "reptation", is used to describe a stabilization process in which several cycles are required before a stable minor loop is generated. Typically, successive loops shift progressively upwards in the hysteresis, towards a stable limit loop.

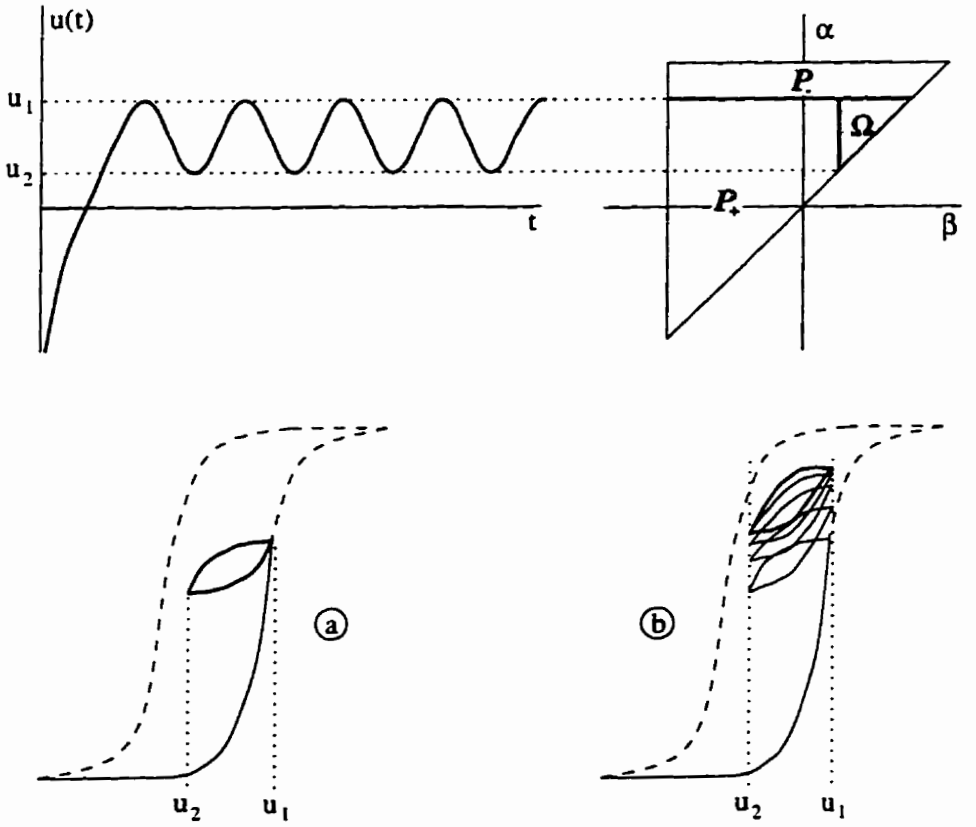

Figure 3.9: Minor Loop Accommodation

Figure 3.9 demonstrates this behaviour. The input oscillates between the same two values, sweeping the region Ω once in each direction for each input period. Thus, one minor loop is generated by each period of the input. Every time the input sweeps Ω, the boundary is identical, so that the output must also be identical,

and successive minor loops coincide exactly. This is depicted in Figure 3.9a. Figure 3.9b shows a typical example of accommodation behaviour. Extensions of the classical model have been proposed which are able to account for this accommodation behaviour[43]. Preisach model extensions will be reviewed in more detail in Section 3.5.

3.4 Preisach Model Identification

In [43], Mayergoyz proposes a technique to determine the Preisach weighting surface μ from experimental data. The identification involves the generation of several "first-order descending curves", from which μ can be determined.

A first-order descending curve (FOD) is generated by first bringing the input to negative saturation, followed by a monotonic increase to a value $u = \alpha_1$, then a decrease to $u = \beta_1$. Any such input is parameterized by α_1 and β_1, and will be denoted $u_{\alpha_1\beta_1}$. This process is illustrated in Figure 3.10. The measured output values are labeled y_{α_1}, corresponding to $u = \alpha_1$, and $y_{\alpha_1\beta_1}$ when u has reached β_1.

The term "descending" refers to the direction of the final branch of the graph. The addition of "first-order" indicates that only one reversal has occurred. Similar terminology leads to the definition of higher-order descending or ascending curves, collectively called "n^{th}-order transition curves".

After the input peaks at α_1, the decrease sweeps out Ω, generating the descending branch inside the major loop. The change in output along the descending branch can therefore be written (Proposition 3.2)

$$y_{\alpha_1} - y_{\alpha_1\beta_1} = 2 \iint_{\Omega} \mu(\alpha, \beta) d\alpha d\beta. \tag{3.4}$$

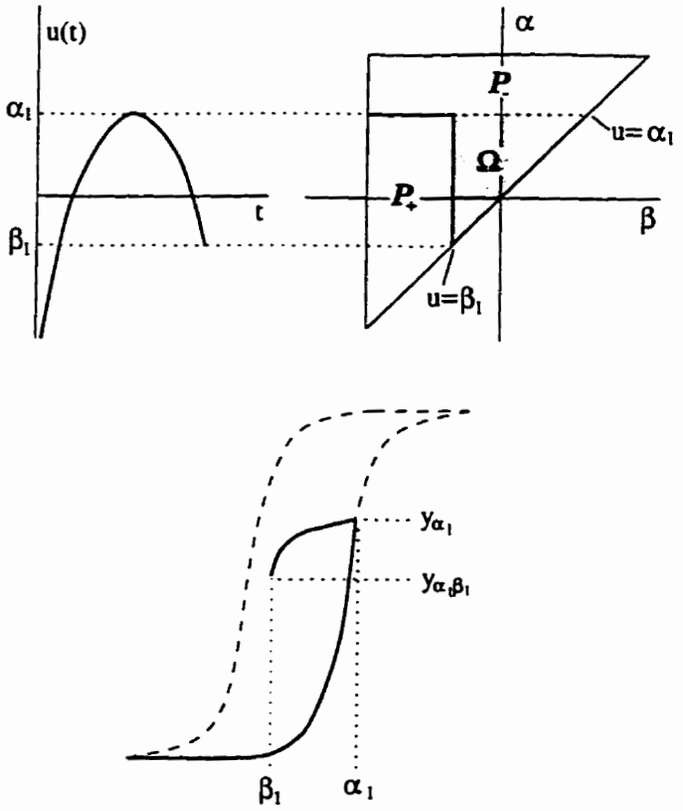

Figure 3.10: Sample Identification Input

Defining the function $F(\alpha_1,\beta_1)=y_{\alpha_1}-y_{\alpha_1\beta_1}$, rewriting the integral and then taking partial derivatives of both sides gives the following relationship for μ.

$$\begin{aligned} F(\alpha_1,\beta_1) &= 2\int_{\beta_1}^{\alpha_1}\int_{\beta}^{\alpha_1}\mu(\alpha,\beta)d\alpha d\beta \\ \frac{\partial}{\partial\beta_1}F(\alpha_1,\beta_1) &= -2\int_{\beta}^{\alpha_1}\mu(\alpha,\beta_1)d\alpha \\ \frac{\partial^2}{\partial\alpha_1\partial\beta_1}F(\alpha_1,\beta_1) &= -2\mu(\alpha_1,\beta_1). \end{aligned}$$

Then the value of the weighting function at any point $(\alpha_1,\beta_1)\in\mathcal{P}_r$ can be determined from

$$\mu(\alpha_1,\beta_1) = -\frac{1}{2}\frac{\partial^2}{\partial\alpha_1\partial\beta_1}F(\alpha_1,\beta_1)$$

$$= \frac{1}{2}\frac{\partial^2 y_{\alpha_1\beta_1}}{\partial\alpha_1\partial\beta_1}.$$

If the value $y_{\alpha\beta}$ could be identified for all points in $\mathcal{P}_r$, it is clear on physical grounds that the surface $y(\alpha,\beta)$ formed of all points $y_{\alpha\beta}$ should be smooth. This surface could then be differentiated to obtain the weighting function,

$$\mu(\alpha,\beta) = \frac{1}{2}\frac{\partial^2 y(\alpha,\beta)}{\partial\alpha\partial\beta}. \tag{3.5}$$

More realistically, the hysteresis domain $[u_-, u_+]$ is divided into n segments, defined by the ordered partition $\{u_i\}_{i=0,\ldots,n}$. FOD curves are then obtained for all pairs (u_i, u_j) with $j \leq i$, resulting in $\frac{n}{2}(n+3)$ FOD data points. A smooth approximation surface $\tilde{y}(\alpha,\beta)$ is then fit to these data points, and this FOD surface is differentiated to obtain an approximate weighting surface $\tilde{\mu}$.

Based on the fact that the major hysteresis is closed, as well as the smooth nature of the FOD curves for physical systems and their relationship to μ (3.5), the following standing assumption on μ is made.

Assumption 3.2

It will be assumed that the Preisach weighting function is at least piecewise continuous, that it is bounded on $\mathcal{P}_r$, and that there exists at least one point $(\alpha,\beta) \in \mathcal{P}_r$ with $\mu(\alpha,\beta) \neq 0$.

It should be noted that the output of the Preisach model can be computed directly from knowledge of the boundary configuration and the FOD data. The formula is a simple linear combination of FOD surface values at points in $\mathcal{P}_r$ given by the corners of the boundary. The need to perform the surface fit (and differentiation) mentioned above is thus eliminated, by using an appropriate interpolation

scheme to approximate FOD surface values which were not directly measured. The method is described in [e.g. 43].

The disadvantage of the interpolation method is that the weighting function is never actually determined, even approximately. In this work, the form of μ and its properties are of greater interest than model implementation, and the identification strategy used will be that of surface fitting and differentiation.

3.5 Extensions to the classical Model

In his monograph[43], Mayergoyz collects results, due to himself and others, which present various extensions to the classical Preisach model. Each of these is briefly discussed in this section. The intent is to summarize the effect of the extension on representation conditions and the complexity of the identification task. For details of the extended models, the reader is referred to [43].

Non-Linear Preisach Model

The intent of this extension is to relax the congruent minor loop requirement, which is that which is most often violated. With this model, comparable minor loops (cf. Definition 3.2) are no longer required to have the same shape, but instead must have vertical chords of equal length. In other words, for any two minor loops generated as the input oscillates between u_1 and u_2, then for every $u^* \in (u_1, u_2)$ the chord $u = u^*$ must have the same length in each loop. Along with the wiping out property, this property of equal vertical chords form the necessary and sufficient conditions for representation.

The cost of this less stringent minor loop condition is an increase in the complexity of the identification task. The procedure is similar in flavour to the classical model identification scheme, but requires second-order transition curve data as well as first-order. This results in an identification hypersurface with domain in $\mathbf{R}^3$.

Restricted Preisach Model

The restricted Preisach model, despite its name, is a further generalization of the non-linear model. While the weighting function of the non-linear form depended only on the current input value, that of an n^{th}-order restricted model depends on the n previous dominant input maxima and minima. The accuracy of the model representation increases with increasing order.

The representation conditions are stated in the same manner as those of the classical Preisach model: the wiping out property must hold and comparable minor loops must have the same shape. However, the definition of comparable minor loops is somewhat relaxed. Two loops are now called comparable if they are generated by input variation between the same two values *and after an identical set of n most recent maxima and minima.*

The identification task becomes more involved with this model. Where the identification surface for the classical model is three-dimensional, an n^{th}-order restricted model requires the identification of a hypersurface in $(2+n)$-space. This must be done through systematic measurement of first- to n^{th}-order transition curves. The number of identification inputs required, and hence the time required for the procedure, is of order n. As well, the complexity of the subsequent surface fit to determine the weighting function is greatly increased.

Accommodation Preisach Model

In order to model accommodation behaviour, a second weighting function ν is introduced, which multiplies μ. This additional weighting is a function of *output* extrema, and it is assumed that the form of ν is known *a priori*. The identification of μ is carried out in the same manner as for the classical model. The representation conditions for this model have not been addressed.

Other Models

Further extensions have been proposed to model dynamic hystereses as well as those having multiple independent inputs. In particular, the latter extension may be required for a full modelling of magnetostrictive or shape memory alloy behaviour in response to time-varying stresses. However, it will be seen in Chapter 5 that if the stress variations are small, the classical form can provide an adequate match. These models are more general than those outlined previously and are further complicated in their identification techniques and representation conditions.

3.6 Summary

This chapter introduced the classical form of the Preisach hysteresis model. A formula was derived for the computation of the output variation to a monotonic input, as an area integral in the Preisach plane. Necessary and sufficient conditions for existence of a Preisach model were given, the identification technique was discussed, and several extensions to the Preisach model were briefly outlined.

Chapter 4

Preisach Model Properties

In this chapter, some mathematical properties of the Preisach model are shown. The first section deals with the continuity of the operator defined by the Preisach model. These and other properties have been investigated in the past, notably by the mathematician Visintin[6, 64]. The authors of those works consider the general case where μ is a Borel measure on an unbounded set, giving the model form

$$y(t) = \int_{\mathcal{P}} [\gamma(u)](t) d\mu.$$

Unfortunately, the proofs are difficult to follow without a strong mathematical background. Here, the more realistic case where the measure can be written as a product of a function with a Lebesgue measure, $d\mu = \mu(\alpha, \beta) d\alpha d\beta$, is examined. The proofs of continuity are simpler in this more restrictive case.

The second section discusses conditions under which the weighting function is non-negative. This has implications for many results in the existing literature[6, 43].

First, several classes of weighting function μ are defined.

Definition 4.1 (Classes of μ)

$\boxed{\mathcal{M}_{PC}}$ *is the set of all functions* $\mu : \mathcal{P}_r \mapsto \mathbf{R}$ *which are bounded and piecewise continuous.*

$\boxed{\mathcal{M}_{P}}$ *is the set of all functions* $\mu : \mathcal{P}_r \mapsto \mathbf{R}$ *which are bounded and piecewise continuous, and satisfying* $\mu(\alpha, \beta) \geq 0$ *for all points* $(\alpha, \beta) \in \mathcal{P}_r$.

Note that $\mathcal{M}_P \subset \mathcal{M}_{PC}$ by definition.

4.1 Continuity

The Preisach model has so far been treated as a map from $\mathbf{R}$ to $\mathbf{R}$, with memory. The model can also be viewed as an operator, Γ, on the space of continuous functions C^0, so that for $u \in C^0$, we write $y = \Gamma u$. This section is concerned with showing continuity of Γ on C^0 and also on the Sobolev space W_1^0 (defined later).

In analyzing the continuity of Γ, it will be useful to define horizontal and vertical strips in $\mathcal{P}_r$, of width ξ:

$$\begin{aligned} h(\lambda, \xi) &\triangleq \{(\alpha, \beta) \in \mathcal{P}_r | \lambda \leq \alpha \leq \lambda + \xi\}, \\ v(\lambda, \xi) &\triangleq \{(\alpha, \beta) \in \mathcal{P}_r | \lambda \leq \beta \leq \lambda + \xi\}. \end{aligned}$$

These are illustrated in Figure 4.1. For convenience, notation for the integrated strips is also defined:

$$\begin{aligned} H(\lambda, \xi) &\triangleq \iint_{h(\lambda,\xi)} \mu(\alpha, \beta) d\alpha d\beta, \\ &= 2 \int_{\lambda}^{\lambda+\xi} \int_{u^{-1}(\alpha)}^{\alpha} \mu(\alpha, \beta) d\beta d\alpha, \end{aligned}$$

$$V(\lambda,\xi) \triangleq \iint_{v(\lambda,\xi)} \mu(\alpha,\beta)d\alpha d\beta$$
$$= 2\int_{\lambda}^{\lambda+\xi}\int_{\beta}^{u_+^{sat}} \mu(\alpha,\beta)d\alpha d\beta.$$

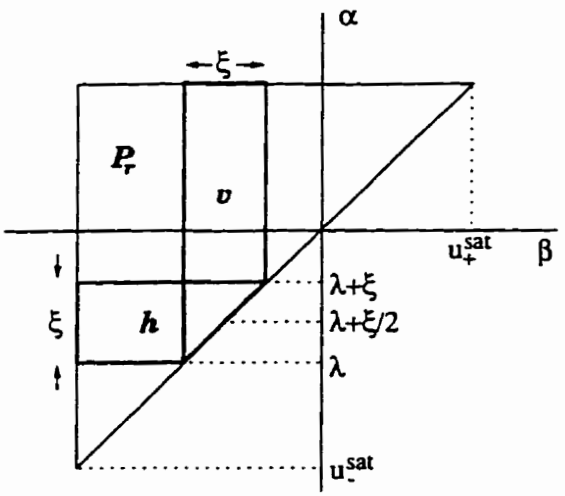

Figure 4.1: Definition of h and v

For any $\xi \in [0, u_+^{sat} - u_-^{sat}]$ and $\lambda \in [u_-^{sat}, u_+^{sat} - \xi]$, define also the functions

$$k(\lambda,\xi) \triangleq \max\{H(\lambda,\xi),\ V(\lambda,\xi)\}$$

and

$$K(\xi) \triangleq \max_{\lambda\in[u_-^{sat},u_+^{sat}-\xi]} k(\lambda,\xi).$$

The value $|K(\xi)|$ is the maximum change in output which can result from a monotonic input variation of magnitude ξ.

Lemma 4.1

If $\mu \in \mathcal{M}_{PC}$, then $k(\cdot,\cdot)$ is continuous.

Proof

The areas of integration defined by $h(\lambda,\xi)$ and $v(\lambda,\xi)$ are clearly continuous in

both λ and ξ. Since μ is piecewise continuous over $\mathcal{P}_r$, both $H(\lambda,\xi)$ and $V(\lambda,\xi)$ are continuous functions of λ and ξ. So H and V are continuous functions on a compact subset of $\mathbf{R}^2$, and it is required to show that the pointwise maximum of these two functions is itself continuous.

Let $T \subset \mathbf{R}^2$ be the compact metric space defined by $\xi \in [0, u_+^{sat} - u_-^{sat}]$ and $\lambda \in [u_-^{sat}, u_+^{sat} - \xi]$, with the standard Euclidean metric $d(\cdot,\cdot)$. Let $B_r(\lambda_o,\xi_o)$ denote the disc of center (λ_o,ξ_o) and radius r so that $d((\lambda_o,\xi_o),(\lambda,\xi)) < r$ for all $(\lambda,\xi) \in B_r(\lambda_o,\xi_o)$.

Now, choose any $\varepsilon > 0$. It is required to show that for any point $(\lambda_o,\xi_o) \in T$, there exists a $\delta > 0$ such that $|k(\lambda_o,\xi_o) - k(\lambda,\xi)| < \varepsilon$ for all $(\lambda,\xi) \in B_\delta(\lambda_o,\xi_o)$. Choose any point $(\lambda_o,\xi_o) \in T$ and suppose, without loss of generality, that $V(\lambda_o,\xi_o) > H(\lambda_o,\xi_o)$, so that $k(\lambda_o,\xi_o) = V(\lambda_o,\xi_o)$. Since V and H are continuous, there exists $\delta_k > 0$ so that for any point in $B_{\delta_k}(\lambda_o,\xi_o)$, $k(\lambda,\xi) = V(\lambda,\xi)$. Also, there exists $\delta_v > 0$ so that

$$|V(\lambda,\xi) - V(\lambda_o,\xi_o)| < \varepsilon, \quad \forall (\lambda,\xi) \in B_{\delta_v}(\lambda_o,\xi_o).$$

Setting $\delta = \min\{\delta_k, \delta_v\}$, for all $(\lambda,\xi) \in B_\delta(\lambda_o,\xi_o)$,

$$\begin{aligned} |k(\lambda,\xi) - k(\lambda_o,\xi_o)| &= |V(\lambda,\xi) - V(\lambda_o,\xi_o)| \\ &< \varepsilon. \end{aligned}$$

Thus, k is continuous at the point (λ_o,ξ_o). A similar argument shows continuity if $H(\lambda_o,\xi_o) > V(\lambda_o,\xi_o)$.

If $V(\lambda_o,\xi_o) = H(\lambda_o,\xi_o)$, then choose $\delta_v > 0$ and $\delta_h > 0$ so that

$$|V(\lambda,\xi) - V(\lambda_o,\xi_o)| < \varepsilon, \quad \forall (\lambda,\xi) \in B_{\delta_v}(\lambda_o,\xi_o),$$

and

$$|H(\lambda,\xi) - H(\lambda_o,\xi_o)| < \varepsilon, \quad \forall (\lambda,\xi) \in B_{\delta_h}(\lambda_o,\xi_o).$$

Set $\delta = \min\{\delta_v, \delta_h\}$. Since $k(\lambda_o, \xi_o) = V(\lambda_o, \xi_o) = H(\lambda_o, \xi_o)$, then within $B_\delta(\lambda_o, \xi_o)$, the farthest any point on V or H can be from $k(\lambda_o, \xi_o)$ is ε. In particular,

$$|k(\lambda, \xi) - k(\lambda_o, \xi_o)| < \varepsilon, \quad \forall (\lambda, \xi) \in B_\delta(\lambda_o, \xi_o).$$

This shows that if $V(\lambda_o, \xi_o) = H(\lambda_o, \xi_o)$, k is continuous at (λ_o, ξ_o). But (λ_o, ξ_o) was arbitrary, so this completes the proof. ■

Lemma 4.2 (Properties of $K(\xi)$)

The function $K(\xi)$ satisfies the following properties:

1. $K(0) = 0$,
2. *if $\mu \in \mathcal{M}_{PC}$, $K(\xi)$ is continuous, and*
3. *if $\mu \in \mathcal{M}_{PC}$, then there exists $C > 0$ such that $K(\xi) \leq C\xi$.*

Proof

Property 1

From the definition of H and V, $k(\lambda, 0) = 0$ for any $\lambda \in [u_-^{sat}, u_+^{sat}]$, since the area of integration is empty for $\xi = 0$. The fact that $K(0) = 0$ then follows directly from the definition of $K(\xi)$.

Property 2

Let T be the compact subset of $\mathbf{R}^2$ defined by $\xi \in [0, u_+^{sat} - u_-^{sat}]$ and $\lambda \in [u_-^{sat}, u_+^{sat} - \xi]$, as shown in Figure 4.2. Choose any $\varepsilon > 0$ and any $\xi_o \in [0, u_+^{sat} - u_-^{sat}]$. Since $\mu \in \mathcal{M}_{PC}$, k is continuous from Lemma 4.1. Then for every $\lambda \in [u_-^{sat}, u_+^{sat} - \xi_o]$ there is a $\delta_\lambda > 0$ and $R_\lambda = B_{\delta_\lambda}(\lambda, \xi_o)$ where $|k(\lambda, \xi) - k(\lambda, \xi_o)| < \varepsilon/2$. The collection of all regions R_λ is an infinite number of circles of varying radii δ_λ and centres on the

vertical line $\xi = \xi_o$ in T (cf. Figure 4.2). For every point (λ, ξ) inside any one of these circles, the shortest distance to the line $\xi = \xi_o$ is $|\xi - \xi_o| < \delta_\lambda$, and

$$|k(\lambda, \xi) - k(\lambda_o, \xi_o)| < \varepsilon/2.$$

Since $[u_-^{sat}, u_+^{sat} - \xi_o]$ is compact, a finite subset of these regions $\mathcal{R} = \{R_i\}$ can be chosen which contains all the points of the line $\xi = \xi_o$ in T.

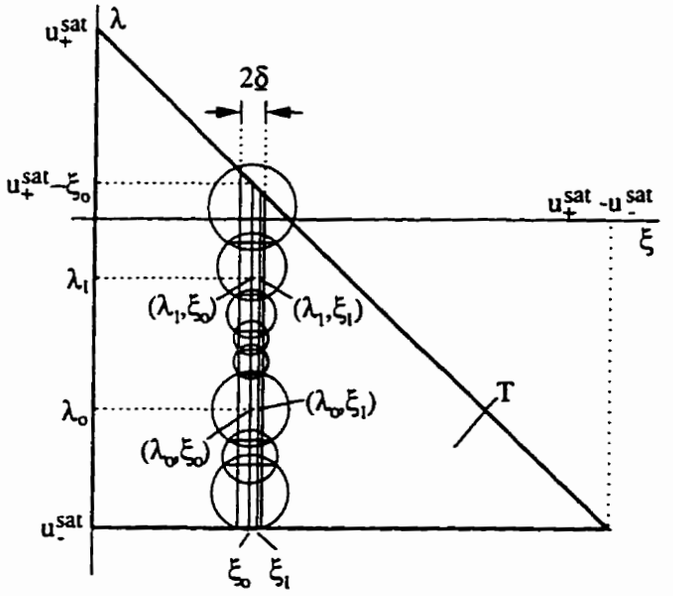

Figure 4.2: Continuity of $K(\xi)$

Since the regions R_i are open and cover the line $\xi = \xi_o$, then every R_i overlaps one next to it, and they share a common chord of non-zero length in this intersection (cf. Figure 4.2). Let $2\delta_i$ be the length of the common chord between R_i and R_{i+1}, and set $\underline{\delta} = \min_i\{\delta_i\}$. Then for any ξ such that $|\xi_o - \xi| < \underline{\delta}$ and any $\lambda \in [u_-^{sat}, u_+^{sat} - \xi_o]$,

$$|k(\lambda, \xi) - k(\lambda, \xi_o)| < \varepsilon/2. \tag{4.1}$$

Now, choose any point ξ_1 such that $|\xi_1 - \xi_o| < \underline{\delta}$, and define

$$\lambda_o \triangleq \operatorname*{argmax}_{\lambda \in [u_-^{sat}, u_+^{sat} - \xi_o]} k(\lambda, \xi_o),$$

$$\lambda_1 \triangleq \operatorname*{argmax}_{\lambda \in [u_-^{sat}, u_+^{sat} - \xi_1]} k(\lambda, \xi_1).$$

Since k is continuous with respect to λ, these values are well-defined. Then $K(\xi_o) = k(\lambda_o, \xi_o)$ and $K(\xi_1) = k(\lambda_1, \xi_1)$. From (4.1),

$$|k(\lambda_o, \xi_o) - k(\lambda_o, \xi_1)| < \varepsilon/2 \tag{4.2}$$

and

$$|k(\lambda_1, \xi_1) - k(\lambda_1, \xi_o)| < \varepsilon/2. \tag{4.3}$$

From the definition of λ_o and λ_1,

$$k(\lambda_o, \xi_o) \geq k(\lambda_1, \xi_o) \tag{4.4}$$

and

$$k(\lambda_1, \xi_1) \geq k(\lambda_o, \xi_1). \tag{4.5}$$

From equations (4.2) and (4.5),

$$\begin{aligned} |k(\lambda_o, \xi_o) - k(\lambda_o, \xi_1)| &< \varepsilon/2 \\ k(\lambda_o, \xi_o) - k(\lambda_o, \xi_1) &< \varepsilon/2 \\ k(\lambda_o, \xi_o) &< \varepsilon/2 + k(\lambda_o, \xi_1) \\ &\leq \varepsilon/2 + k(\lambda_1, \xi_1) \\ k(\lambda_o, \xi_o) - k(\lambda_1, \xi_1) &\leq \varepsilon/2. \end{aligned}$$

Similarly, from (4.3) and (4.4),

$$\begin{aligned} k(\lambda_1, \xi_1) &< \varepsilon/2 + k(\lambda_1, \xi_o) \\ &\leq \varepsilon/2 + k(\lambda_o, \xi_o) \\ k(\lambda_1, \xi_1) - k(\lambda_o, \xi_o) &\leq \varepsilon/2. \end{aligned}$$

So for any two points satisfying $|\xi_o - \xi_1| < \delta$.

$$\begin{aligned} |K(\xi_o) - K(\xi_1)| &= |k(\lambda_o, \xi_o) - k(\lambda_1, \xi_1)| \\ &\leq \varepsilon/2 \\ &< \varepsilon \end{aligned}$$

and K is continuous.

Property 3

Since $\mu \in \mathcal{M}_{PC}$, the weighting function is bounded by definition. Choose any finite positive constant

$$M > \max_{\mathcal{P}_r} \mu(\alpha, \beta)$$

and $\xi \in [0, u_+^{sat} - u_-^{sat}]$. Then for any $\lambda \in [u_-^{sat}, u_+^{sat} - \xi]$,

$$\begin{aligned} k(\lambda, \xi) &= \max\{2H(\lambda, \xi), 2V(\lambda, \xi)\} \\ &= \max\left\{2\iint_{h(\lambda,\xi)} \mu(\alpha,\beta)d\alpha d\beta, 2\iint_{v(\lambda,\xi)} \mu(\alpha,\beta)d\alpha d\beta\right\} \\ &\leq M \max\left\{2\iint_{h(\lambda,\xi)} d\alpha d\beta, 2\iint_{v(\lambda,\xi)} d\alpha d\beta\right\}. \end{aligned} \tag{4.6}$$

But the value of the integrals in (4.6) are simply the areas defined by h and v. From the definition of these regions (cf. Figure 4.1), and of the function K,

$$\begin{aligned} K(\xi) &\leq 2M \max_{\lambda \in [u_-^{sat}, u_+^{sat} - \xi]} \left\{\xi\left(\lambda + \xi/2 - u_-^{sat}\right), \xi\left(u_+^{sat} - \lambda - \xi/2\right)\right\} \\ &= 2M\left[\xi\left(u_+^{sat} - u_-^{sat} - \xi/2\right)\right] \\ &\leq 2M(u_+^{sat} - u_-^{sat}) \cdot \xi. \end{aligned}$$

Since M is independent of λ, setting $C = 2M(u_+^{sat} - u_-^{sat})$ gives $K(\xi) \leq C\xi$ for every $\xi \in [0, u_+^{sat} - u_-^{sat}]$. ∎

Theorem 4.3 (Continuity on C^0)

If $\mu \in \mathcal{M}_{PC}$ then the Preisach model maps continuous inputs to continuous outputs.

Proof

Choose any $\varepsilon > 0$, and define

$$\xi^* \triangleq \sup\{\xi_o \,|\, |K(\xi)| < \varepsilon,\ \forall \xi \leq \xi_o\}.$$

$K(0) = 0$, and $\mu \in \mathcal{M}_{PC}$, so K is continuous. Then ξ^* is well-defined, $\xi^* > 0$, and $|K(\xi)| \leq |K(\xi^*)|$ for all $\xi \leq \xi^*$.

For $u \in C^0$, choose $\delta > 0$ so that $|t_2 - t_1| < \delta$ implies $|u(t_2) - u(t_1)| < \xi^*$. Recalling that $|K(\xi)|$ is the maximum output variation for an input change of magnitude ξ, then $|t_2 - t_1| < \delta$ implies

$$\begin{aligned} |y(t_2) - y(t_1)| &\leq |K(|u(t_2) - u(t_1)|)| \\ &\leq |K(\xi^*)| \\ &< \varepsilon, \end{aligned}$$

and the Preisach operator is continuous on C^0. ∎

Another space of interest is the Sobolev space, denoted W_1^2.

Definition 4.2 (Sobolev Space)

The Sobolev space $W_1^2[0,T]$ is the space of real-valued functions u for which the Sobolev norm is finite:

$$\|u\|_{W_1^2} = \sqrt{\int_0^T \dot{u}^2 + u^2 dt}.$$

These signals have bounded energy and bounded velocity.

In [6], the following theorem is proven.

Theorem 4.4 ([6], Theorem 4.13)

Suppose μ is finite and non-negative on $\mathcal{P}$. The Preisach operator maps $W_1^2[0,T]$ into itself if and only if there exists $C > 0$ such that $K(\xi) \leq C\xi$ for all $\xi > 0$.

In the context of [6], the Preisach plane $\mathcal{P}$ is not assumed bounded.

Corollary 4.5

If $\mathcal{P}$ is restricted to $\mathcal{P}_r$ and $\mu \in \mathcal{M}_P$ then $\Gamma : W_1^2[0,T] \mapsto W_1^2[0,T]$.

Proof

Since $\mathcal{M}_P \subset \mathcal{M}_{PC}$, the required constant C exists, from Property 3 of Lemma 4.2. Then the conditions of Theorem 4.4 are satisfied, and the Preisach model $\Gamma : W_1^2[0,T] \mapsto W_1^2[0,T]$. ∎

4.2 Positivity of the Weighting Function

Many references which treat the mathematical properties of the Preisach model mention the positivity of μ[e.g. 6, 43]. Specific results, such as Theorem 4.4, may be derived for Preisach systems for which the weighting function satisfies $\mu \geq 0$. In this section a graphical test for the positivity of μ is discussed.

Mayergoyz mentions weighting function positivity in [43], in relation to the FOD curves and equation (3.5):

$$\mu(\alpha,\beta) = \frac{1}{2}\frac{\partial^2 y(\alpha,\beta)}{\partial\alpha\partial\beta}.$$

For any pair (α_o, β_o), the partial derivative $\frac{\partial y(\alpha_o,\beta_o)}{\partial\beta}$ is the slope of the tangent to the FOD curve at the point $(\beta_o, y_{\alpha_o\beta_o})$ in the input-output plane (cf. Figure

4.3). Assuming the output direction follows that of the input, the FOD curves are monotonic and this slope is always positive. If the rate of change of this slope is non-negative for increasing α (higher and higher FOD curves), then $\mu(\alpha_o, \beta_o) \geq 0$. If this is true at every point on the FOD curves, then $\mu \geq 0$. Mayergoyz makes the comment, without proof, that all that is required to ensure this is that "all first-order transition curves are monotonically increasing functions of β, and they do not intersect inside the major loop but merge together at the point where the descending and ascending branches of the major loop meet one another". The FOD curves of Figure 4.3 exemplify this behaviour.

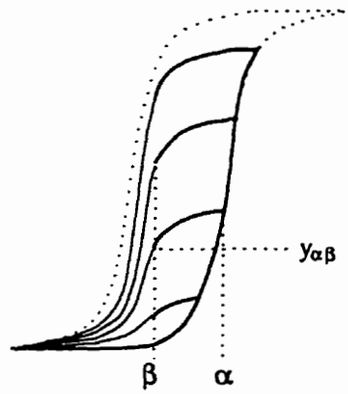

Figure 4.3: FOD Curves

Mayergoyz uses the terminology "first-order transition curves", which includes both first-order ascending and descending curves. A first-order ascending (FOA) curve is, as the name would imply, a curve which undergoes one reversal and whose last branch is ascending. Such a curve is the dual of an FOD, and is generated by first bringing the system to positive saturation, then decreasing to β, reversing, and increasing to $\alpha > \beta$. Note that monotonicity of the FOD and FOA curves is tantamount to the standing assumption that the direction of the output follows that of the input.

The full proof of Mayergoyz' statement remains elusive. The following Proposition provides a partial proof, as well as a graphical test which indicates when a weighting function has negative regions.

Proposition 4.6

If $\mu \in \mathcal{M}_P$, and $\frac{\partial y(\alpha,\beta)}{\partial \beta}$ is continuous in α, then none of the FOD curves cross inside the major loop.

Proof

The proposition is proven by contradiction. Figure 4.4 helps to illustrate the proof. Choose any $\alpha_2 > \alpha_1$, and suppose that the curves $y(\alpha_1, \beta)$ and $y(\alpha_2, \beta)$ cross inside the major loop.

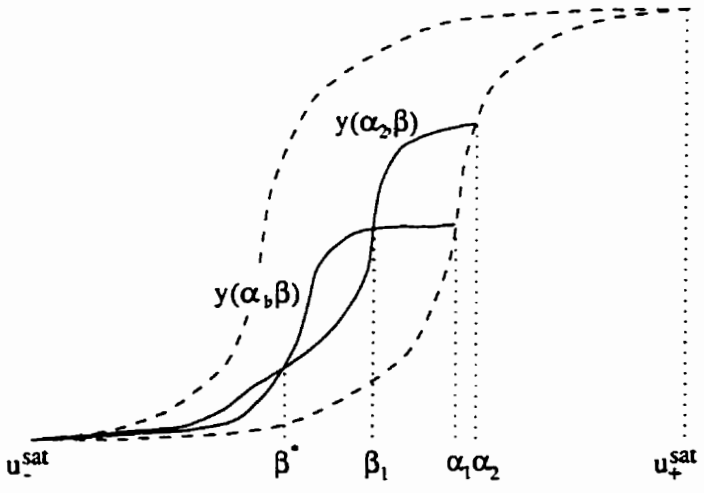

Figure 4.4: Crossing FOD Curves

Define

$$\beta_1 \triangleq \max\{\beta \in (u_-, u_+) | y(\alpha_1, \beta) = y(\alpha_2, \beta),\ y(\alpha_1, \beta - \Delta\beta) > y(\alpha_2, \beta - \Delta\beta)\}$$

$$\beta^* \triangleq \max\{\beta \in [u_-, \beta_1) | y(\alpha_1, \beta) = y(\alpha_2, \beta)\}.$$

β_1 exists by hypothesis, and all FOD curves merge at $\beta = u_-$, so β^* exists. Since $y(\alpha_1, \beta) > y(\alpha_2, \beta)$ for all $\beta \in (\beta^*, \beta_1)$ and $y(\alpha_1, \beta^*) = y(\alpha_2, \beta^*)$,

$$\begin{aligned}\frac{\partial y(\alpha_2, \beta^*)}{\partial \beta} &= \lim_{\Delta\beta \to 0} \frac{y(\alpha_2, \beta^* + \Delta\beta) - y(\alpha_2, \beta^*)}{\Delta\beta} \\ &< \lim_{\Delta\beta \to 0} \frac{y(\alpha_1, \beta^* + \Delta\beta) - y(\alpha_1, \beta^*)}{\Delta\beta} \\ &= \frac{\partial y(\alpha_1, \beta^*)}{\partial \beta}.\end{aligned}$$

But from the assumption of continuity of $\frac{\partial y(\alpha, \beta^*)}{\partial \beta}$ in α, then by the mean value theorem there exists a point $\alpha^* \in (\alpha_1, \alpha_2)$ such that

$$\begin{aligned}\frac{\partial^2 y(\alpha^*, \beta^*)}{\partial \alpha \partial \beta} &= \frac{1}{\alpha_2 - \alpha_1} \left[\frac{\partial y(\alpha_2, \beta^*)}{\partial \beta} - \frac{\partial y(\alpha_1, \beta^*)}{\partial \beta} \right] \\ &< 0,\end{aligned}$$

so $\mu(\alpha^*, \beta^*) < 0$. This implies that if $\mu \in \mathcal{M}_P$, then the FOD curves do not cross within the major loop. ∎

The proof of Proposition 4.6 provides a "negative test": crossing FOD curves indicate a weighting surface that has negative values.

4.3 Summary

The first section of this chapter dealt with the continuity of the Preisach operator on the space of continuous functions and also on the space of square-integrable functions with square-integrable first derivatives. Although the results of that section were also derived in [6], the dependence on results from measure theory in that paper can make it difficult to understand for many readers. Aside from Theorem 4.4, the results here were derived independently. The less general framework al-

lows the use of simpler mathematical arguments than those from previous works, resulting in proofs which are hopefully more accessible.

Section 2 discussed the positivity of μ for a given system. A test based on experimental data is quoted from [43], but the proof of this result remains elusive. It was shown that if a system's FOD curves cross inside the major loop, then some points on the weighting function must be negative. This provides a graphical test which can indicate when $\mu \notin \mathcal{M}_P$.

Chapter 5

Preisach Modelling of Shape Memory Alloys

This chapter is concerned with applying the identification procedure of Chapter 3 to two SMA wire actuators: a single-wire under constant-load, and a two-wire differential actuator. The first section provides background for the identification procedure. The experimental apparatus are described, some previous research in Preisach modelling of SMA is discussed, and the approach taken in this work is outlined. The second section describes the experimental methods used.

In Section 3, the actuators are tested for the wiping out and congruent minor loop properties. Once these have been verified, Section 4 describes the collection of experimental data and the fit of an appropriate surface. This surface is differentiated to obtain the weighting function. In Section 5, the models are verified against experimental identification data, and the results are discussed.

It should be noted that results have appeared very recently which treat the problem of the estimation of the Preisach weighting function from a more theoret-

ical standpoint[3]. In that work, the well-posedness of the problem of determining the weighting function from experimental data is shown, and a convergent approximation method is given. It will be seen that the results obtained here using surface fitting techniques are somewhat inconsistent, and support the continued investigation of more rigorous identification techniques.

5.1 SMA Modelling Background

5.1.1 Experimental Apparatus

This section describes the physical configuration of each experimental apparatus used in this research. The single-wire actuator is described in the first section. The second part describes the differential actuator.

One-Wire Actuator

The experiment consists of a 38cm length of 0.3mm diameter NiTi wire, biased by a load of 2kg. This represents a constant stress on the wire of roughly 277 MPa. The wire is routed over a 3cm diameter pulley, with a contact arc length of approximately 90 degrees. The shaft of the pulley drives a 2000 count/revolution optical encoder, for a linear resolution of less than $1/20^{\text{th}}$ of a millimeter. Position data is fed from the optical encoder to a PC-486/50MHz computer, which is also responsible for output of reference signals. Output signals are intentionally saturated, limiting wire current to 1 Amp. Current drive is provided by a voltage-controlled current amplifier, with a transconductance of 1 Amp/Volt.

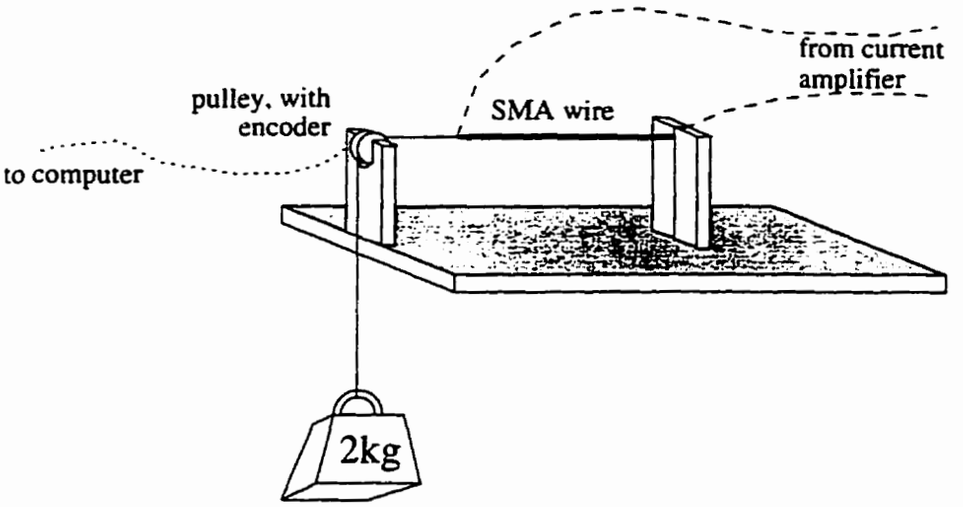

Figure 5.1: One-Wire SMA Actuator

Two-Wire Actuator

The mechanical details of the differential actuator are shown in Figure 5.2 (electrical connections are omitted). The mid-point of a length of SMA wire is anchored at the centre of the 6mm shaft by a set screw. This shaft is equipped with a 2000 count/revolution optical encoder, giving an angular resolution of 0.18 degrees, or less than 10μm change in length of the SMA wire. A total of 35cm of 0.3mm NiTi wire is used to provide two 15cm lengths of active wire. The wires have a common electrical connection at the shaft, and the two "free" ends have electrical lugs crimped over a knot tied in the wire. The lugs provide an electrical connection to the ends of the SMA wire, and also allow the wire ends to be secured to a terminal block. This terminal block is mobile, and can be positioned by means of a screw. The screw is adjusted to give 3% pre-strain in the SMA wire.

The computer hardware is identical to the one-wire case. Bipolar reference signals are used, with two series diodes routing current to one or the other SMA

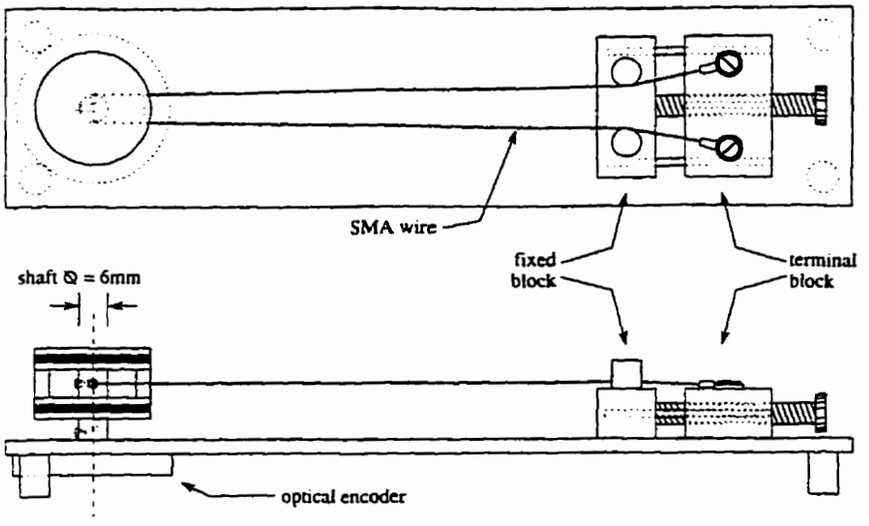

Figure 5.2: Differential SMA Actuator

wire, depending on the sign of the current. The convention adopted in the remainder of this chapter is that negative currents and temperatures refer to one wire, while positive values refer to the other.

In this configuration, each wire individually is subjected to a time-varying stress. As one wire contracts, the opposing wire is stretched, exerting more force on the wire being heated. Generally, this time-varying stress would cause a bi-variate hysteresis behaviour to appear, with the shape of the $T-\varepsilon$ characteristic dependent on the (time-varying) stress. Previous attempts to model this actuator have been put off because of this complexity, in favour of achieving a better understanding of the one-wire actuator first. It had always been assumed that at least a two-input Preisach model would be required for the differential actuator.

In this chapter, it is seen that the single-input Preisach model can represent the hysteresis in the two-wire actuator as well as the one-wire. Discussion of a possible reason for this interesting result is included in the final section of the chapter.

5.1.2 Previous Preisach Modelling

Preisach models have been successfully applied to shape memory alloys in the past. Ortín[49] identified a model for isothermal stress-strain hysteresis in a single crystal of CuZnAl SMA. A very good quantitative match is observed between simulated output from the model and experimental data.

In [30], the author describes a complicated extension of the Preisach model. Four-parameter hysteresis kernels are used, rather than the two-parameter relays of the classical model. Furthermore, it is suggested that the switching values of these operators vary as a function of temperature (the control is stress, in this case) in order to model the bi-variate behaviour. However, a technique for identifying this complex model is lacking, and only qualitative results are obtained.

Probably the most interesting SMA Preisach modelling results, in the context of this work, are those of Hughes & Wen. In their experiments, a shape memory alloy wire is fixed between the hub and tip of a flexible beam. Wire contraction is controlled by Joule-heating, current is the model input, and beam strain the output. In [27], representation testing is carried out, and the results support the application of the Preisach model to this experiment, but only for slowly varying current inputs. In [26] an identification is performed and an attempt is made to fit a polynomial surface to the data, with mixed results. In more recent work[29], Hughes has opted for an interpolation, rather than a surface fitting, strategy. A good match is achieved, but again only for slowly varying currents. A possible reason for this limitation is discussed in the next section.

5.1.3 Modelling Philosophy

It was seen in Chapter 3 that an hysteretic system has a classical Preisach model representation if and only if it displays the wiping out and congruent minor loop properties[43]. In previous Preisach modelling of an SMA actuator, it has been shown that the relationship between control current and wire strain satisfied these two properties for slowly varying inputs[27]. The probable cause of the failure of the classical model to represent the response to rapidly changing currents is minor loop accommodation introduced by the lag in temperature response.

In order to verify this hypothesis. the one-wire actuator described in Section 5.1.1 was subjected to two inputs designed to generate comparable minor loops. Each increases from zero, then varies back and forth between two distinct values, generating five minor loops in the process. The low-frequency input generated a new minor loop approximately every eight minutes, while the higher-frequency current generated a new minor loop every eight seconds. The results are shown in Figure 5.3.

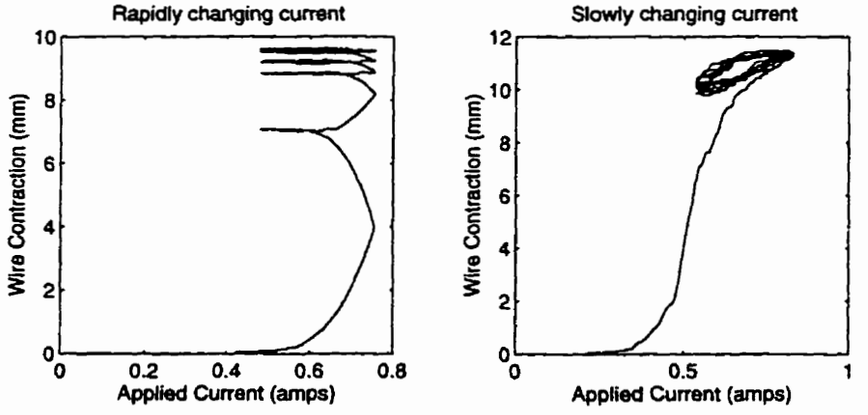

Figure 5.3: Experimental Evidence of Accommodation in SMA

The response to the higher-frequency current (left-hand plot) is problematic in

two ways. After the first input reversal, the wire continues to contract even as the current decreases. This is evidence of the lag between current and temperature, since it implies that the wire temperature is still increasing. As well, minor loop accommodation is clearly seen, as progressive loops shift upwards towards a final stable loop.

Looking at the low-frequency response (right-hand plot), nearly all decreasing input segments generate decreasing outputs. This is an indication that the temperature follows current much more closely. Furthermore, the drift in minor loops is insignificant, compared to that seen in the response to higher frequency current.

Given these results, it is clear that in order to model directly the relationship between current and strain using a Preisach-type model, the Accommodation Preisach model should be applied (cf. Section 3.5). However, this model has a much more complicated form, and the problem of determining the Preisach weighting surface from experimental identification data has not yet been fully addressed.

An alternative approach is to consider the heating behaviour as the driving element for hysteresis occurring between temperature and strain. This is in fact an approach which is truer to the actual physical mechanisms of shape memory, since the phase change occurs as a function of temperature and is independent of the heating method used. The remainder of this chapter is concerned with applying the classical Preisach model form to the temperature-strain characteristic of the SMA actuator.

In modelling the relationship between temperature and strain, it would be ideal to control and measure wire temperature *directly*. One possibility would be to have the wire immersed in a water bath whose temperature could be controlled and measured. In the absence of such a setup, current could be used to slowly heat the

wire, and temperature could be measured.

However, direct temperature measurement of SMA wires is not simple. While several researchers have had some success with thermocouples[25, 37], this is achieved with large wire diameters (1mm in [25]). When smaller diameter wires are used, the thermal mass of the thermocouple bead becomes a factor. The bead acts to partially sink heat away from the wire, lowering the temperature locally. The current carried by the SMA wires further complicates the task, introducing the need for some form of electrically isolating, yet thermally conductive paste between the thermocouple and the wire. In addition, the relatively large currents present in the wire can induce currents in the thermocouple itself, corrupting temperature readings. Aside from thermocouples, some degree of success has been reported using an infra-red sensor based on a pyroelectric detector[53], but this device is not yet refined enough to be useful.

In the absence of an accurate and reliable temperature measurement technique, the temperature must be estimated from a heating model. A lumped-parameter approximation for the relationship between input current, i, and temperature above ambient, T, is shown in equation (5.1). The change in heat energy in the wire is equal to the electrical energy input less the energy lost to the environment through convection. For a more detailed discussion of heat transfer, see [e.g. 35].

$$\rho c_p V \frac{dT}{dt} = Ri(t)^2 - hAT(t) \tag{5.1}$$

The parameters in the heating model are:

- ρ density of the wire material,
- V volume of the wire,
- A surface area of the wire,
- R electrical resistance of the wire,

h heat transfer coefficient to the cooling medium, and

c_p specific heat of the wire material.

A linear transfer function for the heating relationship between i^2 and T may be written

$$H(s) \triangleq \frac{T(s)}{i^2(s)} = \frac{\frac{R}{hA}}{1 + \frac{\rho c_p V}{hA} s}. \tag{5.2}$$

The time constant of this equation is

$$\tau = \frac{\rho c_p V}{hA},$$

and the steady-state value attained for a step current input i is

$$T_{ss} = \lim_{s \to 0} sH(s) \cdot \frac{1}{s} = \frac{R}{hA} i^2. \tag{5.3}$$

It is well known that the physical parameters of equation (5.1) are not constant over the transformation range of an SMA, although this is often assumed[e.g. 39, 41]. While actual parameter values and their variation during the transformation are highly dependent on alloy composition and processing, representative trends can be discerned from [14], an excellent reference for properties of Ni-Ti alloys. In this source, the authors indicate that the volume change during the transformation is small (0.16%). Significant change is noted in c_p and R, however. The specific heat of the martensite phase is lower than that of the austenite phase, and a large peak (approximately 500% of base value) is present at transformation temperatures. This difference in specific heats is consistent with the ready observation that the heating time constant is smaller than that observed on cooling[e.g. 41]. Since specific heat is difficult to measure experimentally, input signals used in the course of this experimental work were restricted to step currents. Position readings were taken only after the measured actuator position had reached a steady-state value. This allows the use of the steady-state relationship (5.3), which doesn't depend on c_p.

In [14], the resistance characteristic for the alloy considered displays only slight hysteresis over the range of temperatures between M_f and A_f. Resistance measurements were taken in the martensite and austenite phases and the average of the two values was used in equation (5.3).

Measurements for the one-wire actuator were $R_M = 5.0\Omega$ and $R_A = 4.5\Omega$, giving an average value of 4.75Ω. Normally, the resistivity of NiTi is higher in the austenite phase than in the martensite phase[14]. However, it is indicated in [16] that NiTi is sometimes doped with Cu (at the expense of Ni) to decrease production cost and reduce the hysteresis. It is noted that one effect of Cu doping, even at low levels, is to flip the resistivity characteristic so that resistance is lower in the austenite phase. This leads to the presumption that the alloy employed contains some Cu. In the shorter-length two-wire actuator, the average resistance value was 2.0Ω.

5.2 Experimental Methods

This section details the experimental methods used during the testing and identification of the SMA actuators.

5.2.1 Data Collection

As mentioned in the previous section, piecewise constant current inputs were used during testing and identification. Each current value was applied until the measured actuator position had reached a steady-state. This position was then associated with the steady-state temperature found from (5.3) to form one point on the input-output graph. Specifically, the procedure was as follows:

1. Choose a desired temperature profile, $T(t)$.

2. Sample $T(t)$ at N evenly spaced points, obtaining $\{T_i\}_{i=1..N}$.

3. Compute the constant currents $\{I_i\}$ from equation (5.3):

$$I_i = \sqrt{\frac{hA}{R}T_i}.$$

4. Apply each current I_i to the actuator in sequence.

5. For each current I_i, wait until the position has been constant for twenty-five seconds, assign the steady-state output value to p_i, and apply I_{i+1}.

6. When the test is complete, join the points (T_i, p_i) by straight line segments to obtain an approximate input-output characteristic. The closer together the points T_i, the better the approximation.

It should be noted that, because of uncertainties and variation in the heating model parameters, all temperatures indicated in this chapter should be considered approximate.

5.2.2 Actuator Initialization

The left graph of Figure 5.4 shows two major loops from the two-wire actuator, each generated using the same temperature profile. The shape of the loops is nearly identical, but there is a significant offset between them. This offset is due to remnant hysteresis in the actuator at the start of the test input. Since a relative encoder is used, outputs generated for identical inputs will be shifted unless the actuator begins in the same location at each trial.

If all trace of remnant hysteresis can be removed before a trial, repeatable results are obtained. In Chapter 3, it was mentioned that it was possible to approximate the anhysteretic state by applying a decaying sinusoid to the actuator. This technique was used on this same actuator in [20]. Here again, in order to remove the remnant hysteresis, the actuator was "initialized" before each test input was applied. This was accomplished by subjecting it to a decaying sinusoidal signal corresponding to a temperature input of

$$\frac{180 - t}{180} \cdot 185 \sin(0.2\pi t).$$

This signal takes three minutes to decay from maximum temperature input to zero, and has only 18 maxima and 18 minima.

The right plot of Figure 5.4 shows one major loop (dashed) superimposed on another (solid), traced during the congruent minor loop test[1]. The actuator was initialized before this test, and it can be seen that the saturation values are symmetric and the match with the major loop is excellent. Initialization of the one-wire actuator was not required, since there is no remnant hysteresis present at room temperature.

5.3 Representation Testing

In this section, each actuator is tested for the presence of the wiping out and congruent minor loop properties. These are the required properties for existence of a Preisach model for the actuators.

[1]The results of the congruent minor loop test are discussed in a later section.

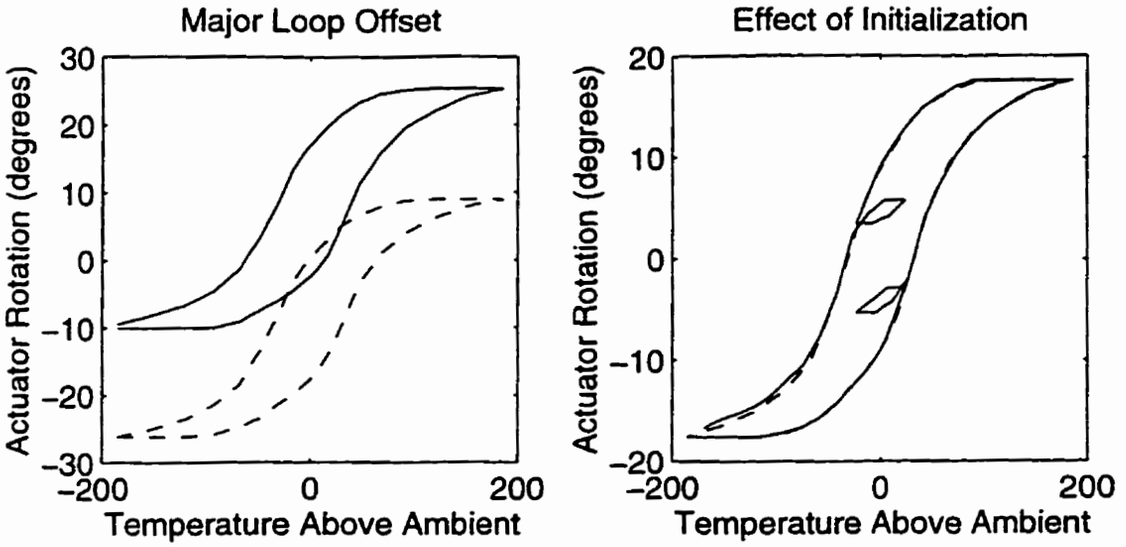

Figure 5.4: Remnant Hysteresis and the Effect of Initialization

5.3.1 Wiping Out Test

The temperature input used to test the wiping out property in the one-wire actuator is shown in Figure 5.5. Each of the two marked segments (A & B) generates four nested branches, as illustrated in the sketch. If the SMA wire displays the wiping out property, the peak at the start of segment B should remove any memory of input up to that point, and the loops traced for input segment B should re-trace exactly those generated by A.

Figure 5.6 shows the actual current input and corresponding measured output. The current plateaus indicate the time taken for the position to stabilize before the next current step was applied (note the time scale). In order to obtain an input-output graph, the steady-state position values for each of the current plateaus was plotted against the corresponding steady-state temperature. These points were then joined by straight line segments. The results, shown in Figure 5.7, show

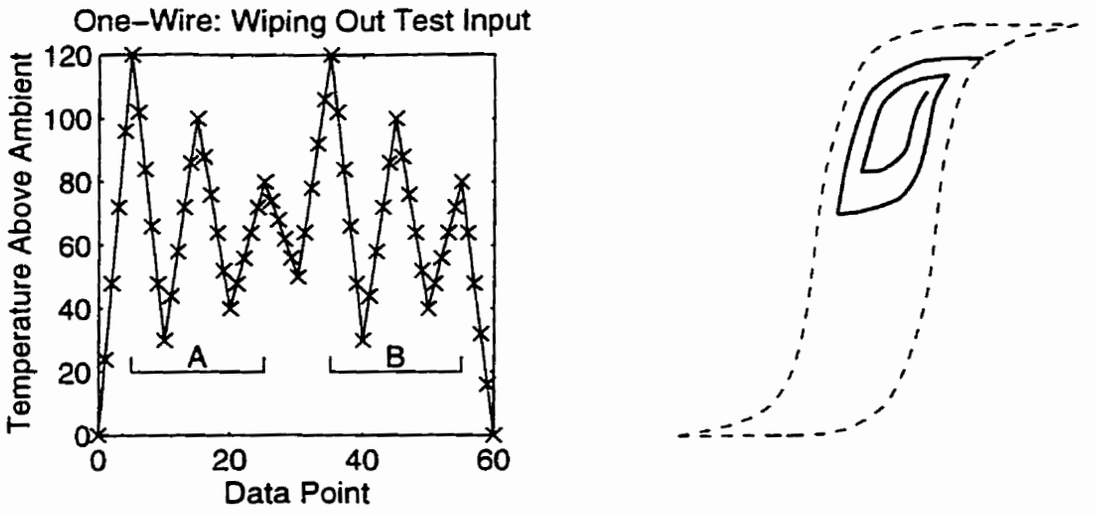

Figure 5.5: Wiping Out Test Input and Nested Branches

strong support for concluding that the temperature-strain characteristic of the SMA actuator does satisfy the wiping out property. On the left, the response is shown up to the end of segment A. The first four nested branches are traced. On the right, the entire response is shown, and the branches traced in response to input segment B coincide with those of segment A.

The analogous graphs for the two-wire actuator are shown in Figure 5.8. It can be seen that they also support the application of the Preisach model.

5.3.2 Congruent Minor Loop Test

The results of the congruent minor loop test of the one-wire actuator are shown in Figure 5.9. The first plot shows the temperature input designed to generate two minor loops which, if the system displays the congruent minor loop property, should have the same shape. The first minor loop is traced by input segment A, while the second is generated by B. The intervening peak has the effect of shifting the second

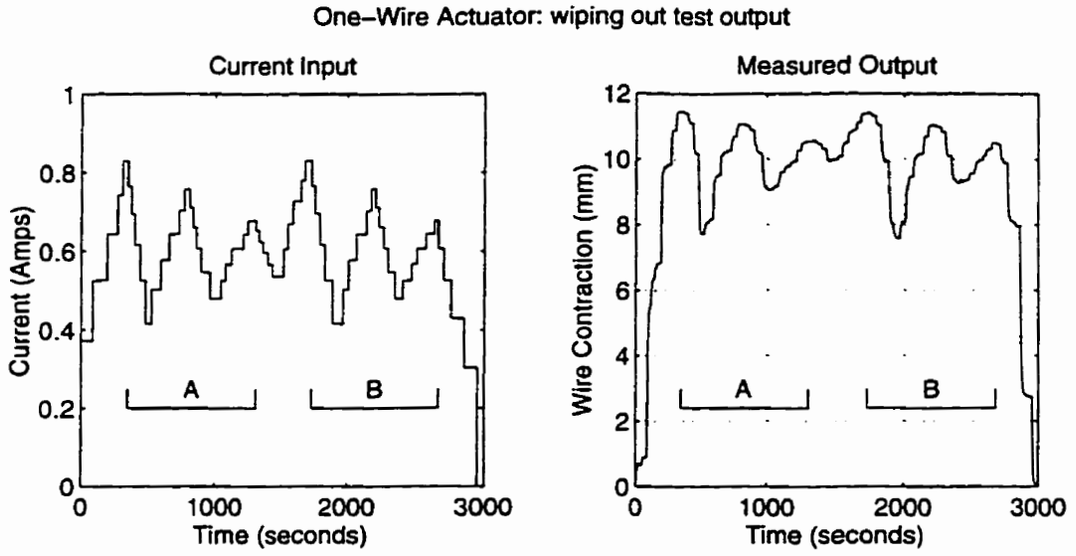

Figure 5.6: One-Wire Wiping Out Test Output

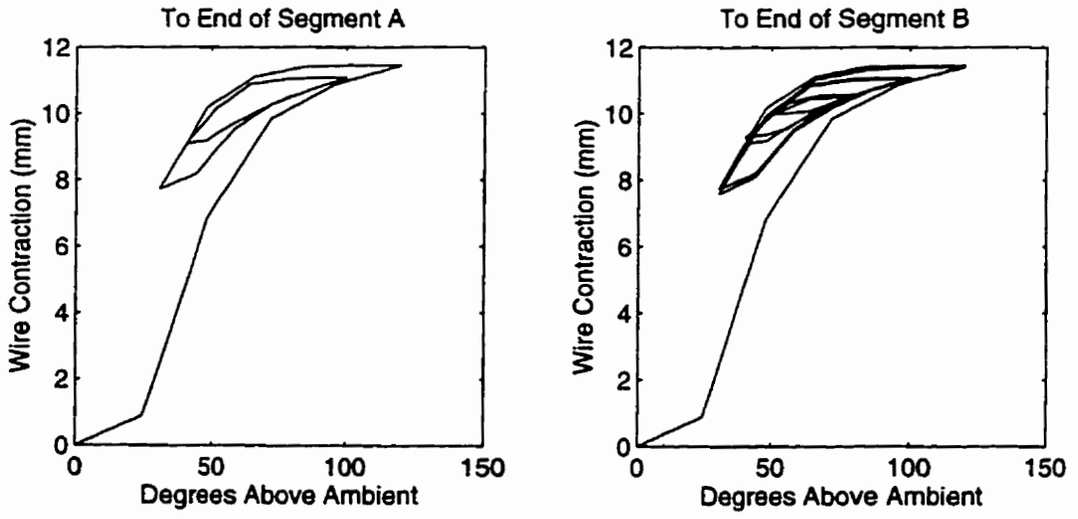

Figure 5.7: One-Wire Wiping Out Test Hysteresis

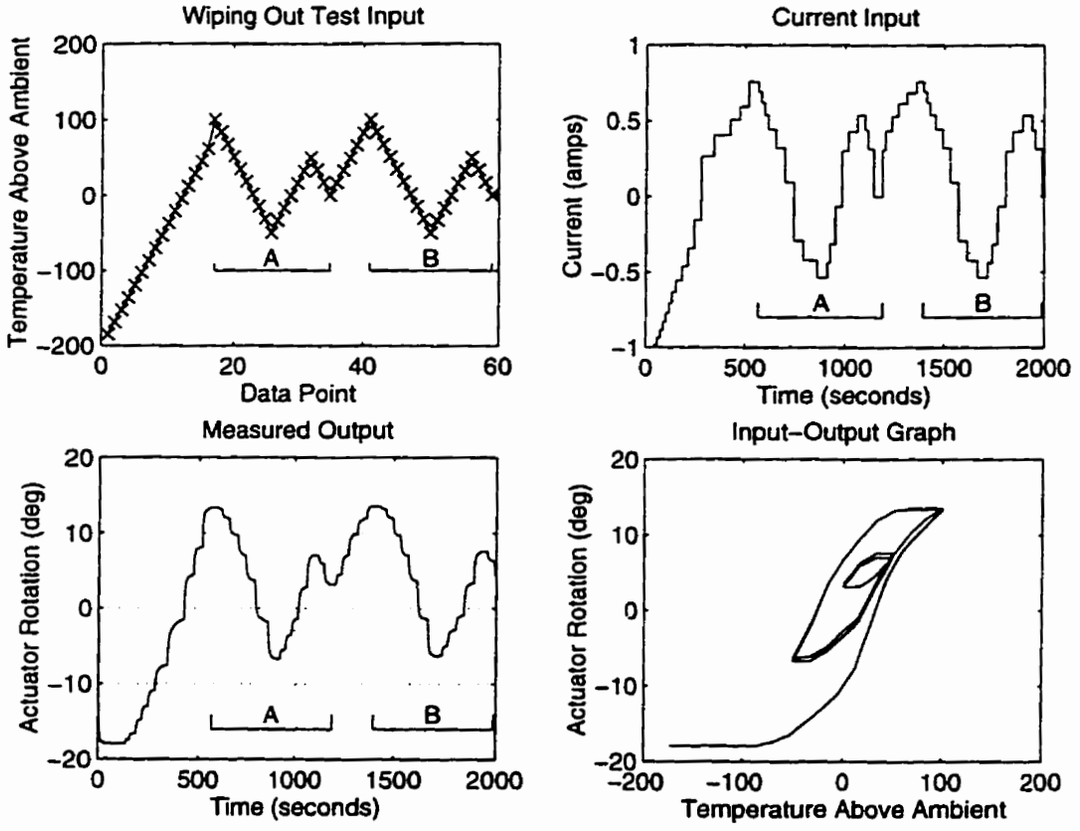

Figure 5.8: Two-Wire Wiping Out Test

loop upwards. The actual current input and measured output are also shown in Figure 5.9. Once again, the plateaus reflect the time required for the position to stabilize. The final plot is the input-output graph, obtained in the same manner as for the wiping out test. The sections of the output corresponding to the two minor loops are shown in different line styles in order to distinguish them from each other and from the major loop. Although the loops are not exactly congruent, their general shapes are similar. The congruency is similar to that which was observed in [27]. Figure 5.10 shows the results of this test for the differential actuator. Better congruency is seen in this case than for the one-wire actuator.

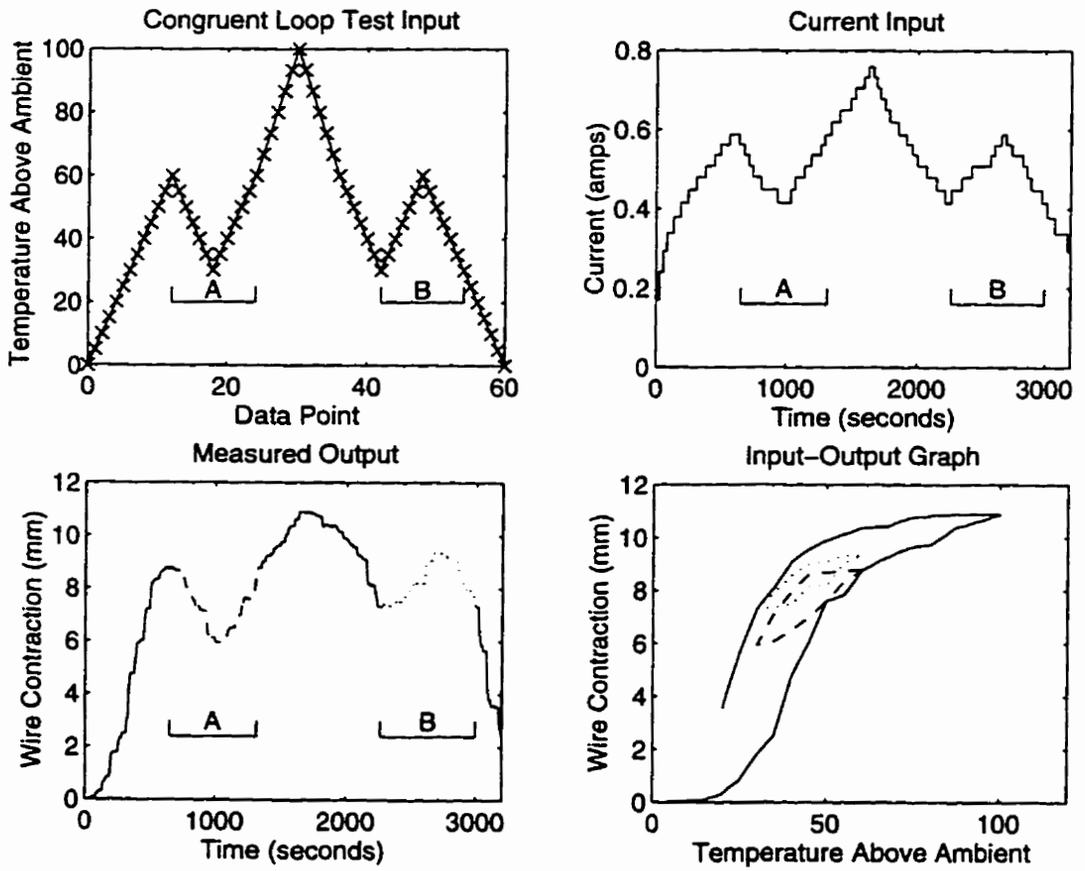

Figure 5.9: One-Wire Congruent Minor Loop Test

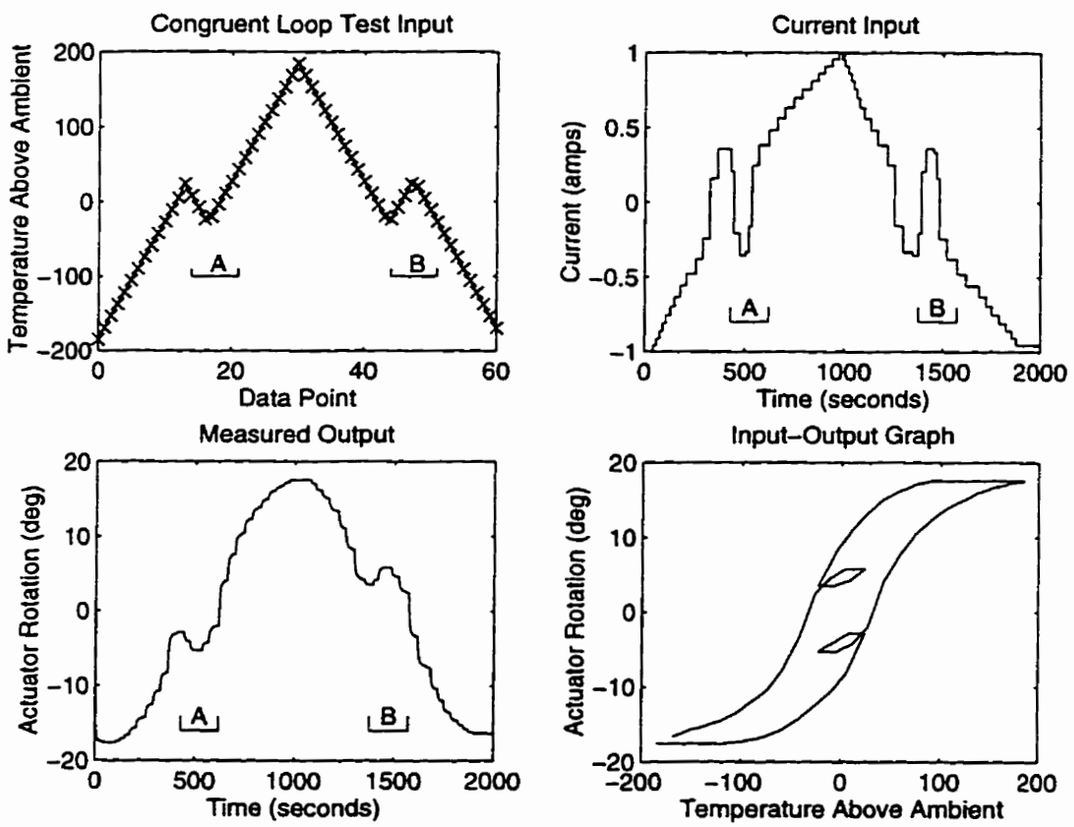

Figure 5.10: Two-Wire Congruent Minor Loop Test

5.4 Model Identification

The model identification section is divided into three subsections. The first subsection presents the experimental identification data. In the second subsection, a surface $\tilde{y}(\alpha, \beta)$ is fit to the identified data. This surface is then differentiated to obtain the approximate weighting function $\tilde{\mu}(\alpha, \beta)$. The results are discussed in the final subsection.

5.4.1 Identification Data

One-Wire Actuator

The range of input currents for the one-wire actuator is $[0, 1]$ Amps. A current of 1 Amp corresponds approximately to a steady-state temperature of 175°C. The temperature input range was divided into the partition

$$\{T_i\} = \{\ 0.0 \quad 1.7 \quad 7.0 \quad 15.7 \quad 27.8 \quad 43.5 \quad 62.7 \quad 85.3 \quad 111.4 \quad 141.0 \quad 174.1\ \}.$$

A temperature sequence, shown in Figure 5.11, was then constructed to generate the nine FOD curves.

The measured outputs of the corresponding FOD curves are shown in Figure 5.12. Data points are joined by line segments to show the general shape of the hysteresis.

Several observations can be made regarding these curves. First, although it is not easily seen from the figure, the FOD curves do not cross within the major loop, even in the bottom "knee". Second, motion is achieved at lower temperatures than expected. Finally, the shape of the curve is somewhat skewed. The last two observations can be partially explained by the use of the average resistance value

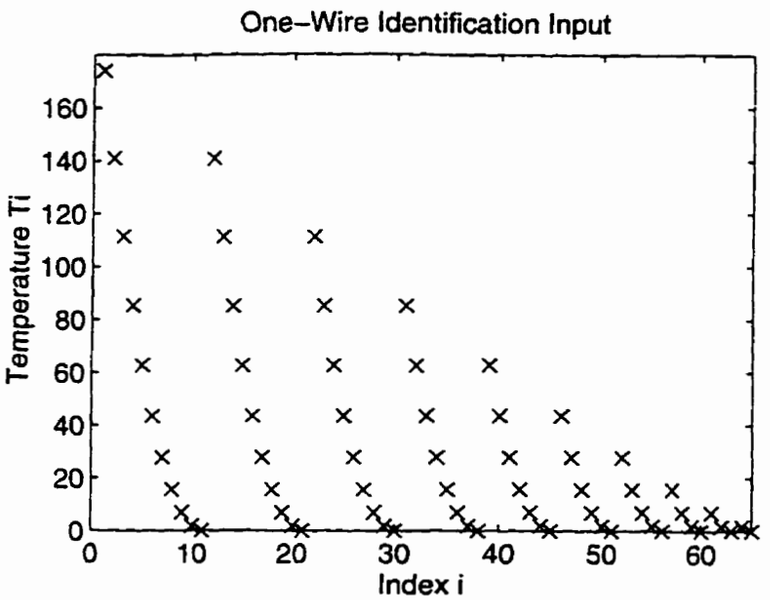

Figure 5.11: One-Wire Identification Input

in computing the temperature axis values. Since the martensite resistance is higher than that measured for austenite, use of the average value tends to widen the top of the hysteresis and narrow the bottom.

Two-Wire Actuator

For the two-wire actuator, the range of input currents is $[-1, 1]$ Amps, corresponding to temperatures of approximately $[-185, 185]$ degrees above ambient. This temperature range was partitioned into

$$\{T_i\} = \{\ -185\ \ -145\ \ -105\ \ -75\ \ -45\ \ -15\ \ 15\ \ 45\ \ 75\ \ 105\ \ 145\ \ 185\ \}$$

and a temperature input sequence similar to that of Figure 5.11 was constructed. This input was applied using the steady-state technique previously described, generating eleven FOD curves. The measured outputs and the corresponding first

order descending curves are shown in Figure 5.13.

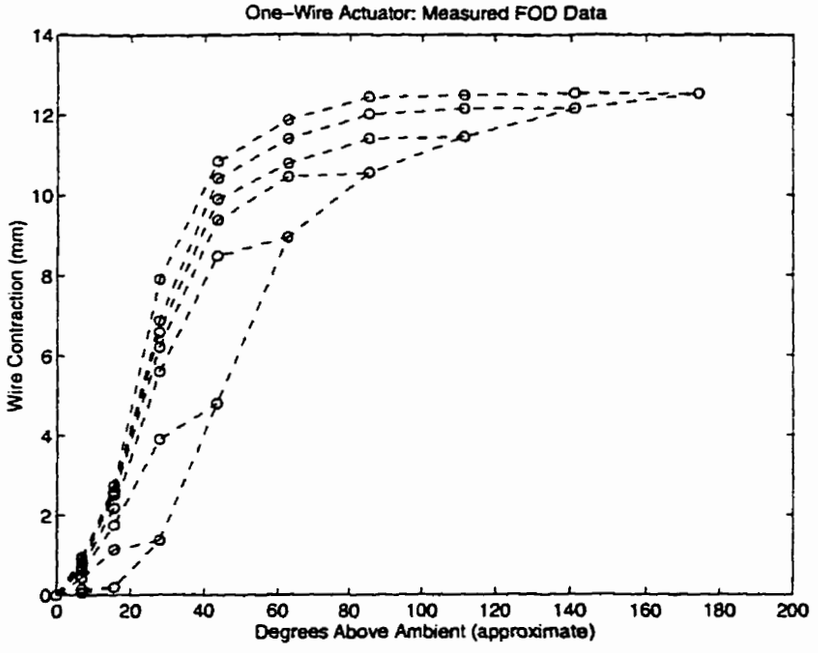

Figure 5.12: One-Wire Measured FOD Data

It is apparent from this data that the actuator was not fully exercised: higher temperatures should have been used. Because of this, the lower end of the FOD curves do not merge. From the angle at which the major ascending branch approaches the upper FOD curve, the upper limit is likely not reaching saturation either. Projecting the curves to the left of the data shows that a temperature range of $[-250, 250]$ may have been more appropriate, although this seems excessively high for NiTi wire.

Figure 5.14 shows three-dimensional plots of the FOD data for the one- and two-wire actuators. In order to determine the weighting functions for these systems, a surface $\tilde{y}(\alpha, \beta)$ is fit to each measured FOD data set, then differentiated to obtain $\tilde{\mu}$.

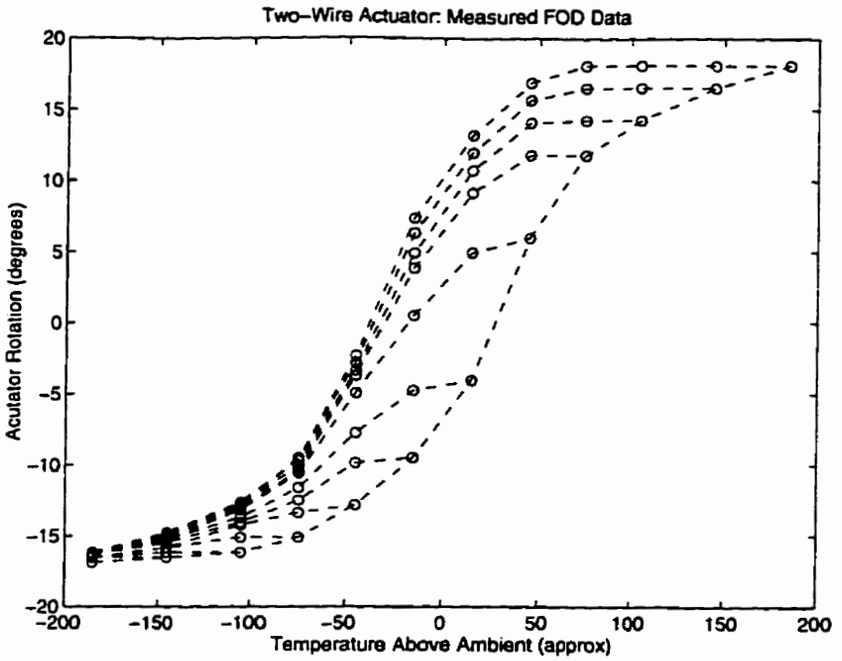

Figure 5.13: Two-Wire Measured FOD Data

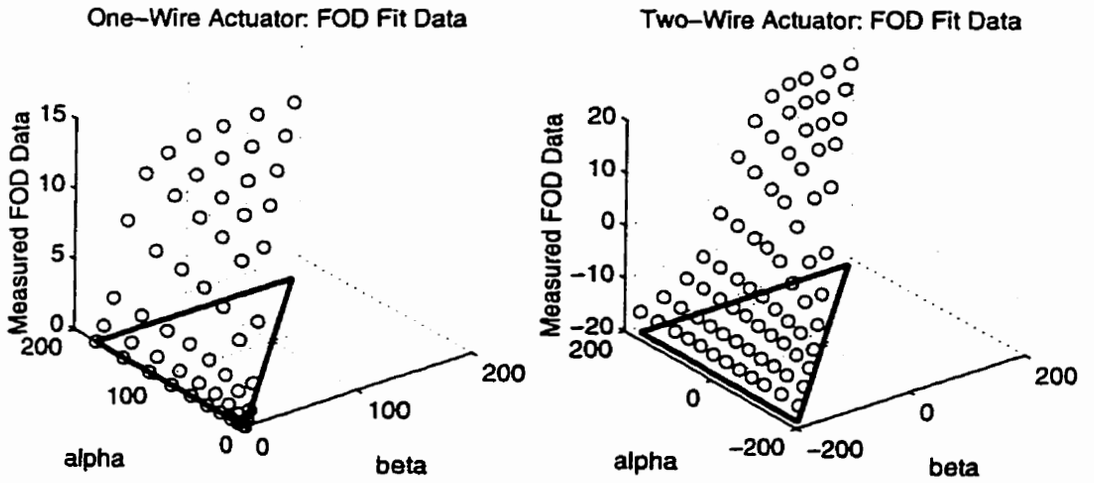

Figure 5.14: Three-dimensional FOD Fit Data

5.4.2 FOD Surface Fit

Previous attempts to fit a polynomial surface to FOD data for SMA have failed[29], mainly because the FOD curves generated by SMA wire have three regions with distinct slopes. Low-order polynomials are unable to properly match this behaviour. While polynomial surfaces of higher order may effectively match the measured data points, they may exhibit highly oscillatory behaviour between points. This conflicts with the smooth behaviour observed experimentally, and has serious implications if the surface is to be differentiated to obtain $\tilde{\mu}$.

While it is unclear what type of three-dimensional surface might best fit the data, experience shows that the individual FOD curves might be well-approximated by an exponential curve. In one of the initial works on modelling of SMA hysteresis[32], two curves of the form

$$y(u) = \frac{x_1}{1 + e^{-x_2(u+x_3)}} \tag{5.4}$$

were used to simulate the major loop of the hysteresis. Equation (5.4) saturates asymptotically at both low and high values of u. The parameter x_1 determines the upper saturation value, while x_2 and x_3 control the slope and point of inflection of the central portion of the curve.

A more recent work[41] used curves of the same form to achieve a good qualitative match of minor loop behaviour as well, by allowing the parameters of the curve to vary as a function of alloy phase. In [2], it has been proposed that the hysteresis relay γ be replaced with two shifted "ridge" functions, similar in behaviour to (5.4).

Curve Fitting

To determine an appropriate form of a candidate three-dimensional surface $\tilde{y}(\alpha,\beta)$, a least-squares fit of the function

$$\tilde{y}_\alpha(\beta) = \frac{b_1}{1+e^{-b_2(\beta+b_3)}} + b_4$$

is performed for each FOD curve (constant α). The offset is added to allow a match of the two-wire FOD curves, which are negative in the lower range of α. A candidate surface is then determined by looking at how the parameters of the resulting family of curves $\tilde{y}_\alpha(\beta)$ vary as a function of α.

A Nelder-Mead simplex algorithm[48], as implemented in the MATLAB `fmins` command, was used to do a least-squares fit. The results are shown in Figure 5.15. A good match is achieved, except for FOD curves with few data points, in which case the simplex algorithm used failed to converge. This is thought to be due to the linearity of the data points on these curves. For the type of curves being fit, this may result in many minima, close together in parameter-space, causing the algorithm to fail to converge.

Candidate Surface

The initial proposed candidate surface, denoted $\tilde{y}'$, is of the form

$$\tilde{y}'(\alpha,\beta) = \tilde{y}_\alpha(\beta) = \frac{b_1(\alpha)}{1+e^{-b_2(\alpha)(\beta+b_3(\alpha))}}.$$

An offset is added to this surface in the next section. The variation of the parameters b_1 to b_3 of $\tilde{y}_\alpha(\beta)$ as a function of α is shown in Figure 5.16.

The function $b_1(\alpha)$ was assumed to be another exponential curve:

$$b_1(\alpha) = \frac{x_1}{[1+e^{-x_2(\alpha+x_3)}]}.$$

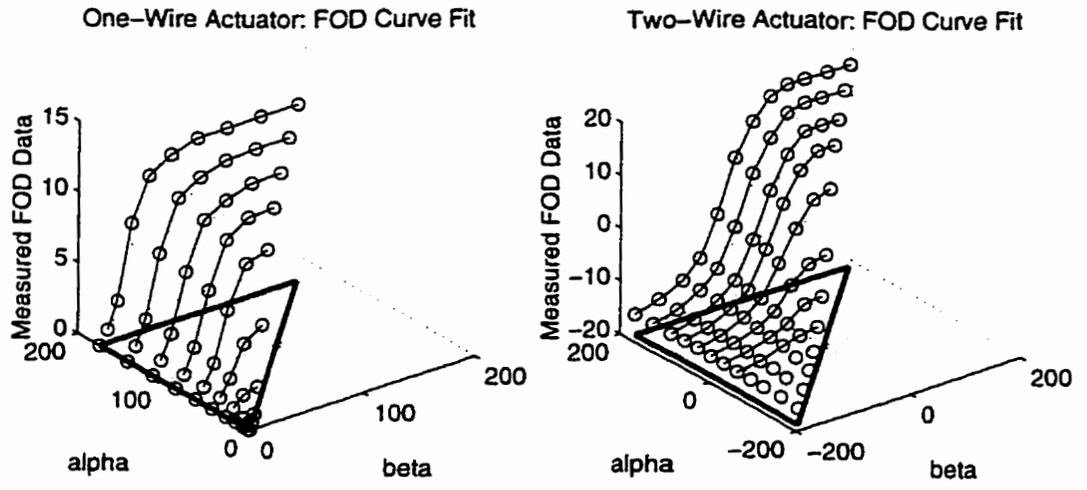

Figure 5.15: FOD Curve Fit

The range of $b_2(\alpha)$ is small, especially in the two-wire case, and nearly constant for most α. The exception is in the one-wire case, where the point $b_2(27.8)$ is approximately double $b_2(\alpha)$ at the rest of the points. In the interest of keeping the number of fit parameters small, it was assumed that $b_2(\alpha) = x_4$. The error in assuming constant b_2 may be mitigated by the fact that the multiplier b_1 is small for low values of α.

Three types of functions were tried for $b_3(\alpha)$: constant, parabolic, and decaying exponential. The form of the surface becomes

$$\tilde{y}'(\alpha,\beta,f) = \frac{x_1}{[1+e^{-x_2(\alpha+x_3)}][1+e^{-x_4(\beta+f(\alpha))}]},$$

with $f(\alpha)$ one of

$$\begin{aligned} f_c(\alpha) &= x_5, \\ f_p(\alpha) &= x_5\alpha^2 + x_6\alpha + x_7, \\ f_e(\alpha) &= x_5 e^{-x_6\alpha} + x_7. \end{aligned}$$

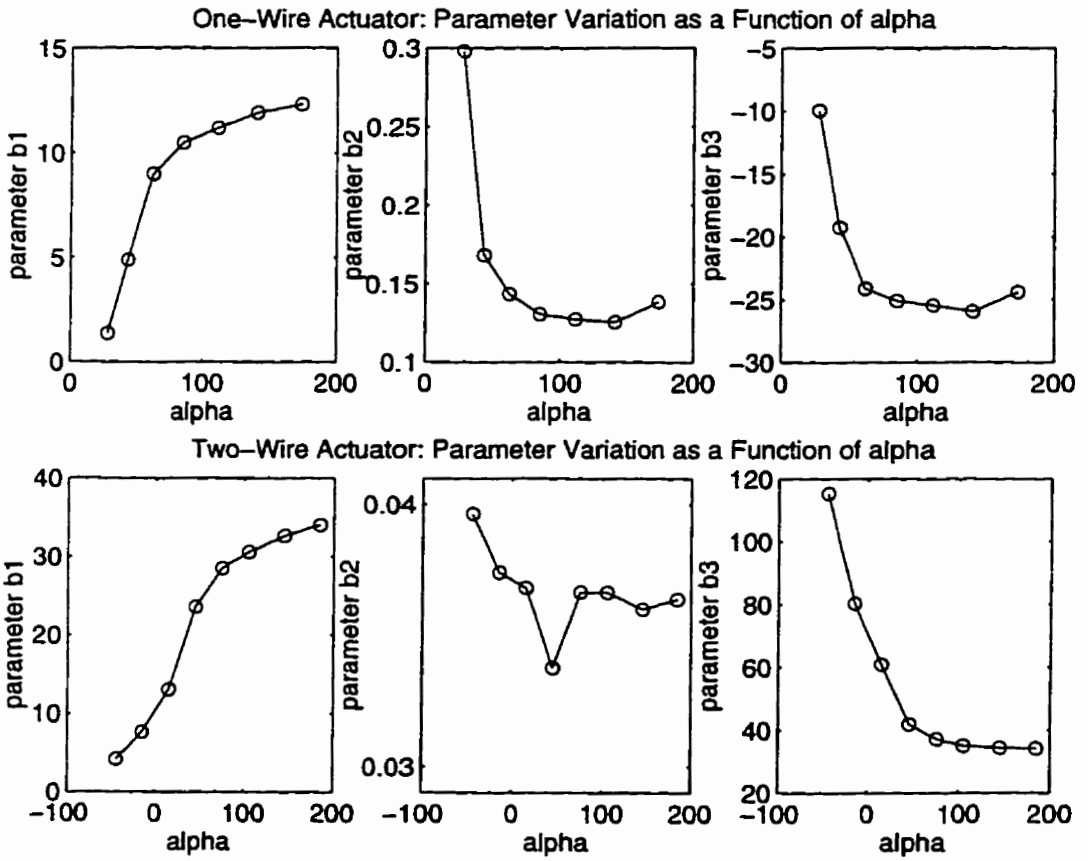

Figure 5.16: Parameter Variation

Before proceeding with the surface fit, the surface $\tilde{y}'$ is modified to obtain the final candidate surface $\tilde{y}$. The following modifications guarantee a perfect match of the model with the experimental output saturation values.

Modified Candidate Surface

Maximum output saturation occurs for increasing input as the input reaches $\overline{u}$, the maximum identification input value. If the input is increased to $\overline{u}$ and then decreased to $\underline{u}$, the minimum identification input value, the major loop is traced. So the minimum output saturation value is $y(\overline{u},\underline{u})$. Since the FOD curves merge at $\underline{u}$, this saturation value is reached on every FOD curve, so that $y(\alpha,\underline{u}) = y(\overline{u},\underline{u})$ for all α. In order to guarantee a match of these saturation values, constraints are imposed on the surface so that $\tilde{y}(\overline{u},\overline{u}) = y(\overline{u},\overline{u})$ and $\tilde{y}(\alpha,\underline{u}) = y(\overline{u},\underline{u})$ for all α. The values $y(\overline{u},\overline{u})$ and $y(\overline{u},\underline{u})$ were measured during the identification process as $y_{\overline{u}}$ and $y_{\overline{u}\underline{u}}$.

The match of the lower output saturation value is easily achieved by adding an offset to the surface:

$$\begin{aligned}\tilde{y}(\alpha,\beta,f) &= \tilde{y}'(\alpha,\beta,f) - \tilde{y}'(\alpha,\underline{u},f) + y(\overline{u},\underline{u}) \\ &= x_1 \cdot \frac{\left[e^{-x_4(\underline{u}+f(\alpha))} - e^{-x_4(\beta+f(\alpha))}\right]}{\left[1+e^{-x_2(\alpha+x_3)}\right]\left[1+e^{-x_4(\beta+f(\alpha))}\right]\left[1+e^{-x_4(\underline{u}+f(\alpha))}\right]} + y(\overline{u},\underline{u}).\end{aligned}$$

In order to match the upper output saturation value, x_1 is removed as a parameter from the minimization, and is instead computed as a function of $y(\overline{u},\overline{u})$, $y(\overline{u},\underline{u})$ and the other parameters x_2, x_3, x_4, and f:

$$x_1 = \left[y(\overline{u},\overline{u}) - y(\overline{u},\underline{u})\right]\frac{\left[1+e^{-x_2(\overline{u}+x_3)}\right]\left[1+e^{-x_4(\overline{u}+f(\overline{u}))}\right]\left[1+e^{-x_4(\underline{u}+f(\overline{u}))}\right]}{\left[e^{-x_4(\underline{u}+f(\overline{u}))} - e^{-x_4(\overline{u}+f(\overline{u}))}\right]}.$$

The final form of the candidate surface was

$$\tilde{y}(\alpha,\beta,f) = [y(\overline{u},\overline{u}) - y(\overline{u},\underline{u})]\frac{[1+e^{-x_2(\overline{u}+x_3)}][1+e^{-x_4(\overline{u}+f(\overline{u}))}]}{[1+e^{-x_2(\alpha+x_3)}][1+e^{-x_4(\beta+f(\alpha))}]} \times \frac{[1+e^{-x_4(\underline{u}+f(\overline{u}))}][e^{-x_4(\underline{u}+f(\alpha))}-e^{-x_4(\beta+f(\alpha))}]}{[1+e^{-x_4(\underline{u}+f(\alpha))}][e^{-x_4(\underline{u}+f(\overline{u}))}-e^{-x_4(\overline{u}+f(\overline{u}))}]} + y(\overline{u},\underline{u}). \quad (5.5)$$

The notation $\tilde{y}_c$, $\tilde{y}_p$ and $\tilde{y}_e$ is used to refer to the surfaces which result when f is chosen to be constant, parabolic, or exponential, respectively. It is easily seen that, for any choice of f, $\tilde{y}(\overline{u},\overline{u}) = y(\overline{u},\overline{u})$ and $\tilde{y}(\alpha,\underline{u}) = y(\overline{u},\underline{u})$.

Surface Fit Results

The measured data values y_α correspond to points on the ascending branch of the major loop, and values $y_{\overline{u}\beta}$ to the descending branch of the major loop. In order to encourage matching of the rest of the major loop, a weighted least-squares error function was used, penalizing errors at points on the major loop by a factor of two compared to errors inside the loop.

The result of this weighted least-squares surface fit for $\tilde{y}_c$, $\tilde{y}_p$ and $\tilde{y}_e$ are shown in Figures 5.17 and 5.18. The measured data points are indicated in the figure, and it is seen that the match is good. As expected, the surfaces match exactly for $\beta = \underline{u}$ and at $(\overline{u},\overline{u})$. The details of the surface parameters are shown in Table 5.1, along with the standard and weighted least-squares error for each surface.

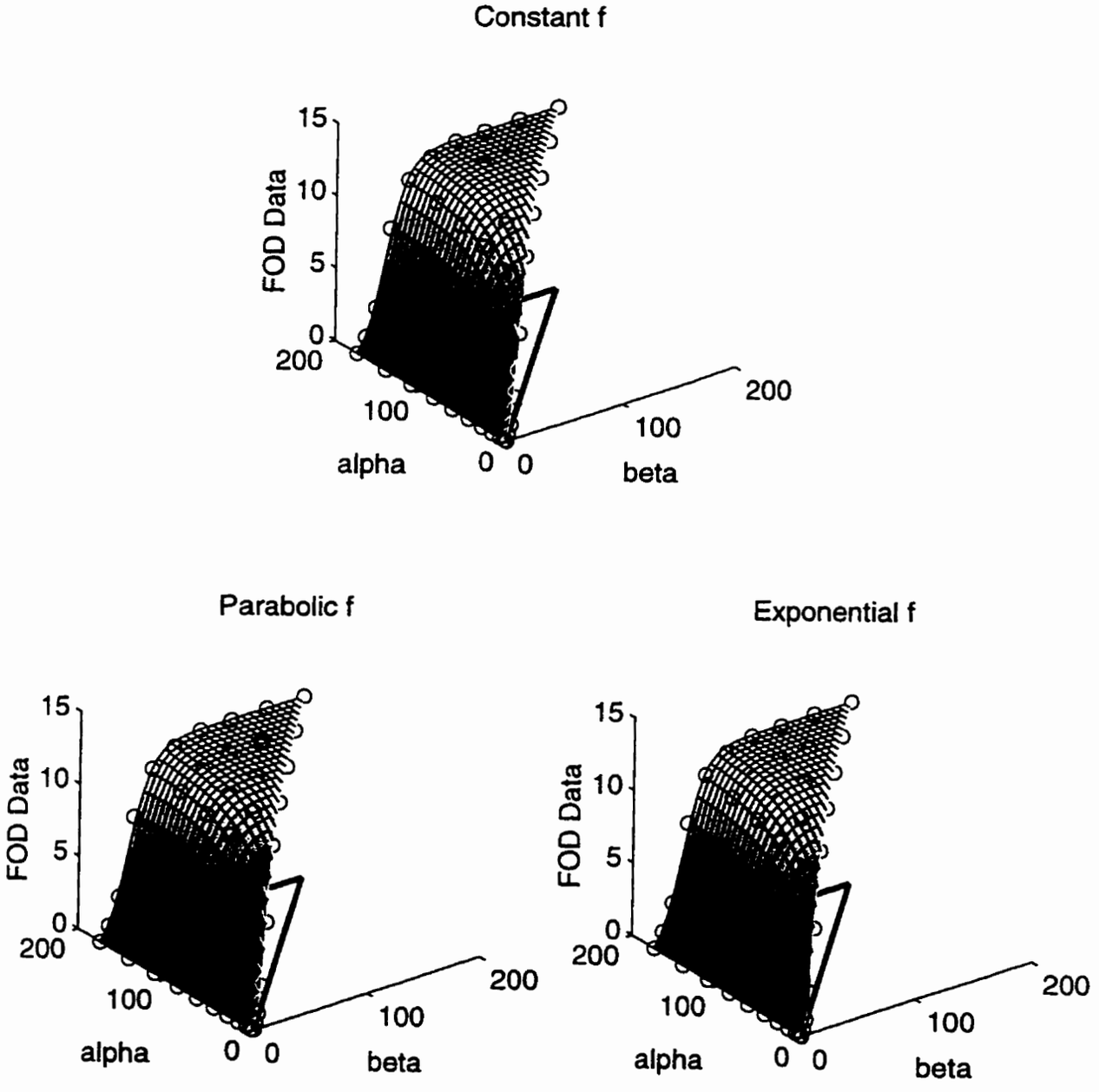

Figure 5.17: One-Wire FOD Surface Fit

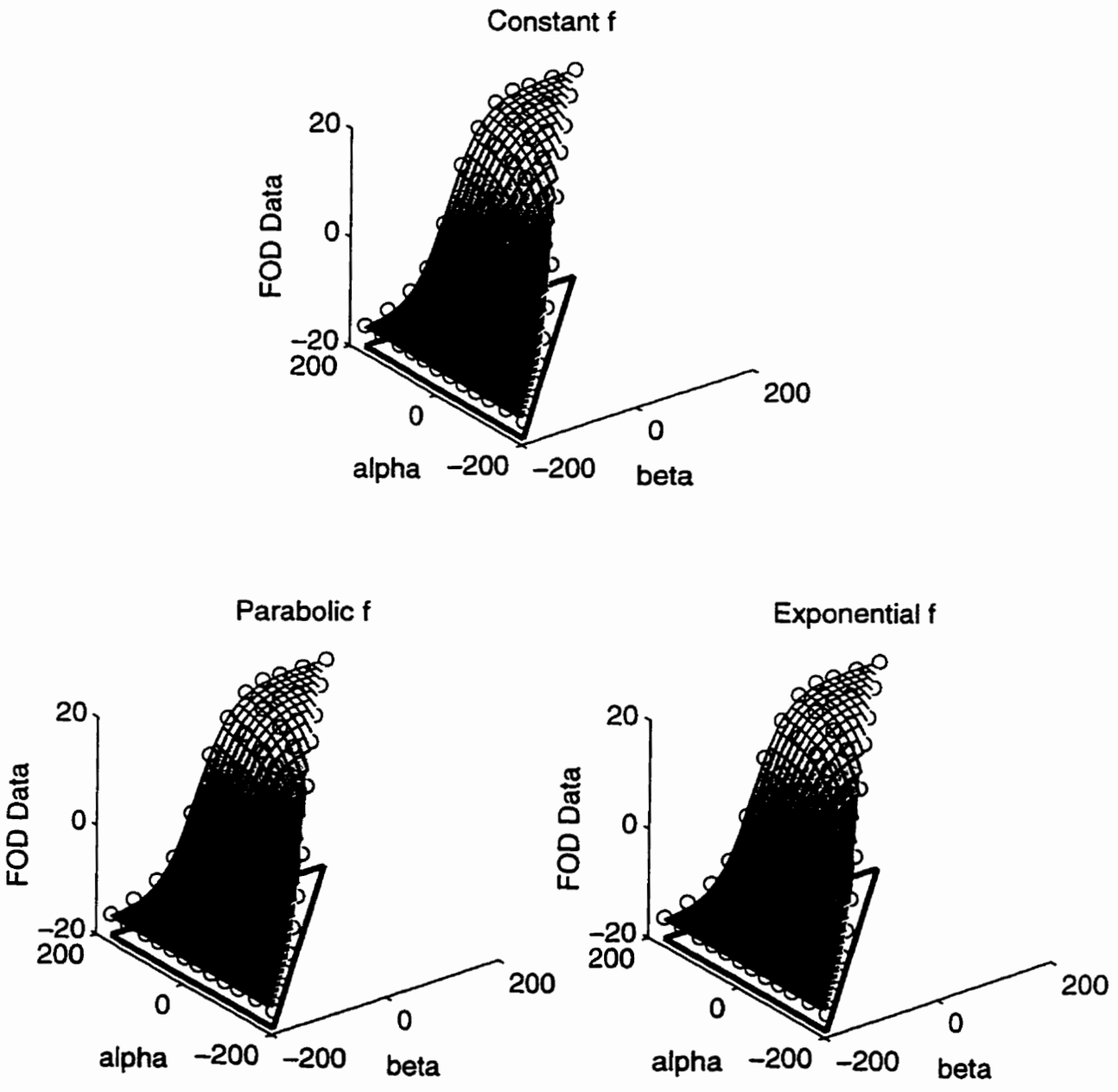

Figure 5.18: Two-Wire FOD Surface Fit

actuator	one-wire			two-wire		
surface	$\tilde{y}_c$	$\tilde{y}_p$	$\tilde{y}_e$	$\tilde{y}_c$	$\tilde{y}_p$	$\tilde{y}_e$
x_2	0.0483	0.0439	0.0394	0.0255	0.0297	0.0293
x_3	-47.2120	-44.1660	-43.0003	-16.7731	-25.0694	-24.2772
x_4	0.1041	0.0996	0.1034	0.0330	0.0344	0.0343
x_5	-23.7060	-0.0010	269.6849	38.4726	0.0017	27.2773
x_6	—	0.2392	0.0765	—	-0.4900	0.0207
x_7	—	-36.3101	-23.6099	—	68.6903	36.0267
$\overline{u}$	174.1	174.1	174.1	185.0	185.0	185.0
$\underline{u}$	0.0	0.0	0.0	-185.0	-185.0	-185.0
$y(\overline{u}, \overline{u})$	12.54	12.54	12.54	18.1055	18.1055	18.1055
$y(\overline{u}, \underline{u})$	0.0	0.0	0.0	-16.5234	-16.5234	-16.5234
weighted error	3.8446	3.5901	3.2668	9.5914	7.3254	7.3415
standard error	2.8149	2.8807	2.3780	7.3717	5.2065	5.2144

Table 5.1: FOD Surface Fit Data

5.4.3 Weighting Surfaces

Differentiating the surface which results from the model identification gives the weighting surface for the one-wire actuator:

$$\tilde{\mu}(\alpha,\beta) = \frac{1}{2}\frac{\partial \tilde{y}(\alpha,\beta,f)}{\partial\alpha\partial\beta}.$$

The surfaces $\tilde{\mu}_c$, $\tilde{\mu}_p$ and $\tilde{\mu}_e$ for the one-wire actuator are shown in Figure 5.19. The two-wire weighting functions are shown in Figure 5.20.

In Chapter 4, several classes of weighting function were defined. It was seen that for those in $\mathcal{M}_P$, the Preisach model was continuous on C^0 and on the Sobolev space W_1^2. It is interesting to determine to which of these classes each of $\tilde{\mu}_c$, $\tilde{\mu}_p$ and $\tilde{\mu}_e$ belong.

Obviously, by the choice of $\tilde{y}(\alpha,\beta)$, each of the weighting functions is continuous and bounded over $\mathcal{P}_r$, so $\tilde{\mu} \in \mathcal{M}_{PC}$. The plots of Figures 5.19 and 5.20 clearly show that $\tilde{\mu}_p$ and $\tilde{\mu}_e$ are not in $\mathcal{M}_P$. For $\tilde{\mu}_c$, $f(\alpha) = x_5$ and, grouping constant terms in (5.5), $\tilde{y}_c$ can be written

$$\tilde{y}_c(\alpha,\beta) = c_1\frac{[e^{-x_4(\underline{u}+x_5)} - e^{-x_4(\beta+x_5)}]}{[1+e^{-x_2(\alpha+x_3)}][1+e^{-x_4(\beta+x_5)}]} + y(\overline{u},\underline{u}),$$

with

$$c_1 = [y(\overline{u},\overline{u}) - y(\overline{u},\underline{u})]\frac{[1+e^{-x_2(\overline{u}+x_3)}][1+e^{-x_4(\overline{u}+f(\overline{u}))}][1+e^{-x_4(\underline{u}+f(\overline{u}))}]}{[1+e^{-x_4(\underline{u}+f(\alpha))}][e^{-x_4(\underline{u}+f(\overline{u}))} - e^{-x_4(\overline{u}+f(\overline{u}))}]}.$$

Since $y(\overline{u},\overline{u}) > y(\overline{u},\underline{u})$ and $\overline{u} > \underline{u}$, $c_1 > 0$. Differentiating to obtain $\tilde{\mu}_c$:

$$\begin{aligned}\tilde{\mu}_c(\alpha,\beta) &= \frac{1}{2}\frac{\partial^2\tilde{y}_c(\alpha,\beta)}{\partial\alpha\partial\beta} \\ &= \frac{c_1}{2}\frac{\partial}{\partial\alpha}\left\{\frac{x_4e^{-x_4(\beta+x_5)}}{[1+e^{-x_2(\alpha+x_3)}][1+e^{-x_4(\beta+x_5)}]} + \frac{x_4e^{-x_4(\beta+x_5)}[e^{-x_4(\underline{u}+x_5)} - e^{-x_4(\beta+x_5)}]}{[1+e^{-x_2(\alpha+x_3)}][1+e^{-x_4(\beta+x_5)}]^2}\right\}\end{aligned}$$

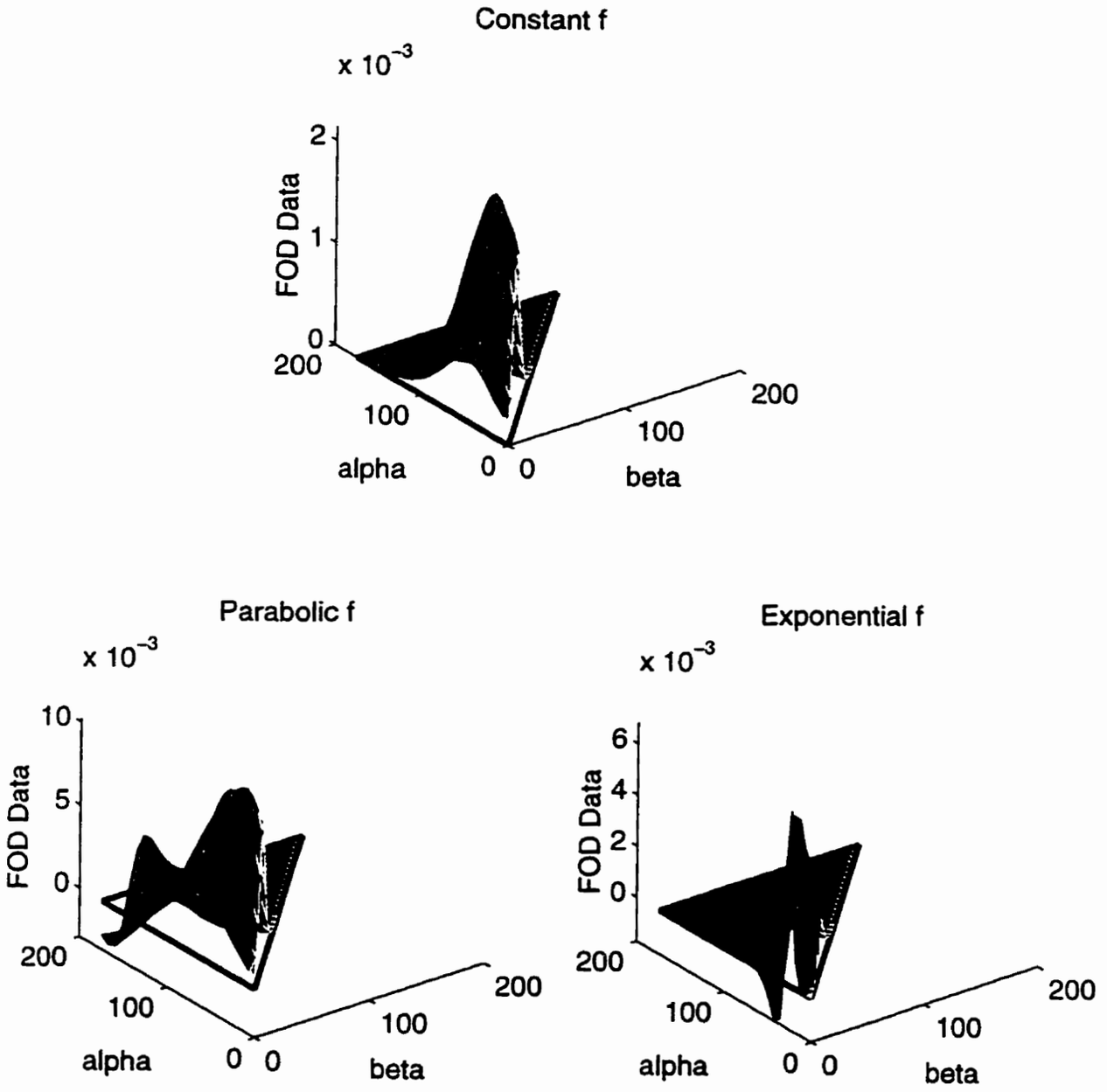

Figure 5.19: One-Wire Identified Weighting Surfaces

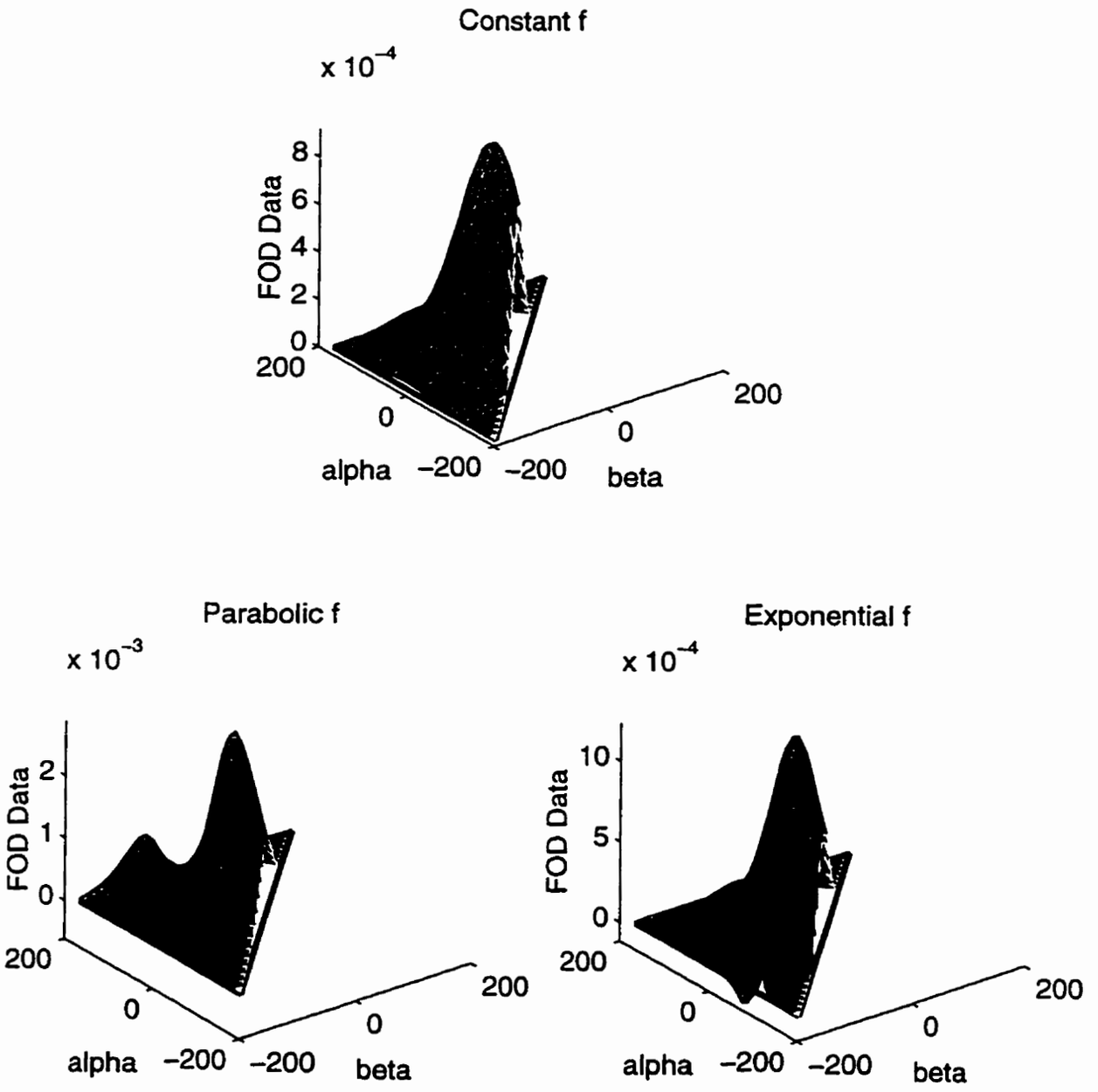

Figure 5.20: Two-Wire Identified Weighting Surfaces

$$= \frac{c_1}{2}\frac{\partial}{\partial\alpha}\left\{\frac{x_4 e^{-x_4(\beta+x_5)}[1+e^{-x_4(\underline{u}+x_5)}]}{[1+e^{-x_2(\alpha+x_3)}][1+e^{-x_4(\beta+x_5)}]^2}\right\}$$
$$= \frac{c_1}{2}\left\{\frac{x_2 x_4 e^{-x_2(\alpha+x_3)}e^{-x_4(\beta+x_5)}[1+e^{-x_4(\underline{u}+x_5)}]}{[1+e^{-x_2(\alpha+x_3)}]^2[1+e^{-x_4(\beta+x_5)}]^2}\right\}.$$

and $\tilde{\mu}_c \geq 0$ for all (α,β) if $x_2 x_4 > 0$. This is the case for both actuators (cf. Table 5.1), so $\tilde{\mu}_c \in \mathcal{M}_P$. Table 5.2 summarizes these results.

surface	$\tilde{\mu}_c$	$\tilde{\mu}_p$	$\tilde{\mu}_e$
$\mu \in \mathcal{M}_{PC}$	Yes	Yes	Yes
$\mu \in \mathcal{M}_P$	Yes	No	No

Table 5.2: Weighting Surface Categorization

5.5 Model Verification

In order to verify the models, the output to the identification input sequence was simulated for each of the derived weighting functions. The results are shown in Figures 5.21 and 5.22. The measured FOD data are plotted in the figure and joined by dashed line segments to represent the experimental hysteresis.

As expected, output saturation values are matched exactly for each curve of the one-wire model output. The two-wire actuator was not fully exercised during identification, so that the measured FOD curves do not merge at $\underline{u}$. In the surface fitting for this actuator, the mean value of the measured $y(\alpha, \underline{u})$ was used as the negative saturation output. It is this mean value (cf. Table 5.1) which is matched by the simulation.

In order to secure a merge of the simulated two-wire FOD curves at $\underline{u}$, the model output is significantly low in the bottom "knee". This demonstrates model inaccuracies which result when the full hysteretic range is not used during identification.

Constant f

For both actuators, the surface $\tilde{y}_c$ had the largest fit error to the measured FOD data. This weighting function also provides the poorest qualitative match of the three. The shape of the upper minor loops is similar to that seen in experiment. The lower minor loops, corresponding to smaller values of α, do not match as well. This is expected, since it is at lower values of α that $b_2(\alpha)$ and $b_3(\alpha)$ deviated most from their assumed constant form. This is particularly true of b_3, since it determines the point of inflection of $\tilde{y}_\alpha(\beta)$. By setting $b_3(\alpha) = x_5$, the points of inflection of the descending curves are constrained to a vertical line in the input-output plane. In the one-wire case this is around 20, and -40 for the two-wire response. These match

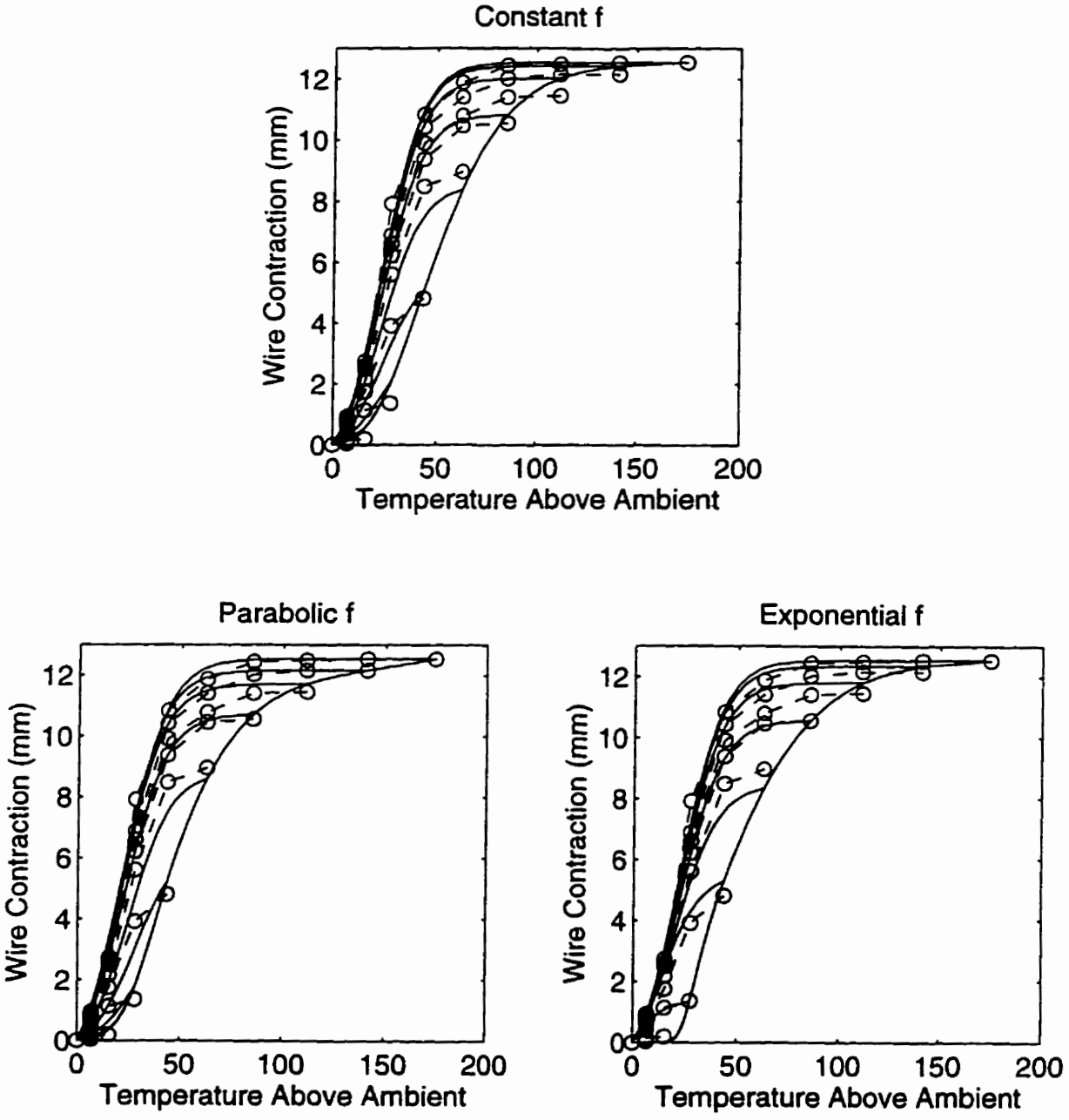

Figure 5.21: One-Wire Simulation Output

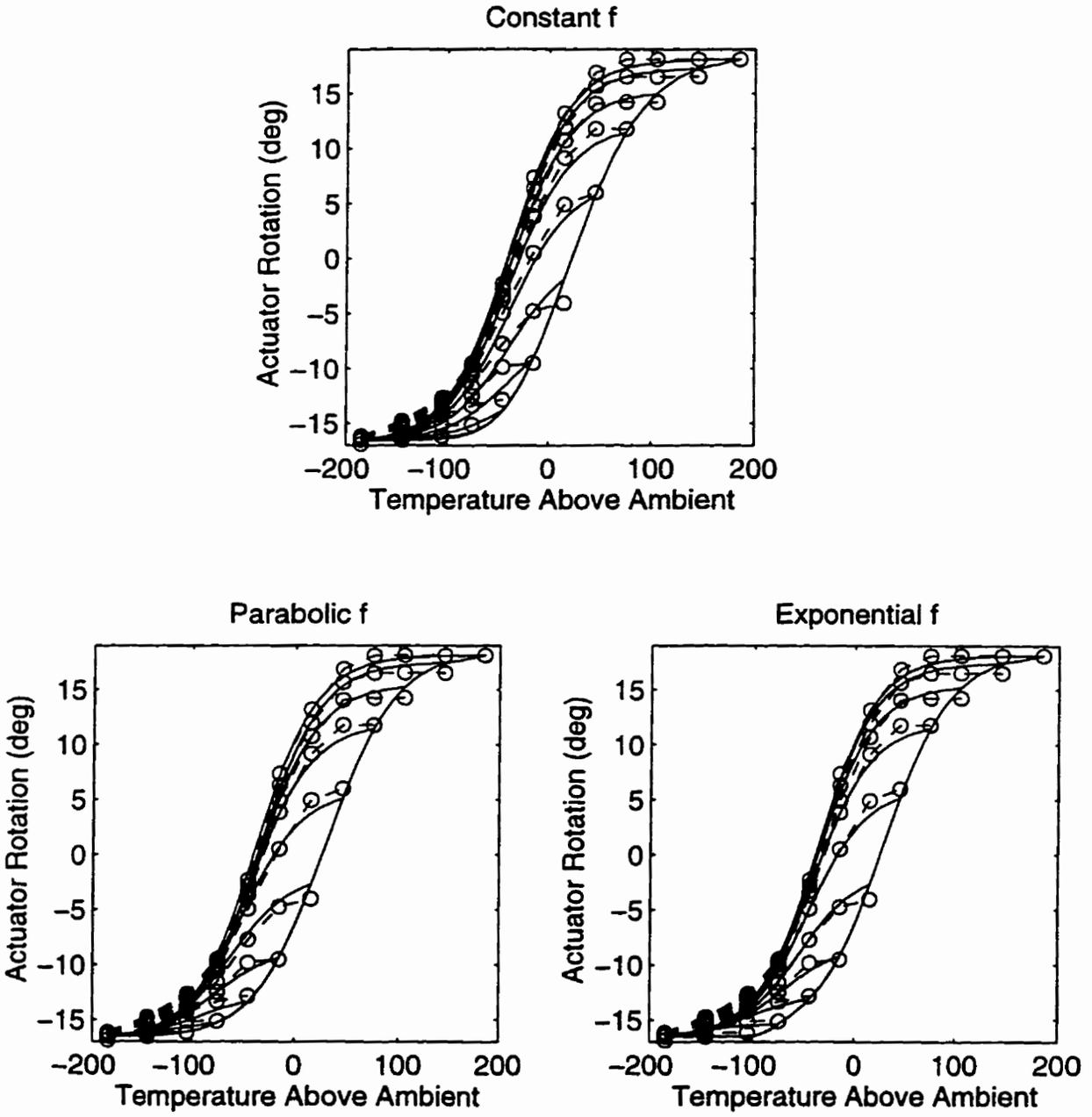

Figure 5.22: Two-Wire Simulation Output

with the values of x_5 for these actuators in Table 5.1. The simulated response of the one-wire actuator also shows some bunching of the descending curves in the upper portions of the hysteresis.

Parabolic f

For the one-wire actuator, the weighted fit error for $\tilde{y}_p$ was better than for $\tilde{y}_c$, but the unweighted error was slightly worse. It is seen in the output for $\tilde{\mu}_p$ that major loop points are better matched than for $\tilde{\mu}_c$, which explains the decrease in weighted error. The upper curves are not as bunched as with $\tilde{\mu}_c$. However, no significant improvement is noted for the lower descending curves.

For the two-wire actuator, the qualitative match using $\tilde{\mu}_p$ was much better than that obtained for $\tilde{\mu}_c$. Notably, an excellent match is achieved for the lower descending curves.

Exponential f

In the case of the one-wire actuator, this surface provided the lowest fit errors, and also the nicest qualitative output. Although the upper curves have bunched up slightly compared to those resulting from $\tilde{\mu}_p$, the reproduction of lower branching behaviour is much better.

For the two-wire actuator, the fit errors were nearly identical for both $\tilde{y}_p$ and $\tilde{y}_e$, and very little difference is seen in the output simulations.

5.5.1 Comments on the Differential Actuator Results

As previously mentioned, the effectiveness of the classical model form in the case of the differential actuator is somewhat surprising. Although the reasons for this unexpected result are not yet entirely clear, this section sketches a possible answer, using an analysis of the stress-strain curves of the wires.

The analysis is done from the perspective of one wire, which is to be heated. This wire will be called the "actuator", while the other is the "load". Figure 5.23 shows the stress-strain curve for the martensite and austenite states of the SMA wire used in the construction of the differential actuator. The values were determined empirically in [40]. Note the characteristic martensite strain plateau, the slope of which is exaggerated here for clarity.

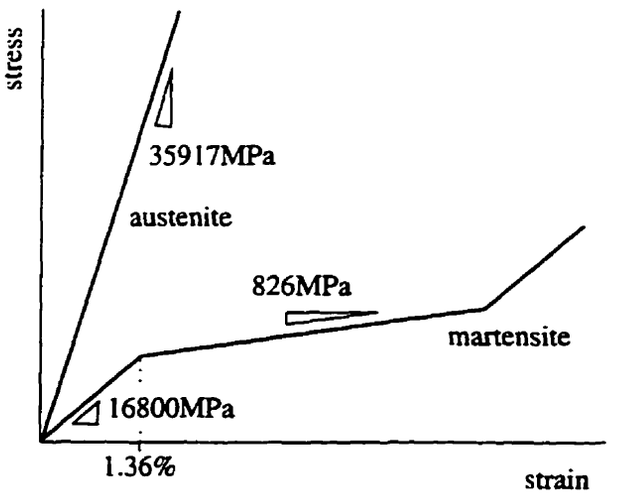

Figure 5.23: Stress-Strain Curves for SMA Wire

In a differential actuator, the wires are mechanically fixed to each other at one end and to the support structure at the other (cf. Figure 5.2). The wires are then pre-strained, to 3% in this particular case. Assuming the support structure

is sufficiently rigid, the total strain in the wire remains constant at 6%. Also, ignoring dynamic effects, the stress in the wires is the same at any point in time. The diagram of Figure 5.24 shows the martensite and austenite characteristics of the actuator wire (solid), with the martensite characteristic of the load wire flipped and overlayed (dashed). Note that for any vertical line, the total strain in the actuator and the load is 6%.

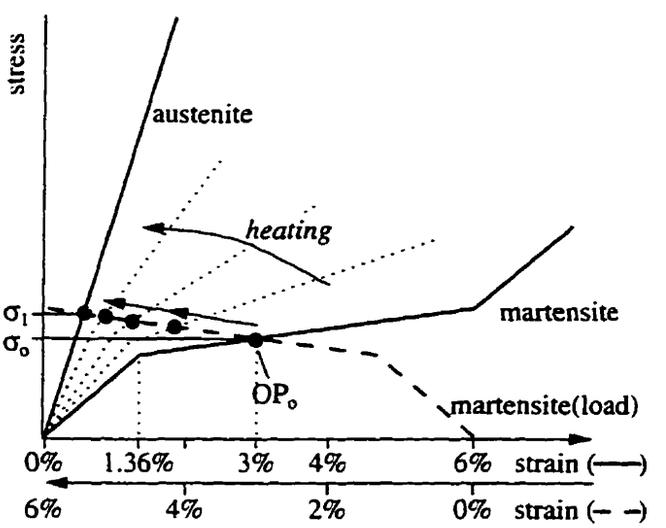

Figure 5.24: Differential Actuator Stress Analysis

Initially, when both wires are cool and in the martensite state, the operating point OP_o is at the intersection of the martensite curves, at 3%. The stress in the system is σ_o. Now, suppose the actuator wire is heated. As it undergoes an internal phase transformation, its stress-strain characteristic changes, shifting towards the straight-line behaviour of full austenite. This is represented by the dotted lines in Figure 5.24. At any point during the transformation, the operating point is at the intersection of the changing actuator characteristic and the load martensite curve. The stress in the wires has increased accordingly.

The change in wire stress during heating, then, is a function of the slope of the martensite plateau for the alloy employed. Assuming that the wires begin cool, both in the martensite state, and one is heated to full austenite, the change in stress can be calculated from the values in Figure 5.23. The initial stress is

$$\begin{aligned} \sigma_o &= 16800(0.0136) + 826(0.03 - 0.0136), \\ &= 242 \text{ MPa} \end{aligned}$$

If ε_a is the final strain in the wire being heated, then the final strain in the load is $(0.06 - \varepsilon_a)$, and the final stress is

$$\begin{aligned} \sigma_1 &= 35917\varepsilon_a \\ &= \sigma_o + 826(0.03 - \varepsilon_a). \end{aligned}$$

Solving this for ε_a gives

$$\begin{aligned} \varepsilon_a &= \frac{\sigma_o + 826(0.03)}{35917 + 826} \\ &= 0.7\%, \end{aligned}$$

and the change in stress upon heating from martensite to austenite:

$$\begin{aligned} \Delta\sigma &= \frac{\sigma_1 - \sigma_o}{\sigma_o} \\ &= \frac{35917(0.007) - 242}{242} \\ &= 7.77\%. \end{aligned}$$

It is hypothesized that this relatively small change in stress, along with the continuous fashion in which it occurs, is at least partially responsible for the ability to represent the behaviour of the actuator with a single-input Preisach model. A more detailed investigation of the reasons behind this observation will hopefully be the subject of future research.

5.6 Summary

In this chapter, identification of Preisach models for two different SMA actuator configurations was considered. It was shown that the actuators satisfy the wiping out property quite well, and that comparable minor loops show a certain degree of congruency. While it theoretically requires an input of infinite length to return a system to the anhysteretic state, it was demonstrated using the two-wire actuator that this could be achieved to satisfaction using a reasonable input.

Preisach weighting surfaces of three different forms were identified for two shape memory alloy actuator configurations. The results differ from existing literature[27] in that exponential surfaces were successfully fit to experimental data. The success of the classical model in representing the differential actuator configuration is intriguing, since actuator motion produces time-varying stresses in the wires. It was shown that the change in stress over the range of motion of the actuator is limited to less than 10%, which may account for this result. Still, further investigation is needed into the mechanisms of this surprising behaviour.

The advantage of surface fitting over interpolation is that the weighting function is known analytically. This is important if the continuity results of Chapter 4 or dissipativity result of Chapter 7 are to be applied. It is only with an analytical expression for μ that the weighting function, and hence model properties, can be understood with full confidence.

In this case, each identified model was characterized in terms of weighting function classes defined in Chapter 4. A positive weighting surface $\tilde{\mu}_c$ was identified for each actuator, which provided a reasonable model match. However, the best match was obtained with $\tilde{\mu}_e$, which was not positive over all of $\mathcal{P}_r$.

It may seem counter-intuitive to think of the Preisach weighting function being

negative-valued. In the energy arguments of Chapter 7, it will be seen that the energy lost in one cycle of a relay is equal to $2\mu(\alpha,\beta)(\alpha-\beta)$. Since $\alpha \geq \beta$, if $\mu(\alpha,\beta) < 0$ does this mean that this relay generates energy? One possible fallacy in this logic is that relays in the Preisach plane cannot be switched in isolation. Rather, they switch in groups along horizontal and vertical line segments corresponding to boundary branches, as these branches sweep through the Preisach plane. Furthermore, it will be seen in Chapter 7 that Preisach weighting functions for magnetostrictive materials must have some negative regions, so this is obviously not precluded in physical systems. This suggests that conditions for the positivity of the Preisach weighting function, and indeed a good understanding of what such positivity implies, would be an appropriate topic for future

investigation.

The fact that three surfaces were identified for each actuator, each having fundamentally different properties in terms of their positivity, suggests the need for a more rigorous identification technique. Recent work has proposed a framework for the estimation of Preisach weighting surfaces in which existence of a unique optimal solution can be shown, and convergent algorithms exist[3]. In the future, this approach to identification may provide a more accurate and robust technique for determination of the weighting function.

Chapter 6

State Space Representation

Chapter 3 discussed the traditional input-output representation of the Preisach model. Non-linear input-output stability theory is largely limited to systems satisfying the conicity and sector conditions proposed by Zames[69]. Some hystereses, such as those found in magnetic materials, do not satisfy these conditions. As a result, the graph of the Preisach model is not, in general, restricted to a sector. Because of this, the input-output stability theory which can be applied to the Preisach model is limited. The current chapter is concerned with developing a state space representation for the Preisach model. By placing the model in a state space framework, non-linear stability techniques such as Lyapunov and dissipativity theory may be applied.

The bulk of this chapter is devoted to defining the state space and the determination of the state transition operator, in the context of Willems' work on dissipative dynamical systems[65]. It will be seen that the nice graphical properties of the Preisach plane can be used by choosing the boundary as the state.

In Section 1, Willems' definition of a dynamical system is recalled. The state

space representation of the Preisach model is developed in Sections 2-4, and properties of the state space are examined in Section 5. This chapter makes use of extensive notation, and tables of nomenclature have been included for reference. They can be found after the summary, in Section 6.6.

6.1 Dynamical Systems

The following definition of a dynamical system is due to Willems, who first introduced the formalism used in the study of dissipative dynamical systems.

Definition 6.1 (Dynamical System [65])
A (continuous stationary) dynamical system Σ *is defined through the sets* U, $\mathcal{U}$, Y, $\mathcal{Y}$, $\mathcal{X}$ *and the maps* ϕ *and* r. *These satisfy the following axioms:*

1. $\mathcal{U}$ *is called the* input space *and consists of a class of* U*-valued functions on* $\mathbb{R}$. *The set* U *is called the set of* input values. *The space* $\mathcal{U}$ *is assumed to be closed under the shift operator* σ_T; *i.e., if* $u \in \mathcal{U}$ *then the function* $\sigma_T u(t) \triangleq u(t+T)$ *also belongs to* $\mathcal{U}$ *for any* $T \in \mathbb{R}$;

2. $\mathcal{Y}$ *is called the* output space *and consists of a class of* Y*-valued functions on* $\mathbb{R}$. *The set* Y *is called the set of* output values. *The space* $\mathcal{Y}$ *is also assumed to be closed under the shift operator;*

3. $\mathcal{X}$ *is an abstract set called the* state space;

4. ϕ *is called the* state transition function *and is a map from* $\mathbb{R}^2 \times \mathcal{X} \times \mathcal{U}$ *into* $\mathcal{X}$. *It obeys the following axioms:*

   (a) *(consistency):* $\phi(t_o, t_o, x_o, u) = x_o$ *for all* $t_o \in \mathbb{R}$, $x_o \in \mathcal{X}$, $u \in \mathcal{U}$;

(b) *(determinism):* $\phi(t_1, t_o, x_o, u_1) = \phi(t_1, t_o, x_o, u_2)$ *for all* $t_o, t_1 \in \mathbb{R}$, $t_1 \geq t_o$, $x_o \in \mathcal{X}$, *and all* $u_1, u_2 \in \mathcal{U}$ *satisfying* $u_1(t) = u_2(t)$ *for all* $t_o \leq t \leq t_1$;

(c) *(semi-group):* $\phi(t_2, t_o, x_o, u) = \phi(t_2, t_1, \phi(t_1, t_o, x_o, u), u)$ *for all* $t_o \leq t_1 \leq t_2$, $x_o \in \mathcal{X}$, $u \in \mathcal{U}$;

(d) *(stationarity):* $\phi(t_1 + T, t_o + T, x_o, \sigma_T u) = \phi(t_1, t_o, x_o, u)$ *for all* $t_o \in \mathbb{R}$, $t_1 \geq t_o$, $T \in \mathbb{R}$, $x_o \in \mathcal{X}$, *and* $u \in \mathcal{U}$;

5. r *is called the* read-out function *and is a map from* $\mathcal{X} \times U$ *into* Y;

6. *the* Y*-valued function* $r(\phi(t, t_o, x_o, u), u(t))$ *defined for* $t \geq t_o$ *is, for all* $x_o \in \mathcal{X}$, $t_o \in \mathbb{R}$, $u \in \mathcal{U}$, *the restriction to* $[t_o, \infty)$ *of a function* $y \in \mathcal{Y}$. *This means that there exists an element* $y \in \mathcal{Y}$ *such that* $y(t) = r(\phi(t, t_o, x_o, u), u(t))$ *for* $t \geq t_o$.

Willems points out: "It should be emphasized that the read-out function is required to be a memory-less map in the sense that the output only depends on the *present* value of the state and the input. All dynamical effects (*i.e.*, those phenomena involving memory) are required to be taken care of by the state."

Although the dynamical system framework is used to establish the state-space representation for the Preisach model, the reader is reminded that the model is, in fact, static. That is, the behaviour depends only on input extrema, and the order in which they occur. As a result, it will turn out in much of what follows that time is rather arbitrary. This will be true for any representation of the Preisach model in isolation.

The following sections set out a state space framework for the Preisach model. First, the input, output, and state spaces are defined. An intermediate space $\mathcal{S}$, which will be used in the construction of the state transition operator, is then

introduced, and mappings between the spaces $\mathcal{U}$, $\mathcal{S}$ and $\mathcal{B}$ are defined. Finally, the state transition function ϕ and read-out function r are defined, and it is shown that both functions satisfy the axioms of Definition 6.1.

6.2 System Spaces

6.2.1 The Input Space

Let C^0 denote the space of real-valued continuous functions defined on the bi-infinite real line. The input space $\mathcal{U}$ is defined, for some system-dependent $\hat{u} > 0$, as

$$\mathcal{U} \triangleq \{u \in C^0 \,|\, |u(t)| \leq \hat{u} \ \forall t \text{ and } \lim_{t \to -\infty} u(t) = 0\}.$$

$\mathcal{U}$ is obviously closed under the shift operator. For any interval $[t_0, t_1]$ in $\mathbf{R}$, the notation $u_{[t_0,t_1]}$ denotes the restriction of u to $[t_0, t_1]$. The notation $\mathcal{U}[t_0, t_1]$ denotes the set obtained when every element of $\mathcal{U}$ is restricted to $[t_0, t_1]$.

The input restriction $|u(t)| \leq \hat{u}$ allows the Preisach plane to be bounded, as in Chapter 3, and arises naturally in systems where input signals are subject to saturation. In the context of previous chapters, $\hat{u} = \max\{|u_-^{sat}|, |u_+^{sat}|\}$.

Recall that at any time t, the point in $\mathcal{P}_r$ where the boundary intersects the line $\alpha = \beta$ is $(u(t), u(t))$. The initial boundary B^*, at $t = -\infty$, is assumed to be the line $\alpha = -\beta$, which intersects $\alpha = \beta$ at $(0, 0)$. Since the Preisach model is not defined for piecewise continuous inputs, the limitation

$$\lim_{t \to -\infty} u(t) = 0$$

is required to preserve the continuity of the input at this initial condition.

6.2.2 The Output Space

The output space $\mathcal{Y} \subset C^0$, $Y = \mathbf{R}$, and $\mathcal{Y}$ is also closed under the shift operator.

6.2.3 The State Space

In defining the state of the Preisach model it seems logical to look to the Preisach plane, since that is where the memory of the model is "stored". There are a number of possible choices for the state space. For instance:

- the set of all possible configurations of the continuum of relays in $\mathcal{P}$;
- the set of all boundaries which separate the above relay configurations;
- the set of all alternating sequences of extrema which generate those boundaries.

Each of these choices stores the complete memory of the system, as required by the dynamical systems formalism. In fact, they are equivalent in that each can be generated from the other. However, the choice of the boundary as the state results in a nice graphical interpretation of state dynamics.

In characterizing the set of all boundaries, it is useful to recall some of the key boundary features from Chapter 3. It was seen that Preisach boundaries are non-increasing "staircase" graphs in $\mathcal{P}$, composed of horizontal and vertical segments, with possibly one diagonal segment corresponding to the initial condition. As in Chapter 3, the input restriction $u(t) \in [-\hat{u}, \hat{u}]$ further limits boundaries to those contained in the triangle $\mathcal{P}_r \subset \mathcal{P}$ defined by $\mathcal{P}_r \triangleq \{(\alpha, \beta) \in \mathcal{P} | -\hat{u} \leq \beta \leq \alpha \leq \hat{u}\}$. The assumption that the initial boundary is $\alpha = -\beta$, along with this input restriction, means that all boundaries contain the point $(-\hat{u}, \hat{u})$. The following definition characterizes the state space in terms of these properties.

Definition 6.2 (The State Space)

The state space $\mathcal{B}$ is defined to be the set of (possibly multivalued) continuous graphs B in $\mathbb{R}^2$ whose points $(\beta, B(\beta))$ satisfy the following properties (for all values of $B(\beta)$):

($BP1$) *bounded input restriction:* $-\hat{u} \leq \beta \leq B(\beta) \leq \hat{u}$;

($BP2$) *initial condition:* $B(-\hat{u}) = \hat{u}$;

($BP3$) *non-increasing:* $B(\beta_2) \leq B(\beta_1), \quad \forall \beta_2 > \beta_1$.

This definition encompasses all the characteristics of Preisach plane boundaries, and fits Willems' definition of a state space. In addition, it purposefully includes curves which are bounded and non-increasing, but not necessarily made up of horizontal or vertical line segments. The inclusion of these elements completes the space, as will be seen in Section 6.5.4.

Note that ($BP2$) implies that every boundary contains the point $(-\hat{u}, \hat{u})$. There is a subtlety which arises as a result of this, which is illustrated in Figure 6.1. The boundary on the left is not a member of $\mathcal{B}$, since it does not include $(-\hat{u}, \hat{u})$; the boundary on the right does, and is an acceptable state. While the two are equivalent in terms of the resulting output, the inclusion of the point $(-\hat{u}, \hat{u})$ will facilitate the mathematical details of Section 6.5.

Zero Element

It seems logical in choosing a zero element in $\mathcal{B}$ to be guided by the idea of minimum energy. In discussing energy storage in the Preisach model in Chapter 7, it will be seen that there is no *unique* state of minimum stored energy. However, in the

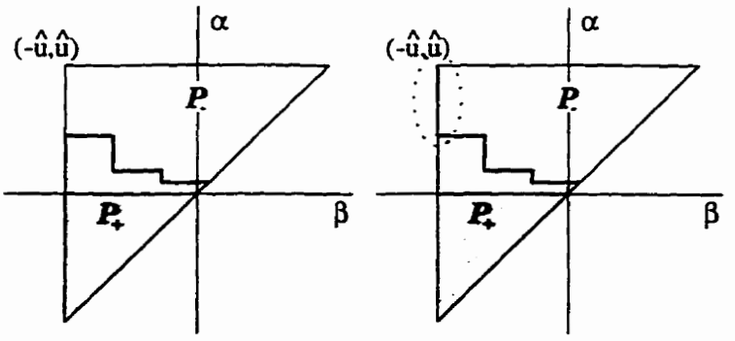

Figure 6.1: Effect of the Initial Condition on the State

anhysteretic state, no remnant hysteresis is present in the system, and zero input gives zero output. It will be seen in Chapter 7 that this is in fact a state of zero stored energy. Since it is also assumed to be the initial state of the system, it is logical to choose this as the zero state, denoted

$$B^* \triangleq \{(\alpha, \beta) \in \mathcal{P}_r | \alpha = -\beta\}.$$

6.2.4 Reachability

In control theory, the success of a control problem often relies in part on the ability of the controller to move the system to a desired state by applying an input. This concept is known as reachability.

Definition 6.3 (Reachability)

A system Σ is said to be "reachable from x_o" if for every $x \in \mathcal{X}$ there exists a time $t < \infty$ and an admissible input $u \in \mathcal{U}(t_o, t]$ such that $\phi(t_o + t, t_o, x_o, u) = x$. If Σ is reachable from every $x_o \in \mathcal{X}$, it is said to be "reachable".

As the input to the Preisach model evolves, it generates boundaries composed only of alternating horizontal and vertical segments, plus a segment of the line $\alpha =$

$-\beta$ if any memory of the initial condition remains. One such boundary is illustrated in Figure 6.2. However, boundaries in $\mathcal{B}$ may contain segments of *arbitrary* negative slope. For finite time T, there is no input in $\mathcal{U}(-\infty, T]$ which can generate such a segment *exactly*, so the entire state space $\mathcal{B}$ is not reachable.

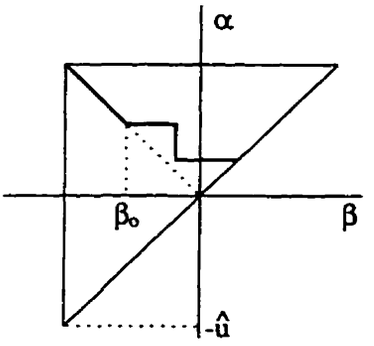

Figure 6.2: Example of a Reachable Boundary

The reachable subspace of $\mathcal{B}$ can be defined as follows. For $n \geq 0$, denote by $\mathcal{B}^n$ the set of all boundaries $B \in \mathcal{B}$ for which there exists a real number $\beta_o \in [-\hat{u}, 0]$ such that $B(\beta) = -\beta$ for all $\beta \leq \beta_o$ (segment of slope -1), and which consist of n connected alternating horizontal and vertical segments for $\beta > \beta_o$. For example, the boundary of Figure 6.2 is an element of $\mathcal{B}^3$. Note also that $\mathcal{B}^0 = B^*$. Any $B \in \mathcal{B}^n$ can be reached from B^* by an input having n input reversals over $(-\infty, T]$, for any $T < \infty$. Then the subspace of boundaries which is reachable from B^* is

$$\mathcal{B}_r \triangleq \bigcup_{n<\infty} \mathcal{B}^n,$$

the set of all "staircase" boundaries with a finite number of "stairs". The reachability properties of $\mathcal{B}$ will be further discussed in Section 6.5.2.

6.3 Reduced Memory Sequences

In this section, the intermediate space $\mathcal{S}$ of *reduced memory sequences* is introduced, along with mappings between $\mathcal{S}$ and the input and state spaces. These mappings will be used in the next section to construct the state transition operator.

6.3.1 Memory Sequences

Branching in static hystereses occurs whenever the input switches direction, at input extrema. In general, the output of a static hysteresis is dependent at any particular time on the current input value as well as the values of all past input extrema. A hysteresis "remembers" the effect of these past input extrema, and the set of previous extrema form a *memory sequence*[64]. The wiping out property of the Preisach model implies that the dependence of the output on previous input extrema is restricted to a particular subset of the memory sequence. This subset is referred to by Mayergoyz as the set of *dominant input extrema*[43], and by Visintin[64] as the *reduced memory sequence*. The terminology of Visintin is adopted here.

The wiping out property was described in Chapter 3. In essence, any input maximum which exceeds previous maxima will wipe out the memory of those maxima, and minima can be similarly "wiped out". At a given time t, only certain past extrema are retained and affect the output. They form an alternating set of input maxima and minima, in which each maximum is smaller in amplitude than the previous one, and each minimum is larger than the previous one, until the two series converge at $u(t)$. Since the boundary corners are defined by these extrema, this results in the characteristic "staircase" appearance of the boundaries.

Examples of the construction of the reduced memory sequence associated with

an input can be found in [e.g. 43, 64]. The following construction is based on that of [64].

For any input $u \in \mathcal{U}(-\infty, T]$ and any $\tau \leq T$, set $s_0 = 0$ and $\eta = \max_{t\in(-\infty,\tau]} |u(t)|$. This is well-defined, since $\lim_{t\to-\infty} u(t) = 0$. Let $t_1 = \max\{t \in (-\infty, \tau] \,|\, |u(t)| = \eta\}$, and define the elements s_i (i=1, 2, ...) of the reduced memory sequence $s(u, \tau)$ as follows:

$$\begin{aligned} i = 1: &\quad s_1 = u(t_1), \\ s_{i-1} < s_{i-2}: &\quad s_i = \max_{t\in(t_{i-1},\tau]} u(t), \quad \text{and} \quad t_i = \max\{t \in (t_{i-1}, \tau] | u(t) = s_i\}, \\ s_{i-1} > s_{i-2}: &\quad s_i = \min_{t\in(t_{i-1},\tau]} u(t), \quad \text{and} \quad t_i = \max\{t \in (t_{i-1}, \tau] | u(t) = s_i\}, \end{aligned} \tag{6.1}$$

terminating the sequence if $t_i = \tau$.

Note that the values s_i are well-defined: by definition of s_{i-1} in (6.1), $u(t) > s_{i-1}$ (or $u(t) < s_{i-1}$) over $(t_{i-1}, \tau]$. Since u is continuous, the required maximum (or minimum) is well-defined. The times t_i are similarly well-defined, since the maximum is being taken over a non-empty set and τ is finite. The sequence $\{t_i\}$ is merely used to construct $\{s_i\}$, and then discarded: the time at which extrema occur is of no significance in the Preisach model.

If the input u has a finite number of extrema in $(-\infty, \tau]$, the above sequence has finite length N, $t_N = \tau$ and $u(t_n) = u(\tau)$. In this case, the tail of the sequence is formed by setting $s_i = s_N$ for $i > N$. If the sequence is infinite, then setting $t^* = \sup\{t_i\}$, the input u must be constant over $[t^*, \tau]$. Note that in both cases,

$$\lim_{i\to\infty} s_i = u(\tau). \tag{6.2}$$

The elements of the sequence $s(u, \tau)$ change depending on the time τ at which the reduced memory sequence is computed. Figure 6.3 shows the reduced memory sequence $s(u, t_i)$ for a sample input u at various times.

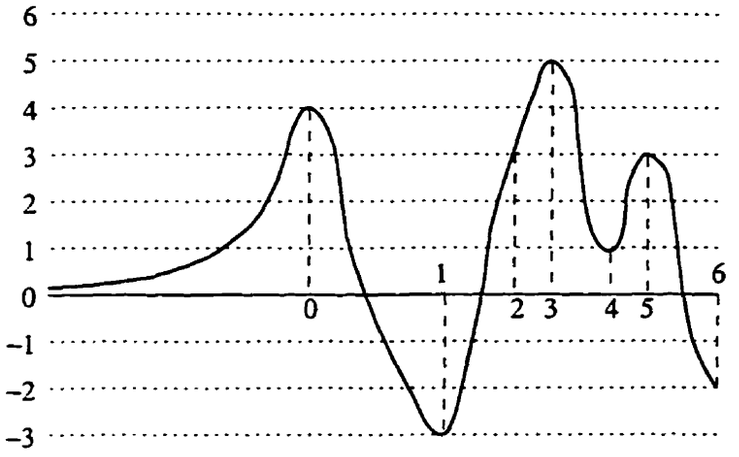

i	s(u,t)
0	{4,4,4,...}
1	{4,-3,-3,-3,...}
2	{4,-3,3,3,3,...}
3	{5,5,5,...}
4	{5,1,1,1,...}
5	{5,1,3,3,3,...}
6	{5,-2,-2,-2,...}

Figure 6.3: Example of Construction of Reduced Memory Sequences

This section will make use of the notation

$$N(s) \triangleq \sup\{i | s_{i-1} \neq s_i\}, \tag{6.3}$$

which, for any reduced memory sequence $s(u,\tau)$, is the index beyond which s_i is constant and equal to $u(\tau)$. If u has a finite number of extrema in $(-\infty,\tau]$, then $N(s(u,\tau))$ is finite; otherwise, $N(s)$ may be infinite. Also, for any sequence $s = \{s_i\}$, let s^e and s^o denote the even and odd subsequences $s^e \triangleq \{s_i\}_{i=2,4,\ldots} = \{s_i^e\}$ and $s^o \triangleq \{s_i\}_{i=1,3,\ldots} = \{s_i^o\}$.

Definition 6.4 (Space of Reduced Memory Sequences)

The space of reduced memory sequences, $S \subset l_\infty$, is composed of all sequences s with $\|s\|_\infty \leq \hat{u}$, and for which the even subsequence s^e and odd subsequence s^o satisfy

1. *s^e is strictly decreasing (strictly increasing) up to $N(s)$, and constant thereafter (if $N(s)$ is finite).*

2. *s^o is strictly increasing (strictly decreasing) up to $N(s)$, and constant thereafter (if $N(s)$ is finite).*

3. $\lim_{i\to\infty} s_i^e = \lim_{i\to\infty} s_i^o$.

Figure 6.4 shows examples of elements of $\mathcal{S}$ which have finite and infinite $N(s)$. Note that if $N(s) < \infty$, then $s_i = s_{N(s)} = u(\tau)$ for all $i \geq N(s)$.

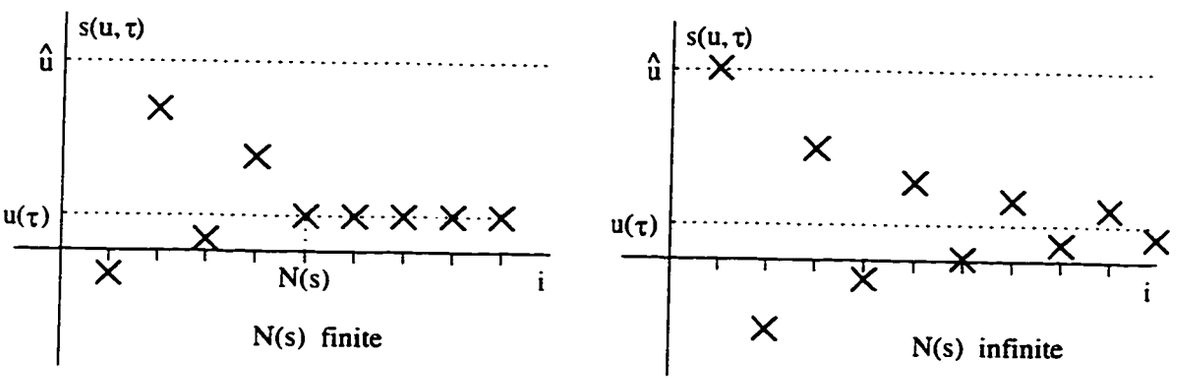

Figure 6.4: Sample Sequences in $\mathcal{S}$

Figure 6.5 shows the spaces defined thus far. The following subsections are concerned with the definition and properties of mappings between these spaces.

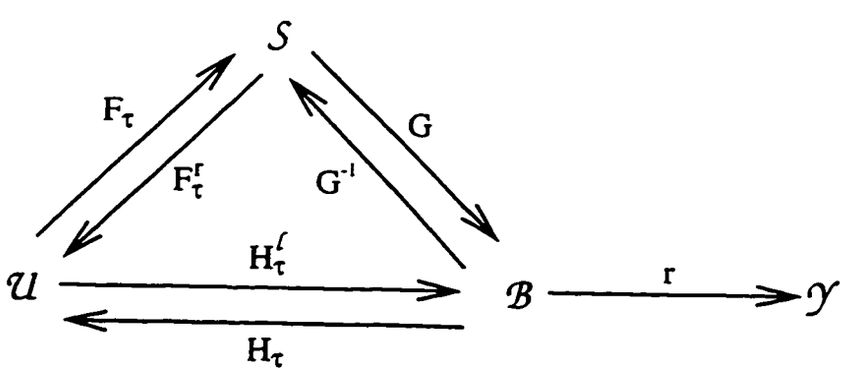

Figure 6.5: Relationship Between System Spaces

$\boldsymbol{F_\tau : \mathcal{U} \mapsto \mathcal{S}}$

For any time $\tau < \infty$ and any input $u \in \mathcal{U}(-\infty, \tau]$, the reduced memory sequence $F_\tau u = s(u, \tau)$ is defined as in (6.1).

$\boldsymbol{F_\tau^\tau : \mathcal{S} \mapsto \mathcal{U}}$

The reduced memory sequence $s(u, \tau)$ captures only the information regarding extrema of $u_{(-\infty,\tau]}$. There are therefore an infinite number of inputs $u_i \neq u$ satisfying $F_\tau u_i = F_\tau u$. Hence, F_τ is not one-to-one, and the inverse mapping is not defined. However, these inputs are equivalent in the sense that they generate the same reduced memory sequence. The operator $F_\tau^\tau : S \mapsto \mathcal{U}(-\infty, \tau]$ is defined by constructing, for any $s \in \mathcal{S}$, an input which is representative of this class of equivalent inputs.

For any $s(\cdot, \tau) \in S$, let $N(s)$ be defined as in (6.3). It is required to construct an input $u \in \mathcal{U}(-\infty, \tau]$ with extrema equal to the elements of s and satisfying $u(\tau) = \lim\{s_i\}$. Note that $N(s)$ could be infinite. Choose any $t_0 < \tau$, and let $\{t_i\}$ be a partition of $[t_0, \tau]$ defined for all $i \geq 0$ by

$$t_i = t_{i-1} + \frac{\tau - t_0}{2} \cdot \frac{1}{i^2}. \tag{6.4}$$

Note that $\lim_{i\to\infty} t_i = \tau$. Set $s_0 = 0$ and define $u(t)$ on $(-\infty, \tau]$ by straight-line interpolation between the points (t_i, s_i):

$$u(t) = \begin{cases} 0 & t \leq t_0 \\ s_i & t = t_i, \\ (t - t_{i-1})\frac{s_i - s_{i-1}}{t_i - t_{i-1}} + s_{i-1} & t_{i-1} < t < t_i. \end{cases} \tag{6.5}$$

The resulting output $u \in \mathcal{U}(-\infty, \tau]$ has extrema corresponding to elements of $s(\cdot, \tau)$, and

$$u(\tau) = \lim_{i\to\infty} s_i.$$

Define the concatenation operator $\diamond$ on $C^0 \times C^0$ by

$$u_{(t_o,t_1]} \diamond v_{(t_1,t_2]} = \begin{cases} u, & t_o < t \leq t_1 \\ v, & t_1 < t \leq t_2. \end{cases}$$

Lemma 6.1

The operators F_τ, F_τ^r satisfy the following properties, for any $\tau < \infty$.

1. *F_τ^r is a right-inverse of F_τ: for any $s \in \mathcal{S}$, $F_\tau F_\tau^r s(\cdot, \tau) = s(\cdot, \tau)$.*

2. *F_τ is deterministic: that is, for any $\tau < \infty$ and $u_1, u_2 \in \mathcal{U}(-\infty, \tau]$ satisfying $u_1(t) = u_2(t)$ over $(-\infty, \tau]$, then $F_\tau u_1 = F_\tau u_2$.*

3. *For any $u \in \mathcal{U}(-\infty, T]$ the composition $F_\tau^r F_\tau$ preserves the continuity of the input for every $\tau < T$; that is,*

$$\left(F_\tau^r F_\tau u_{(-\infty,\tau]}\right) \diamond u_{(\tau,T]} \in \mathcal{U}(-\infty, T].$$

4. *For any $T > \tau$ and $u \in \mathcal{U}(-\infty, T]$, the composition $F_\tau^r F_\tau$ satisfies the identity*

$$F_T \left[\left(F_\tau^r F_\tau u_{(-\infty,\tau]}\right) \diamond u_{(\tau,T]}\right] = F_T u. \tag{6.6}$$

Proof

Property 1

This property is satisfied by definition of F_τ^r. For any $s \in \mathcal{S}$, the extrema of $u = F_\tau^r s(\cdot, \tau)$ are exactly the elements of s, so $F_\tau u = F_\tau F_\tau^r s(\cdot, \tau) = s(\cdot, \tau)$.

Property 2

Since $u_1(t) = u_2(t)$ over all of $(-\infty, \tau]$, then in particular their extrema over this interval are equal. Since F_τ constructs a sequence based only on the extrema of an input over $(-\infty, \tau]$, $F_\tau u_1 = F_\tau u_2$.

Property 3

Choose any $u \in \mathcal{U}(-\infty, T]$, $\tau < T$. Let the reduced memory sequence at τ be $s(u,\tau) = F_\tau u$. and the input which is reconstructed from $s(u,\tau)$ be $\tilde{u} = F_\tau^r s$. From the partition (6.4) used in the construction of $\tilde{u}$, $\lim_{i\to\infty} t_i = \tau$ and from (6.5), $\tilde{u}(\tau) = \lim_{i\to\infty} s_i$. But from the definition of F_τ (6.2), $\lim_{i\to\infty} s_i = u(\tau)$. So $\tilde{u}(\tau) = u(\tau)$ and $F_\tau^r F_\tau u \diamond u_{(\tau,T]} \in \mathcal{U}(-\infty, T]$.

Property 4

For any $u \in \mathcal{U}(-\infty, T]$, let $\tilde{u} = F_\tau^r F_\tau u_{(-\infty,\tau]}$. By construction, $\tilde{u}$ contains all of the same extremum information as $u_{(-\infty,\tau]}$. From Property 3, $\tilde{u}\diamond u_{(\tau,T]} \in \mathcal{U}(-\infty, T]$, so $F_T(\tilde{u}\diamond u_{(\tau,T]})$ is defined. Then $\tilde{u}\diamond u_{(\tau,T]}$ has extrema identical to those of $u_{(-\infty,T]}$, so the identity (6.6) holds. ∎

The following two subsections define mappings between reduced memory sequences and boundaries.

$G : \mathcal{S} \mapsto \mathcal{B}$

For any reduced memory sequence $s(u,\tau) \in \mathcal{S}$, the elements of s define the corners of the corresponding boundary $G(s)$ as follows. For all $i < \infty$, define the set of points $p_i \in \mathbf{R}^2$

$$
\begin{aligned}
p_0 &= (-\hat{u}, \hat{u}) \\
p_1 &= (-|s_1|, |s_1|) \\
p_i &= \begin{cases} (s_i, s_{i-1}), & s_i < s_{i-1} \\ (s_{i-1}, s_i), & s_i > s_{i-1} \end{cases}
\end{aligned}
$$

and the line segments P_i joining p_i to p_{i+1}. Define

$$G(s) = \bigcup_{i=0}^{\infty} P_i.$$

Note that if $N(s) < \infty$, then for all $i > N(s)$,

$$\begin{aligned} p_i &= p_{N(s)} \\ &= (s_{N(s)}, s_{N(s)}) \\ &= (u(\tau), u(\tau)). \end{aligned}$$

If $N(s)$ is infinite, then the boundary $G(s)$ has an infinite number of corners p_i. In this case, since

$$\lim_{i\to\infty} s_i^e = \lim_{i\to\infty} s_i^o = u(\tau),$$

then

$$\lim_{i\to\infty} p_i = (u(\tau), u(\tau)).$$

In both cases, the result is as expected for the Preisach model: the boundary at time τ intersects the line $\alpha = \beta$ at the point $(u(\tau), u(\tau))$.

Note that the range of G, $Ra(G)$, is the set of all boundaries $B \in \mathcal{B}$ which have a finite or countably infinite number of alternating horizontal and vertical segments. This set is not quite $\mathcal{B}$, since $\mathcal{B}$ also contains non-increasing curves of arbitrary negative slope. This will be further discussed in Section 6.5.2, once the concept of distance in $\mathcal{B}$ is introduced. It will be shown that for any $B \in \mathcal{B}$, there is a boundary in $Ra(G)$—in fact, in $\mathcal{B}_\tau \subset Ra(G)$—which is arbitrarily close to B.

$G^{-1} : Ra(G) \mapsto \mathcal{S}$

For every sequence $s \in \mathcal{S}$, the boundary $G(s)$ is unique, by definition of G. Since G is obviously onto $Ra(G)$, the inverse mapping $G^{-1} : Ra(G) \mapsto \mathcal{S}$ exists. The

construction of a sequence $s \in \mathcal{S}$ from any boundary in $B \in Ra(G)$ is defined as follows.

Let $N-1$ be the number of horizontal and vertical segments of B. Then $N \geq 1$ and N may be infinite. Set $p_1 = (\alpha_1, \beta_1)$, the coordinates of the right endpoint of the diagonal segment (if none exists, set $p_1 = (-\hat{u}, \hat{u})$). For $i = 2, \ldots, N$, let p_i be the coordinates (α_i, β_i) of the N remaining corners of the boundary. If the first segment is horizontal, set

$$s_i = \begin{cases} \alpha_i, & i = 1, 3, \ldots \\ \beta_i, & i = 2, 4, \ldots \end{cases}$$

and if the first segment is vertical, set

$$s_i = \begin{cases} \beta_i, & i = 1, 3, \ldots \\ \alpha_i, & i = 2, 4, \ldots \end{cases}$$

The resulting sequence contains N elements. If $N < \infty$, as in the example of Figure 6.6, the reduced memory sequence is completed by setting the tail to $s_i = s_N$ for all $i > N$.

From the definition of G, the construction outlined above is the inverse of G, $G^{-1} : Ra(G) \mapsto \mathcal{S}$, and $GG^{-1} = G^{-1}G = I$.

$\boldsymbol{H_\tau^\ell : \mathcal{U} \mapsto \mathcal{B}}$

$\boldsymbol{H_\tau : Ra(G) \mapsto \mathcal{U}}$

The mappings $H_\tau^\ell : \mathcal{U} \mapsto \mathcal{B}$ and $H_\tau : Ra(G) \mapsto \mathcal{U}$ are defined as the compositions

$$H_\tau \triangleq F_\tau^r G^{-1}, \qquad H_\tau^\ell \triangleq G F_\tau^\ell.$$

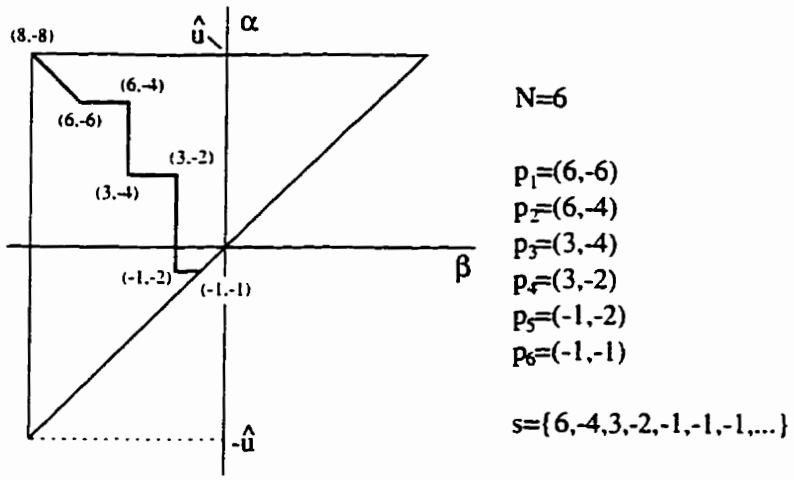

Figure 6.6: Construction of s from B

Lemma 6.2

The operators H_τ, H_τ^ℓ satisfy the following properties, for any $\tau < \infty$.

1. *H_τ^ℓ is a left-inverse of H_τ.*

2. *H_τ^ℓ is deterministic: that is, for any $\tau < \infty$ and $u_1, u_2 \in \mathcal{U}(-\infty, \tau]$ satisfying $u_1(t) = u_2(t)$ over $(-\infty, \tau]$, then $H_\tau^\ell u_1 = H_\tau^\ell u_2$.*

3. *For any $T > \tau$ and $u \in \mathcal{U}(-\infty, T]$, the operators satisfy the identity*

$$H_T^\ell \left[\left(H_\tau H_\tau^\ell u_{(-\infty,\tau]} \right) \diamond u_{(\tau,T]} \right] = H_T^\ell u. \tag{6.7}$$

Proof

Property 1

$$\begin{aligned} H_\tau^\ell H_\tau &= G F_\tau F_\tau^\tau G^{-1} \\ &= G I G^{-1} \\ &= I. \end{aligned}$$

Property 2

Since F_τ is deterministic, then for any two inputs $u_1, u_2 \in \mathcal{U}(-\infty, \tau]$ satisfying $u_1(t) = u_2(t)$ over $(-\infty, \tau]$,

$$\begin{aligned} H^\ell_\tau u_1 &= GF_\tau u_1 \\ &= GF_\tau u_2 \\ &= H^\ell_\tau u_2. \end{aligned}$$

Property 3

Applying Property 4 of Lemma 6.1,

$$\begin{aligned} H^\ell_T \left[H_\tau H^\ell_\tau u_{(-\infty,\tau]} \diamond u_{(\tau,T]} \right] &= GF_T \left[F^\tau_\tau G^{-1} GF_\tau u_{(-\infty,\tau]} \diamond u_{(\tau,T]} \right] \\ &= GF_T \left[F^\tau_\tau F_\tau u_{(-\infty,\tau]} \diamond u_{(\tau,T]} \right] \\ &= GF_T u \\ &= H^\ell_T u. \end{aligned}$$

■

6.4 State Transition and Read-Out Operators

6.4.1 State Transition Operator

The state transition operator ϕ determines the state $B = \phi(t_1, t_o, B_o, u)$ which results from applying an input $u \in \mathcal{U}[t_o, t_1]$ to a system in state B_o at time t_o. Since the Preisach model is only defined for continuous inputs, it is imperative that u be continuous at t_o with the input up to that point. This prompts the following definition of *admissibility*.

Definition 6.5 (Admissible Inputs)

An input $u \in \mathcal{U}(t_o, T]$ is said to be admissible for state B_o if, for any input $u^* \in \mathcal{U}(-\infty, t_o]$ such that $B_o = \phi(t_o, -\infty, B^*, u^*)$, $u^*_{(-\infty,t_o]} \diamond u_{(t_o,T]}$ is in $\mathcal{U}(-\infty, T]$; that is, $u(t_o) = u^*(t_o)$.

This concept of admissibility is presented in more detail in [57].

It is nonsensical, when writing $\phi(t_1, t_o, B_o, u)$, to consider inputs which are not admissible to B_o, or states B_o which are not reachable. The state transition operator is defined, and the axioms proven, under the assumptions that initial states B_o are reachable and inputs u are admissible for the state to which they are applied. While this interpretation is not explicitly clear from Definition 6.1, it can be found in other similar definitions[e.g. 57].

The state transition operator ϕ is defined using the mappings introduced in Section 6.3. Given some interval $[t_0, t_1]$, some reachable initial state B_o at time t_o, and some input $u \in \mathcal{U}[t_0, t_1]$ admissible at B_o, the procedure to determine the state $\phi(t_1, t_o, B_o, u)$ is as follows:

1. determine the memory sequence corresponding to the initial state: $s(\cdot, t_0) = G^{-1} B_o$,
2. construct an input $u_o \in \mathcal{U}(-\infty, t_0]$ which generates $s(\cdot, t_0)$: $u_o = F^r_{t_0} s(\cdot, t_0)$,
3. concatenate the inputs u_o and u to form $\tilde{u} = u_o \diamond u \in \mathcal{U}(-\infty, t_1]$,
4. determine the corresponding boundary B_1 at time t_1: $B_1 = G F_{t_1} \tilde{u}$.

Thus, the state transition function ϕ is given by

$$\phi(t_1, t_o, B_o, u) \triangleq H^{\ell}_{t_1} \left[H_{t_0} B_o \diamond u_{(t_0,t_1]} \right]. \tag{6.8}$$

6.4.2 State Transition Function Axioms

It is now proven that ϕ as defined in (6.8) satisfies the axioms required of a state transition function.

consistency

Choose any $t_o \in \mathbf{R}$, $B_o \in \mathcal{B}_r$, and admissible $u \in \mathcal{U}$. Then

$$\begin{aligned}\phi(t_o, t_o, B_o, u) &= H^{\ell}_{t_o}\left[H_{t_o} B_o \diamond u_{(t_o,t_o]}\right] \\ &= H^{\ell}_{t_o}\left[H_{t_o} B_o\right] \\ &= B_o.\end{aligned}$$

determinism

Choose any $t_1 \geq t_o$, $B_o \in \mathcal{B}_r$, and admissible $u_1, u_2 \in \mathcal{U}$ such that $u_1(t) = u_2(t)$ over $t \in [t_o, t_1]$. Let $u_o = H_{t_o} B_o$. Then

$$\begin{aligned}\phi(t_1, t_o, B_o, u_1) &= H^{\ell}_{t_1}\left(u_o \diamond u_{1(t_o,t_1]}\right), \text{ and} \\ \phi(t_1, t_o, B_o, u_2) &= H^{\ell}_{t_1}\left(u_o \diamond u_{2(t_o,t_1]}\right).\end{aligned}$$

But $u_{1(t_o,t_1]} = u_{2(t_o,t_1]}$, and from Lemma 6.2, H^{ℓ}_{τ} is deterministic, so $\phi(t_1, t_o, B_o, u_1) = \phi(t_1, t_o, B_o, u_2)$.

semi-group

Choose any $t_o \in \mathbf{R}$, $t_2 \geq t_1 \geq t_o$, $B_o \in \mathcal{B}_r$ and admissible $u \in \mathcal{U}$. Let $u_o = H_{t_o} B_o$, $\tilde{u} = u_o \diamond u_{(t_o,t_2]}$, and note that $u_o \diamond u_{(t_o,t_1]} = \tilde{u}_{(-\infty,t_1]}$ and $u_{(t_1,t_2]} = \tilde{u}_{(t_1,t_2]}$. Then

$$\begin{aligned}\phi(t_2, t_1, \phi(t_1, t_o, B_o, u), u) &= H^{\ell}_{t_2}\left[H_{t_1}\left\{\phi(t_1, t_o, B_o, u)\right\} \diamond u_{(t_1,t_2]}\right] \\ &= H^{\ell}_{t_2}\left[H_{t_1}\left\{H^{\ell}_{t_1}\left[H_{t_o} B_o \diamond u_{(t_o,t_1]}\right]\right\} \diamond u_{(t_1,t_2]}\right] \\ &= H^{\ell}_{t_2}\left[H_{t_1}\left\{H^{\ell}_{t_1}\left[u_o \diamond u_{(t_o,t_1]}\right]\right\} \diamond u_{(t_1,t_2]}\right] \\ &= H^{\ell}_{t_2}\left[H_{t_1} H^{\ell}_{t_1} \tilde{u}_{(-\infty,t_1]} \diamond \tilde{u}_{(t_1,t_2]}\right] \\ &= H^{\ell}_{t_2} \tilde{u}\end{aligned}$$

by Property 3 of Lemma 6.2. But

$$\begin{aligned}\phi(t_2, t_0, B_o, u) &= H^\ell_{t_2}\left[H_{t_o}B_o \diamond u_{(t_o,t_2]}\right] \\ &= H^\ell_{t_2}\left[u_o \diamond u_{(t_o,t_2]}\right] \\ &= H^\ell_{t_2}\tilde{u},\end{aligned}$$

and so ϕ satisfies the semi-group property.

stationarity

Choose any $t_o \in \mathbf{R}$, $t_1 \geq t_o$, $B_o \in \mathcal{B}_r$, admissible $u \in \mathcal{U}$ and $T < \infty$. It is required to show that

$$H^\ell_{t_1}\left[H_{t_o}B_o \diamond u_{(t_o,t_1]}\right] = H^\ell_{t_1+T}\left[H_{t_o+T}B_o \diamond \sigma_T u_{(t_o,t_1]}\right]. \tag{6.9}$$

Recall that σ_T is the shift operator. Set

$$\begin{aligned}u_1 &= H_{t_o}B_o \in \mathcal{U}(-\infty, t_o], \\ u_2 &= H_{t_o+T}B_o \in \mathcal{U}(-\infty, t_o + T].\end{aligned}$$

Then

$$s(u_1, t_o) = F_{t_o}u_1 = F_{t_o}F^r_{t_o}G^{-1}B_o = G^{-1}B_o,$$

and similarly, $s(u_2, t_o + T) = G^{-1}B_o$. Now define

$$\begin{aligned}\tilde{u}_1 &= u_1 \diamond u_{(t_o,t_1]}, \\ \tilde{u}_2 &= u_2 \diamond \sigma_T u_{(t_o,t_1]}.\end{aligned}$$

Equation (6.9) can be written

$$H^\ell_{t_1}\tilde{u}_1 = H^\ell_{t_1+T}\tilde{u}_2.$$

Since $s(u_1, t_o) = s(u_2, t_o + T)$, then $s(\tilde{u}_1, t_1) = F_{t_1}\tilde{u}_1$ is the same reduced memory sequence as $s(\tilde{u}_2, t_1 + T) = F_{t_1+T}\tilde{u}_2$. Thus

$$\begin{aligned} H^{\ell}_{t_1}\tilde{u}_1 &= GF_{t_1}\tilde{u}_1 \\ &= GF_{t_1+T}\tilde{u}_2 \\ &= H^{\ell}_{t_1+T}\tilde{u}_2, \end{aligned}$$

and ϕ is stationary.

6.4.3 Read-Out Function

The read-out function r gives the system output which corresponds to a particular state B. In Chapter 3, the output was written as

$$y(t) = \int\int_{\mathcal{P}_+(t)} \mu(\alpha,\beta)d\alpha d\beta - \int\int_{\mathcal{P}_-(t)} \mu(\alpha,\beta)d\alpha d\beta,$$

where $\mathcal{P}_+(t)$ and $\mathcal{P}_-(t)$ were the regions of $\mathcal{P}_r$ where relays were in the +1 and -1 state, respectively, at time t. At any time, these regions can be determined from the boundary B. The operators P_+ and P_- on $\mathcal{B}$ are defined so that $P_+B = \mathcal{P}_+$ and $P_-B = \mathcal{P}_-$:

P_+B is the set of all $(\alpha,\beta) \in \mathcal{P}$ which lie below or to the left of the graph of B in $\mathcal{P}$, as well as the points on the graph of B.

P_-B is the set of all $(\alpha,\beta) \in \mathcal{P}$ which lie above or to the right of the graph of B in $\mathcal{P}$.

Then the read-out function $r : \mathcal{B} \mapsto Y$ is given by

$$y(t) = r(B) = \int\int_{P_+B} \mu(\alpha,\beta)d\alpha d\beta - \int\int_{P_-B} \mu(\alpha,\beta)d\alpha d\beta.$$

Note that the boundary B is implicitly time varying with u.

6.5 Properties of the State Space

This section is devoted to elucidating some of the properties of the state space $\mathcal{B}$. An isomorphic space $\tilde{\mathcal{B}}$ which is more familiar than $\mathcal{B}$ is introduced. Where it is more efficient, the subsequent analysis makes use of this relationship, demonstrating properties of $\mathcal{B}$ by showing they hold in $\tilde{\mathcal{B}}$.

Define an isomorphic mapping on $R : \mathbf{R}^2 \mapsto \mathbf{R}^2$ by

$$R = \begin{bmatrix} \frac{1}{\sqrt{2}} & -\frac{1}{\sqrt{2}} \\ \frac{1}{\sqrt{2}} & \frac{1}{\sqrt{2}} \end{bmatrix}.$$

The effect of this mapping on a boundary $B \in \mathcal{B}$ is illustrated in Figure 6.7.

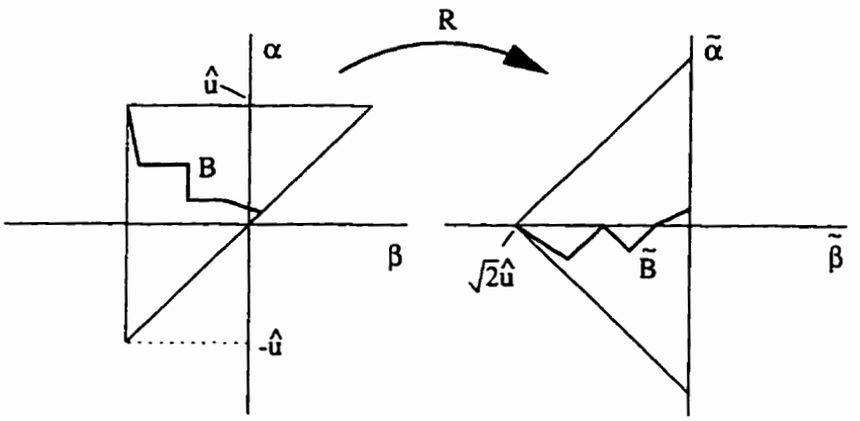

Figure 6.7: The Rotation Mapping R

Essentially, the rotation R maps elements of the state space $\mathcal{B}$ to the set of functions which are Lipschitz continuous on $[-\sqrt{2}\hat{u}, 0]$, with Lipschitz constant 1. While elements of $\mathcal{B}$ may be graphs of multivalued functions of β, these rotated boundaries cannot be multivalued. This simplifies proofs for some of the results which follow. Since isomorphisms preserve distance, properties related to distance are shared by $\mathcal{B}$ and $\tilde{\mathcal{B}}$: what can be proven for $\tilde{\mathcal{B}}$ also holds for $\mathcal{B}$.

Claim 6.3

For any $B \in \mathcal{B}$, the points of the rotated graph

$$\tilde{B} = \left\{(\tilde{\beta}, \tilde{B}(\tilde{\beta}) | [\tilde{\beta}\ \tilde{B}(\tilde{\beta})]^T = R[\beta\ B(\beta)]^T\right\}$$

satisfy the following rotated boundary conditions:

($\tilde{B}P1$) *bounded input restriction:* $\left|\tilde{B}(\tilde{\beta})\right| \leq \sqrt{2}\hat{u} + \tilde{\beta},\ \tilde{\beta} \leq 0$;

($\tilde{B}P2$) *initial condition:* $\tilde{B}(-\sqrt{2}\hat{u}) = 0$;

($\tilde{B}P3$) *Lipschitz condition:* $\left|\tilde{B}(\tilde{\beta}_1) - \tilde{B}(\tilde{\beta}_2)\right| \leq \left|\tilde{\beta}_1 - \tilde{\beta}_2\right|,\ \ \forall \tilde{\beta}_1, \tilde{\beta}_2$.

Proof

For any $B \in \mathcal{B}$, the points $(\beta, B(\beta))$ satisfy properties (BP1-BP2), and are related to points of $\tilde{B}$ by

$$\begin{bmatrix} \beta \\ B(\beta) \end{bmatrix} = R^{-1} \begin{bmatrix} \tilde{\beta} \\ \tilde{B}(\tilde{\beta}) \end{bmatrix} = \begin{bmatrix} \frac{\tilde{\beta}+\tilde{B}(\tilde{\beta})}{\sqrt{2}} \\ \frac{-\tilde{\beta}+\tilde{B}(\tilde{\beta})}{\sqrt{2}} \end{bmatrix}. \tag{6.10}$$

Property ($\tilde{B}$P1) results directly from substituting (6.10) into (BP1), and in turn implies ($\tilde{B}$P2). Although property ($\tilde{B}$P3) can be proven by considering all possible violations of the Lipschitz condition and showing these contradict (BP3), a graphical argument is much clearer, if less rigorous. Suppose that some portion of a curve $\tilde{B}$, satisfying ($\tilde{B}$P1-$\tilde{B}$P2), has a slope whose magnitude is greater than unity. When this curve is rotated, the resulting boundary $B = R^{-1}\tilde{B}$ has segments which are increasing, as shown in Figure 6.8. This is in contradiction with (BP3), and shows that (BP3)$\Longrightarrow$($\tilde{B}$P3). ∎

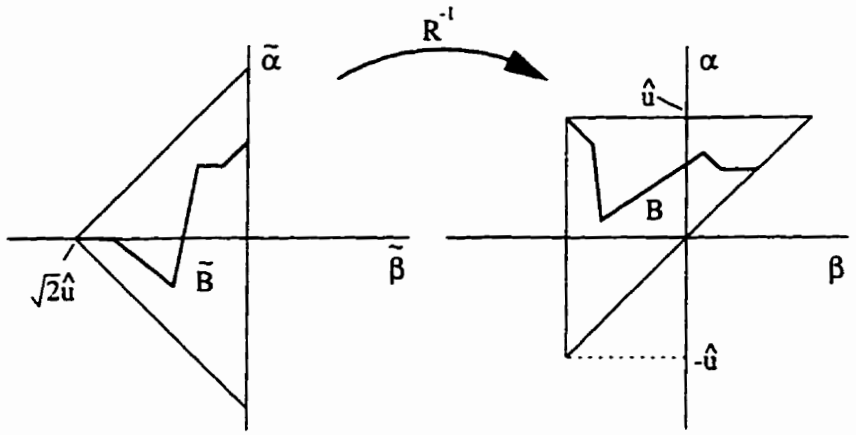

Figure 6.8: Violation of the Lipschitz Condition

This result shows that the state space $\mathcal{B}$ is isomorphic to a space $\tilde{\mathcal{B}} \subset C^0[-\sqrt{2}\hat{u}, 0]$. This fact will be used in demonstrating several properties of the state space in the following subsections.

6.5.1 Metrizing the State Space

Introducing the notation $\mathcal{P}_{B_1 B_2}$, indicating the region in $\mathcal{P}$ bounded by the graphs B_1, B_2 and the line $\alpha = \beta$, the state space can be given a metric defined by the area between two boundaries,

$$d(B_1, B_2) = \iint_{\mathcal{P}_{B_1 B_2}} d\alpha d\beta.$$

Since the mapping R preserves distance between points in $\mathbf{R}^2$, the area between any two boundaries B_1 and B_2 is equal to the area between $\tilde{B}_1$ and $\tilde{B}_2$, which is computed as

$$\int_{-\sqrt{2}\hat{u}}^{0} \left| \tilde{B}_1(\tilde{\beta}) - \tilde{B}_2(\tilde{\beta}) \right| d\tilde{\beta}. \tag{6.11}$$

This is illustrated in Figure 6.9.

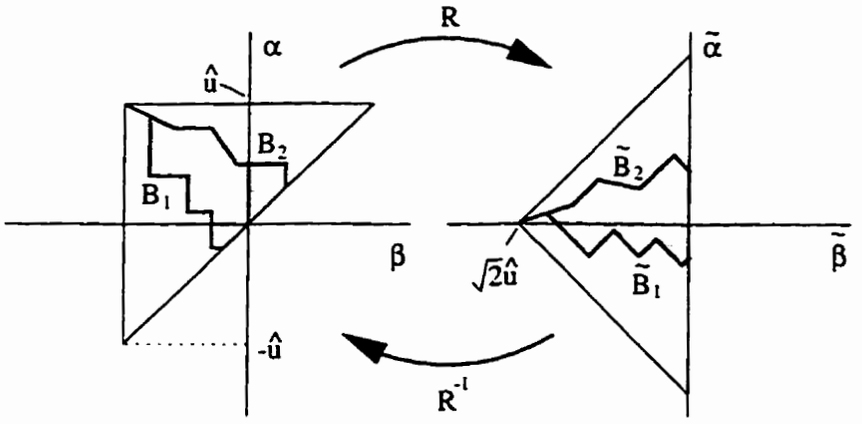

Figure 6.9: The Metric on $\mathcal{B}$

But every element of $\tilde{B}$ is in $C^0[-\sqrt{2}\hat{u}, 0]$, and (6.11) is simply the L_1 norm on $C^0[-\sqrt{2}\hat{u}, 0]$. So for any two boundaries in $\mathcal{B}$, $d(B_1, B_2) = \left\|\tilde{B}_1 - \tilde{B}_2\right\|_1$, and it is clear that $d(\cdot,\cdot)$ satisfies the properties of a metric.

It is worth noting that $\tilde{\mathcal{B}}$ (and hence also $\mathcal{B}$) is not a linear space, since scalar multiplication is precluded by the Lipschitz condition ($\tilde{\text{B}}$P3). Although the distance function in $\tilde{\mathcal{B}}$ is identical to the L_1 norm, the notation $\|\cdot\|_1$ will not be used since this would imply a normed space. The rotated metric space will be denoted $(\tilde{\mathcal{B}}, \tilde{d}(\cdot,\cdot))$ to avoid this confusion, with

$$\tilde{d}(\tilde{B}_1, \tilde{B}_2) = \int_{-\sqrt{2}\hat{u}}^{0} \left|\tilde{B}_1(\tilde{\beta}) - \tilde{B}_2(\tilde{\beta})\right| d\tilde{\beta}.$$

6.5.2 Reachability

The notion of reachability was introduced and briefly discussed in Section 6.5.2. It was pointed out that the state space was not reachable, and the reachable subspace $\mathcal{B}_r$ was defined. Here, the idea of *approximate reachability* is introduced. This concept is similar to that of approximate controllability for infinite-dimensional systems, defined in [10].

Definition 6.6 (Approximate Reachability)

The state space $(\mathcal{X}, d)$ of a dynamical system Σ is said to be "approximately reachable from x_o" if, for any $x \in \mathcal{X}$ and $\varepsilon > 0$, there exists a time $t < \infty$ and admissible input $u \in \mathcal{U}(-\infty, t]$ such that $d(x, \phi(t, t_o, x_o, u)) < \varepsilon$.

Theorem 6.4 (Approximate Reachability)

The state space $\mathcal{B}$ is approximately reachable from $B^\bullet$.

Proof

Consider any $B \in \mathcal{B}$, a continuous, non-increasing function defined on $[-\hat{u}, 0]$. For any $n < \infty$, let $\{\beta_i\}_{i=0,\ldots,n}$ be a partition of $[-\hat{u}, 0]$ into n equal subintervals, with $\beta_o = -\hat{u}$. B can be approximated on $[-\hat{u}, 0]$ by a function g which is piecewise constant over each interval $(\beta_i, \beta_{i+1}]$:

$$g(\beta) = \begin{cases} B(\beta_1), & \beta = -\hat{u} \\ B(\beta), & \beta_i < \beta \leq \beta_{i+1}. \end{cases}$$

Increasing n reduces the L_1 approximation error, and for any $\varepsilon > 0$, $n < \infty$ can be chosen so that the area between B and g is less than ε[e.g. 11].

Since B is non-increasing, the values $\{g(\beta_i)\}$ are also non-increasing, and g is equivalent in the area metric on $\mathcal{B}$ to a non-increasing staircase function B_o with n horizontal segments. Since n is finite for any $\varepsilon > 0$, $B_o \in \mathcal{B}_r$. So for any $B \in \mathcal{B}$ and $\varepsilon > 0$, there exists a $B_o \in \mathcal{B}_r$ such that $d(B, B_o) < \varepsilon$. Since boundaries in $\mathcal{B}_r$ are reachable from $B^\bullet$, the state space $\mathcal{B}$ is approximately reachable from $B^\bullet$. ■

6.5.3 Boundedness

Definition 6.7 (Boundedness[e.g. 36])
A metric space (X, d) is said to be bounded if, for every pair of states $x_1, x_2 \in \mathcal{X}$, $d(x_1, x_2) < \infty$.

By property (BP1), the maximum area between any two boundaries is $2\hat{u}^2$. Hence, $d(B_1, B_2) \leq 2\hat{u}^2$ for all $B_1, B_2 \in \mathcal{B}$, and the state space $\mathcal{B}$ is bounded.

6.5.4 Completeness

In this subsection, it is proven that the metric space $\mathcal{B}$ is complete. The importance of this property will be described after some preliminary definitions.

Definition 6.8 (Cauchy Sequence[e.g. 36])
A sequence $\{x_n\}$ in a metric space X with metric $d(\cdot, \cdot)$ is said to be Cauchy if for every $\epsilon > 0$ there is an $N = N(\epsilon)$ such that $d(x_m, x_n) < \epsilon$ for every $m, n > N$.

Definition 6.9 (Completeness[e.g. 36])
A metric space X is said to be complete if every Cauchy sequence in X converges in X.

Definition 6.10 (Equicontinuity[e.g. 52])
A family of functions $\mathcal{F}$ from a space X into a metric space (Y, d) is said to be equicontinuous at x_o if, for every $\epsilon > 0$, there exists an open neighborhood $\mathcal{O}$ of x_o such that $d(f(x), f(x_o)) < \epsilon$ for all $x \in \mathcal{O}$ and all $f \in \mathcal{F}$. If $\mathcal{F}$ is equicontinuous for all $x_o \in X$, it is said to be equicontinuous.

The key point in this definition is that the size of the neighborhood $\mathcal{O}$ does not depend on f.

The importance of completeness can now be explained. In many applications, it is easier to show that a sequence is Cauchy—that its elements get closer and closer to each other—than it is to show that it converges. This is because the former requires only knowledge of the sequence itself, while the latter supposes some knowledge of the limit. For an example of an application where completeness is important, consider the numerical optimization of a cost function $J : X \mapsto \mathbf{R}$ over a parameter space X. A minimization algorithm generates a sequence of points x_i in X such that $J(x_i) < J(x_{i-1})$, and it may be easy to show that $\{x_i\}$ is Cauchy. Then if X is complete, $\{x_i\}$ converges to a unique limit, say to $x^* \in X$, and $J(x^*) = \min J(x)$; the minimization problem has a unique solution in X. However, if X is not complete, then the sequence $\{x_i\}$ may not converge, and the problem could be ill-posed.

It is now shown that $\tilde{\mathcal{B}}$ is equicontinuous, and later, that it is complete. Since $\mathcal{B}$ and $\tilde{\mathcal{B}}$ are isomorphic, this implies that $\mathcal{B}$ is also complete.

Lemma 6.5 ($\tilde{\mathcal{B}}$ Equicontinuous)

$\tilde{\mathcal{B}}$ is an equicontinuous family of functions mapping $[-\sqrt{2}\hat{u}, 0] \mapsto (\mathbf{R}, |\cdot|)$.

Proof

Choose any $\epsilon > 0$. Every element of $\tilde{\mathcal{B}}$ is Lipschitz continuous with Lipschitz constant 1. Setting $\delta = \epsilon$, then for any $\tilde{B} \in \tilde{\mathcal{B}}$ and any $\beta_o \in [-\sqrt{2}\hat{u}, 0]$, if $|\beta - \beta_o| < \delta$ then

$$\begin{aligned} \left|\tilde{B}(\beta) - \tilde{B}(\beta_o)\right| &\leq |\beta - \beta_o| \\ &< \delta \\ &= \epsilon. \end{aligned}$$

Since δ is independent of $\tilde{B}$ and β_o, the family of curves $\tilde{\mathcal{B}}$ is equicontinuous. ∎

Theorem 6.6 (Arzela-Ascoli[52])

Let $\mathcal{F}$ be an equicontinuous family of real-valued functions on a separable space[1] *X. Then each subsequence $\{f_n\}$ in $\mathcal{F}$ which is bounded at each point (of a dense subset) has a subsequence $\{f_{n_k}\}$ that converges pointwise to a continuous function, the convergence being uniform on each compact subset of X.*

Theorem 6.7 (Completeness)

The metric space $(\mathcal{B}, d)$ is complete.

Proof

The proof is an application of the Arzela-Ascoli theorem, in which $X = [-\sqrt{2}\hat{u}, 0]$ is a compact subset of $\mathbf{R}$ and $\mathcal{F} = \tilde{\mathcal{B}}$. Note that X is separable.

Choose any Cauchy sequence $\{\tilde{B}_n\}$ in $\tilde{\mathcal{B}}$. Then for every n, $\tilde{B}_n(-\sqrt{2}\hat{u}) = 0$ and $\tilde{B}$ is Lipschitz continuous, so for every point $\beta \in [-\sqrt{2}\hat{u}, 0]$,

$$\begin{aligned} \left|\tilde{B}_n(\beta)\right| &= \left|\tilde{B}_n(\beta) - \tilde{B}_n(-\sqrt{2}\hat{u})\right| \\ &\leq \left|\beta + \sqrt{2}\hat{u}\right|, \end{aligned}$$

and the sequence $\{\tilde{B}_n\}$ is pointwise bounded over X. By the Arzela-Ascoli theorem, the sequence $\{\tilde{B}_n\}$ has a subsequence $\{\tilde{B}_{n_k}\}$ which converges both uniformly and pointwise to a continuous function $\tilde{B}$. But pointwise convergence over compact X means that

$$\max_{\beta \in X} \left|\tilde{B}_{n_k}(\beta) - \tilde{B}(\beta)\right| \longrightarrow 0$$

[1] A space X is separable if it has a countable subset which is dense in X. In particular, the real line is separable, since the rationals are countable and dense in $\mathbf{R}$[e.g. 36].

which in turn implies that

$$\int_X \left|\tilde{B}_{n_k}(\beta) - \tilde{B}(\beta)\right| d\beta \longrightarrow 0$$

so $\tilde{B}_{n_k} \longrightarrow \tilde{B}$ in the metric $\tilde{d}$ on $\tilde{\mathcal{B}}$.

Also, $\tilde{d}$ is simply the L_1 norm on $C^0[-\sqrt{2}\hat{u}, 0]$, and L_1 is the completion of C^0. Since $\{\tilde{B}_n\} \subset C^0[-\sqrt{2}\hat{u}, 0]$, $\{\tilde{B}_n\}$ converges in $\tilde{d}$ to a limit $\tilde{B}_o$. Since the limit of a sequence which converges in a metric space is unique[e.g. 36], $\tilde{B}_o = \tilde{B}$, and $\{\tilde{B}_n\} \longrightarrow \tilde{B}$ in $\tilde{d}$.

To prove completeness, it remains to show that $\tilde{B} \in \tilde{\mathcal{B}}$. Choose any $\beta_1, \beta_2 \in [-\sqrt{2}\hat{u}, 0]$. Recall that $\tilde{B}_n(\beta)$ is a bounded sequence of real numbers. Then

$$\begin{aligned}
\left|\tilde{B}(\beta_2) - \tilde{B}(\beta_1)\right| &= \left|\lim_{n\to\infty} \tilde{B}_n(\beta_2) - \lim_{n\to\infty} \tilde{B}_n(\beta_1)\right| \\
&= \left|\lim_{n\to\infty} (\tilde{B}_n(\beta_2) - \tilde{B}_n(\beta_1))\right| \\
&= \lim_{n\to\infty} \left|(\tilde{B}_n(\beta_2) - \tilde{B}_n(\beta_1))\right| \\
&\leq \lim_{n\to\infty} |\beta_2 - \beta_1| \\
&= |\beta_2 - \beta_1| ,
\end{aligned}$$

so $\tilde{B}$ satisfies ($\tilde{\text{B}}$P3).

The pointwise convergence $\{\tilde{B}_n\} \longrightarrow \tilde{B}$ implies that $\tilde{B}(-\sqrt{2}\hat{u}) = 0$, since $\tilde{B}_n(-\sqrt{2}\hat{u}) = 0$ for every n. So $\tilde{B}$ also satisfies ($\tilde{\text{B}}$P2). Together, properties ($\tilde{\text{B}}$P2) and ($\tilde{\text{B}}$P3) imply ($\tilde{\text{B}}$P1), so $\tilde{B} \in \tilde{\mathcal{B}}$.

Hence, the rotated state space $(\tilde{\mathcal{B}}, \tilde{d})$ is complete, and since they are isomorphic, so is the state space $(\mathcal{B}, d)$. ∎

6.6 Summary

A state space definition of the Preisach model has been given for continuous bounded inputs which vanish as $t \to -\infty$. The state space is a complete, bounded metric space, and is approximately reachable.

This is an original contribution which is made possible by the structure of the Preisach model. It opens the door for the application of classical non-linear state-space methods to these highly non-linear systems. In the next chapter, the state-space framework allows the development of a new result on the dissipativity of the Preisach model.

Spaces	
C^0	space of continuous functions
l_∞	space of bounded sequences
$\mathcal{U}$	input space ($\subset C^0$)
$\mathcal{Y}$	output space ($\subset C^0$)
$\mathcal{B}$	state space
$\mathcal{B}_r$	reachable subspace of $\mathcal{B}$ ($\subset \mathcal{B}$)
$\mathcal{B}^n$	set of boundaries in $\mathcal{B}$ with n (finite) horizontal and vertical segments ($\subset \mathcal{B}_r$)
$\tilde{\mathcal{B}}$	rotated state space, isomorphic to $\mathcal{B}$
$\mathcal{S}$	set of reduced memory sequences ($\subset l_\infty$)
$\mathcal{P}$	the Preisach plane ($\subset \mathbf{R}^2$)
$\mathcal{P}_r$	the restricted Preisach plane ($\subset \mathcal{P}$)

Table 6.1: Chapter 6 Nomenclature—Spaces

Elements	
(α, β)	a point in $\mathcal{P}$ or $\mathcal{P}_r$ $(\in \mathbf{R}^2)$
β	the abscissa of a point in $\mathcal{P}$ or $\mathcal{P}_r$ $(\in \mathbf{R})$
B	a boundary; a graph of a function $(\in \mathcal{B})$
B^*	the initial condition; the zero state $(\in \mathcal{B})$
$\tilde{B}$	a rotated boundary $(\in \tilde{\mathcal{B}})$
$s, s(\cdot, \tau), s(u, \tau)$	a reduced memory sequence $(\in \mathcal{S})$
s^e, s^o	even and odd subsequences of s
$N(s)$	index beyond which s_i is constant $N(s) \geq 1$ and $N(s)$ may be infinite
u	an input $(\in \mathcal{U})$
$\hat{u}$	input bound: $\|u\|_\infty \leq \hat{u}$ $(\in \mathbf{R})$

Table 6.2: Chapter 6 Nomenclature—Elements

Mappings (see also Figure 6.5)	
$F_\tau: \mathcal{U} \mapsto \mathcal{S}$	constructs the reduced memory sequence of u at time τ
$F_\tau^r: \mathcal{S} \mapsto \mathcal{U}$	constructs an input $u \in \mathcal{U}$ which generates $s(\cdot, \tau)$
$G: \mathcal{S} \mapsto \mathcal{B}$	constructs a boundary from a reduced memory sequence
$G^{-1}: Ra(G) \mapsto \mathcal{S}$	maps boundaries in $Ra(G)$ back to their generating sequence
$H_\tau^\ell: \mathcal{U} \mapsto \mathcal{B}$	composite map from inputs to boundaries: $H_\tau^\ell = GF_\tau$
$H_\tau: Ra(G) \mapsto \mathcal{U}$	composite map from boundaries to inputs: $H_\tau = F_\tau^r G^{-1}$
$R: \mathcal{B} \mapsto \tilde{\mathcal{B}}$	isomorphic rotation mapping
$d: \mathcal{B} \times \mathcal{B} \mapsto \mathbf{R}$	area metric on $\mathcal{B}$
$\tilde{d}: \tilde{\mathcal{B}} \times \tilde{\mathcal{B}} \mapsto \mathbf{R}$	area metric on $\tilde{\mathcal{B}}$

Table 6.3: Chapter 6 Nomenclature—Mappings

Chapter 7

Energy and the Preisach Model

In the design of controllers for physical systems, it is often useful to have an understanding of the energy properties of the system. Some of the classical results in the design of controllers for non-linear systems are based on generalizations of energy arguments. Passivity theory and Lyapunov's method are two examples.

In the first section of this chapter, formulas for energy storage and loss in the Preisach model are derived. Similar results have been derived in [43], but the assumption made in that work was somewhat restrictive and a more general approach is taken here. In the second section, the dissipativity theory of Willems is introduced. Coupled with the state-space representation of the previous chapter, this framework allows the derivation of an energy dissipation result which is more general than those obtained previously[19, 28].

7.1 Energy Storage in the Preisach Model

This section is concerned with investigating energy storage in Preisach models for which $\mu \in \mathcal{M}_P$, in order to form a basis for the subsequent use of energy arguments in controller design and stability analysis. In doing so, an input-output pair representing instantaneous power is identified and used to compute the total energy input over time. Examples of such "energy pairs" are force and velocity in mechanical systems, and current and voltage in electrical systems.

In actuators, u is often some form of mechanical or electrical force, and y is displacement. Hence, $u\dot{y}$ has units of power. The instantaneous power input at time t is $u(t)\dot{y}(t)$, and the total energy input as a result of applying u from t_o to t_1 is

$$Q = \int_{t_o}^{t_1} u(t)\dot{y}(t)dt.$$

7.1.1 Energy Storage, Recovery & Loss in Relays

In order to understand the energy characteristics of the Preisach model, it is useful to begin with the study of the individual weighted relays which make up the model.

Consider the arbitrary weighted relay $\gamma_{\alpha\beta}$ of Figure 7.1, with weighting $\mu(\alpha, \beta) \geq 0$, and suppose it is subjected to an input that switches the relay into the "up" position and later back into the "down" position: for instance, $u(t) = -u_1 \cos(t)$ with $u_1 > \max\{|\alpha|, |\beta|\}$. The effect of this input is illustrated in Figure 7.2. Since $-u_1 < \beta$, the relay is in the "down" position at time $t = 0$. Suppose the relay switches "up" at t_α and "down" again at t_β. Then

$$\langle u, \dot{y}_{\alpha\beta} \rangle_{2\pi} = \int_0^{2\pi} u\, \dot{y}_{\alpha\beta} dt$$

$$
\begin{aligned}
&= \int_0^{2\pi} u\, 2\mu(\alpha,\beta)[\delta(t-t_\alpha) - \delta(t-t_\beta)]dt \\
&= 2\mu(\alpha,\beta)[u(t_\alpha) - u(t_\beta)] \\
&= 2\mu(\alpha,\beta)(\alpha-\beta).
\end{aligned}
$$

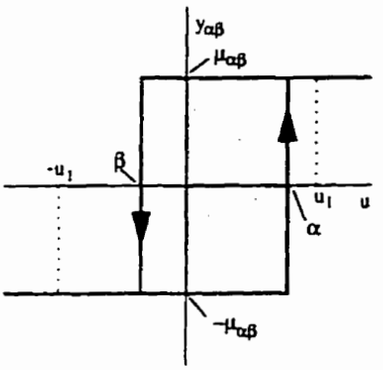

Figure 7.1: Weighted Relay

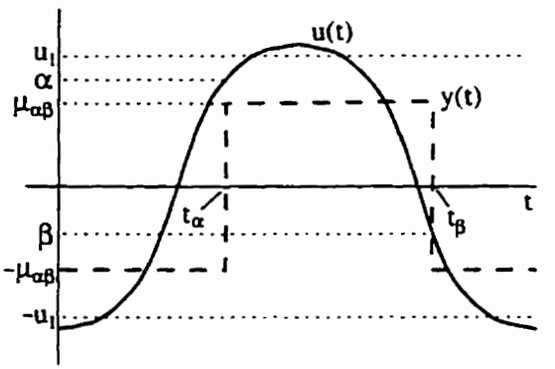

Figure 7.2: Test Cosine Input

Define $q_\alpha \triangleq 2\mu(\alpha,\beta)\alpha$ and $q_\beta \triangleq -2\mu(\alpha,\beta)\beta$. If the product $u\dot{y}_{\alpha\beta}$ has units of power, then q_α and q_β represent the net work involved in switching the relay as u passes α and β, respectively. If either q_α or q_β is negative for a particular relay, this implies that energy is recovered from that relay when it switches. This is a more general approach that that taken in [43], where it was assumed that the total energy loss was split evenly between switches, so that $q_\alpha = q_\beta = \mu(\alpha,\beta)(\alpha-\beta)$. Note that the energy lost in one cycle is equal to the area of the relay. This agrees with the well-known result that the hysteretic energy loss in each cycle of a magnetic circuit is equal to the area of the hysteresis loop[e.g. 1].

7.1.2 Energy Stored in the Preisach Model

If $\mu \in \mathcal{M}_P$, the regions of $\mathcal{P}_r$ in which relays store recoverable energy are delineated by the axes of the Preisach plane. For notational convenience, define the following

"quadrants" (cf. Figure 7.3):

$$\mathcal{Q}_1 \triangleq \{(\alpha,\beta)|\alpha > 0, \beta > 0\} \cap \mathcal{P}_r.$$
$$\mathcal{Q}_2 \triangleq \{(\alpha,\beta)|\alpha \geq 0, \beta \leq 0\} \cap \mathcal{P}_r.$$
$$\mathcal{Q}_3 \triangleq \{(\alpha,\beta)|\alpha < 0, \beta < 0\} \cap \mathcal{P}_r$$

These are three of the four "standard" quadrants, restricted to those points contained in $\mathcal{P}_r$.

Relays which have recoverable stored energy are those for which the next switch results in a negative energy transfer. For example, since $q_\beta = -2\mu(\alpha,\beta)\beta$ and $\beta \geq 0$ in $\mathcal{Q}_1$, relays in that quadrant store recoverable energy whenever their next switch is from $+1$ to -1. The amount of recoverable stored energy is $|q_\beta|$. The energy storage capabilities of individual relays are summarized in Table 7.1.

region of $\mathcal{P}$	current relay state	energy transfer at next switch	recoverable stored energy
$\mathcal{Q}_1$	$+1$	$q_\beta \leq 0$	$\|q_\beta\|$
	-1	$q_\alpha \geq 0$	none
$\mathcal{Q}_2$	$+1$	$q_\beta \geq 0$	none
	-1	$q_\alpha \geq 0$	none
$\mathcal{Q}_3$	$+1$	$q_\beta \geq 0$	none
	-1	$q_\alpha \leq 0$	$\|q_\alpha\|$

Table 7.1: Recoverable Energy Storage in Relays

If $\mu \in \mathcal{M}_P$, the energy storage properties may be conceptualized as follows. Any relay $\gamma_{\alpha\beta}$ in $\mathcal{Q}_2$ may be represented by a mass system with a non-zero coefficient of static friction. Moving the mass is analogous to switching the relay. To move the

mass in either direction (switch $\gamma_{\alpha\beta}$ from -1 to +1, or +1 to -1) requires that the static friction force be overcome. In each case, this represents energy which is lost in moving the mass.

Relays in $\mathcal{Q}_1$ may be thought of as mass-spring systems, again with a non-zero coefficient of static friction[1]. When the mass has been given a positive displacement ($\gamma_{\alpha\beta}$ is in the +1 state), the spring stores some potential energy. This energy is released when the input force is reduced below the static friction force, and the mass moves back ($\gamma_{\alpha\beta}$ switches from +1 to -1). A similar analogy holds for relays in $\mathcal{Q}_3$.

Using the information of Table 7.1, recoverable energy stored in the Preisach model can be computed from the Preisach plane diagram. If $\mu \in \mathcal{M}_P$, recoverable energy is stored in relays in $\mathcal{Q}_1$ which are in the "+1" state, and in relays in $\mathcal{Q}_3$ which are in the "-1" state.

Figure 7.3a shows a sample boundary for $u < 0$, with the quadrants labeled. The shaded region contains points representing those relays in which recoverable energy is stored. The amount of energy stored in each relay is $|q_\alpha|$, and the total recoverable stored energy Q_r is given by

$$Q_r = \iint_\Omega |q_\alpha| \, d\alpha d\beta.$$

Since $\Omega \subset \mathcal{Q}_3$, $\alpha < 0$ and this gives

$$Q_r = -2 \iint_{\mathcal{Q}_3 \cap \mathcal{P}_-} \mu(\alpha, \beta) \alpha d\alpha d\beta.$$

[1]Note that this analogy is not perfect: the relay transitions at $u = \alpha$ and $u = \beta$ have infinite slope, implying a zero spring coefficient.

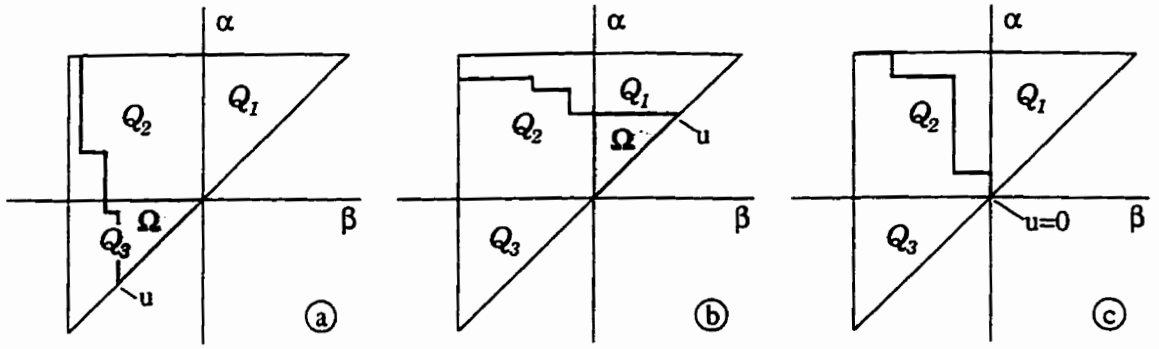

Figure 7.3: Regions of Stored Energy in $\mathcal{P}_r$

If on the other hand the boundary is as in Figure 7.3b, then

$$\begin{aligned} Q_r &= \iint_{Q_1 \cap \mathcal{P}_+} |q_\beta| \, d\alpha d\beta \\ &= 2 \iint_{Q_1 \cap \mathcal{P}_+} \mu(\alpha, \beta) \beta \, d\alpha d\beta. \end{aligned}$$

At any particular instant, the boundary can only intersect one of these quadrants, so any energy stored in the system is *either* in relays in Q_1 *or* in those in Q_3. For any boundary $B \in \mathcal{B}$, $Q_r(B)$ can be written as the sum of two terms, of which one, or possibly both, is zero:

$$\begin{aligned} Q_r(B) &= \iint_{Q_1 \cap \mathcal{P}_+} |q_\beta| \, d\alpha d\beta + \iint_{Q_3 \cap \mathcal{P}_-} |q_\alpha| \, d\alpha d\beta \\ &= 2 \iint_{Q_1 \cap \mathcal{P}_+} \mu(\alpha, \beta) \beta \, d\alpha d\beta - 2 \iint_{Q_3 \cap \mathcal{P}_-} \mu(\alpha, \beta) \alpha \, d\alpha d\beta \\ &= 2 \iint_{Q_1 \cap P_+ B} \mu(\alpha, \beta) \beta \, d\alpha d\beta - 2 \iint_{Q_3 \cap P_- B} \mu(\alpha, \beta) \alpha \, d\alpha d\beta. \end{aligned} \tag{7.1}$$

In determining whether a system dissipates energy, it is often assumed that a state of minimum stored energy can be determined. In stable linear systems, a common approach to the determination of this state is to set the system input to

zero and find the steady state. In the case of the Preisach model, a similar concept may be proposed.

Proposition 7.1 (Zero Energy Storage)
If at any time t the input $u(t) = 0$, then the Preisach model is in a state of zero stored energy.

Proof
Since boundaries are always non-increasing, then for any time t at which $u(t) = 0$, the corresponding boundary B intersects the line $\alpha = \beta$ at $(0,0)$, and must be entirely contained in Q_2 (cf. Figure 7.3c). Recalling that P_+B is the region of $\mathcal{P}_r$ containing relays which are below the graph of B, we see that $Q_1 \cap P_+B = \emptyset$, and similarly, $Q_3 \cap P_-B = \emptyset$.

$$\begin{aligned} Q_r(B) &= 2 \iint_{Q_1 \cap P_+B} \mu(\alpha,\beta)\beta d\alpha d\beta - 2 \iint_{Q_3 \cap P_-B} \mu(\alpha,\beta)\alpha d\alpha d\beta \\ &= 0, \end{aligned}$$

since the areas of integration are empty. ∎

This result implies that there are an infinite number of states in which the Preisach model has zero stored energy. These states correspond to the vertical line $u = 0$ in the input-output plane. The associated output is the remnant hysteresis, the magnitude of which depends on the past history. In particular, the anhysteretic state is a state of zero energy storage.

7.1.3 Energy Transfer in the Preisach Model

In the previous section, a formula was derived for the energy stored in the Preisach model. This section presents a method of computing the total energy transferred

to the system by a given input u.

Theorem 7.2 (Net Energy Transfer)

If u is a monotonic input which sweeps a region Ω in the Preisach plane, then the total energy transferred to the system by u is

$$\begin{aligned} Q &= \iint_{\Omega} 2\mu(\alpha,\beta)\alpha d\alpha d\beta, \quad \text{if } \dot{u} > 0, \\ \text{or} \quad Q &= -\iint_{\Omega} 2\mu(\alpha,\beta)\beta d\alpha d\beta, \quad \text{if } \dot{u} < 0. \end{aligned} \tag{7.2}$$

Proof

Consider an input which increases monotonically from t_1 to t_2, transferring points in the region Ω from $\mathcal{P}_-$ to $\mathcal{P}_+$, as shown in Figure 7.4.

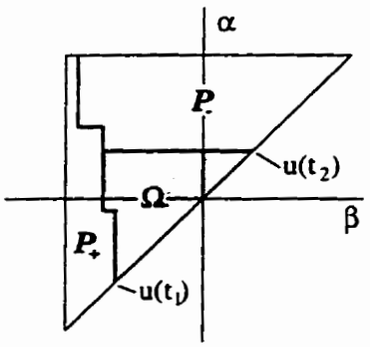

Figure 7.4: Proof of Theorem 7.2

For every relay switched, the energy transferred is $q_\alpha = 2\mu(\alpha,\beta)\alpha$. The total energy input, as u sweeps from $u(t_1)$ to $u(t_2)$, is given by the sum of q_α over all the relays switched:

$$Q = 2\iint_{\Omega} \mu(\alpha,\beta)\alpha d\alpha d\beta.$$

The proof is similar in the case where u is decreasing. ∎

Note that Theorem 7.2 is general, in that no assumptions have been made on μ.

Whether (7.2) represents net energy input or recovered will depend on the shape and sign of $\mu(\alpha,\beta)$ on Ω, and the location of Ω in $\mathcal{P}_r$.

Equation (7.2) can be used to compute the total energy transferred due to any continuous input u composed of monotonic segments. If $\mu \in \mathcal{M}_P$, the result can be combined with the equation for stored energy (7.1) to determine the hysteretic energy loss for a given input u.

7.2 Dissipativity of the Preisach Model

In his pioneering work on dissipative dynamical systems[65], Willems sets out a framework for investigating the energy-dissipating qualities of a system. These qualities are intimately related to system stability, and it was shown[65] that the major input-output stability results can all be cast as special cases of dissipativity theory. In this section, the definition of dissipativity is recalled and the dissipativity of Preisach models with $\mu \in \mathcal{M}_P$ is shown.

Dissipativity is defined in terms of the relationship between two functions known as the *supply rate* and the *storage function*.

Definition 7.1 (Dissipativity [65])
A dynamical system Σ is said to be dissipative with respect to the (locally integrable) supply rate $w : U \times Y \mapsto \boldsymbol{R}$ if there exists a non-negative function $S : \mathcal{X} \mapsto \boldsymbol{R}^+$, called the storage function, such that for all $t_1 \geq t_o$, $x_o \in \mathcal{X}$, and $u \in U$,

$$S(x_o) + \int_{t_o}^{t_1} w(u(t), y(t))dt \geq S(x_1)$$

where $x_1 = \phi(t_1, t_o, x_o, u)$.

Essentially, for a system to be dissipative, the sum of the storage in the initial state and the supply generated by the input must not be less than the storage in the final state. In other words, there is no internal generation of storage. The word "energy" is conspicuously absent from this description: while dissipativity theory is based on energy concepts, the supply rate and storage function are generalizations of the physical concepts of "rate of energy supply" and "amount of stored energy". There need not be any physical energy interpretation in order for the definition or related results to hold.

The more restrictive condition that

$$\int_{t_o}^{t_1} uy\, dt \geq 0,$$

often called "passivity", is a specific case of dissipativity with $w(u,y) = uy$ and $S = 0$. This will be discussed in more detail in Chapter 8.

Although in general, storage functions for physical systems are not unique, it is often the case that the formula for the actual energy stored in a system is a storage function for some related supply rate. It will be shown that the Preisach model is dissipative with respect to the supply rate $w(u,y) = u\dot{y}$, by demonstrating that the recoverable stored energy Q_r is a storage function for this supply rate.

The proof of dissipativity requires the following definition of the characteristic function of a set.

Definition 7.2 (Characteristic Function[e.g. 47])
If A is a subset of a space X, the characteristic function of A, $\chi_A : X \mapsto \{0,1\}$ is defined by

$$\chi_A(x) = \begin{cases} 1, & \text{if } x \in A \\ 0, & \text{if } x \notin A. \end{cases}$$

Lemma 7.3

Let A and B be subsets of a space X. Then for all $x \in X$,

1. *if $A \cap B = \emptyset$, then $\chi_A(x) + \chi_B(x) = \chi_{A \cup B}(x)$, and*
2. *if $B \subset A$, then $\chi_A(x) - \chi_B(x) = \chi_{A \sim B}(x)$,*

where $\sim$ indicates the set difference operation.

Proof

The proof of this Lemma is straightforward. ∎

Theorem 7.4 (Preisach Model Dissipativity)

If $\mu \in \mathcal{M}_P$, the Preisach model is dissipative with respect to the supply rate $w(u, y) = u\dot{y}$.

Proof

The recoverable stored energy, for any $B \in \mathcal{B}$, is

$$Q_r(B) = 2 \iint_{Q_1 \cap P_+ B} \mu(\alpha, \beta) \beta d\alpha d\beta - 2 \iint_{Q_3 \cap P_- B} \mu(\alpha, \beta) \alpha d\alpha d\beta.$$

If $\mu \in \mathcal{M}_P$, then since $\alpha \leq 0$ in Q_3 and $\beta \geq 0$ in Q_1, $Q_r(B) \geq 0$. Also, μ and $\mathcal{P}_r$ are bounded, so $Q_r(B) < \infty$, and $Q_r : \mathcal{B} \mapsto \mathbf{R}^+$. It remains to show that for any initial state B_o and $u \in \mathcal{U}[t_o, t_1]$ such that $B_1 = \phi(t_1, t_o, B_o, u)$, the dissipativity inequality

$$Q_r(B_o) + \int_{t_o}^{t_1} u\dot{y} dt \geq Q_r(B_1) \tag{7.3}$$

is satisfied.

For each relay $\gamma_{\alpha\beta}$, let $n_{\alpha\beta}$ be the number of times that relay is fully cycled (switched twice) by u. The energy transferred in one full cycle is equal to the area of the relay, $2\mu(\alpha,\beta)(\alpha-\beta) \geq 0$. and represents a net energy loss. Suppose first that all $n_{\alpha\beta}$ are finite. The case where $n_{\alpha\beta}$ is infinite for some $\gamma_{\alpha\beta}$ is discussed at the end of the proof.

Let Ω^e be the collection of relays which are switched an even number of times $(2n_{\alpha\beta})$ by u. The energy transfer for each relay in this region is $2n_{\alpha\beta}\mu(\alpha,\beta)(\alpha-\beta) \geq 0$. Denote by $Q^e \geq 0$ the *total* energy transferred to *all* relays in Ω^e.

Let Ω_α be the collection of relays which are switched an odd number of times $(2n_{\alpha\beta}+1)$ by u, and whose last switch was at $u=\alpha$ (from -1 to +1). The energy transferred to each of these relays is $2n_{\alpha\beta}\mu(\alpha,\beta)(\alpha-\beta)+q_\alpha$. Let $Q_\alpha \geq 0$ be the total energy transferred to relays in Ω_α after each has been fully cycled $n_{\alpha\beta}$ times. Each relay then undergoes one final switch from -1 to +1, so that the total energy transfer to relays in Ω_α is

$$Q_\alpha + \iint_{\Omega_\alpha} q_\alpha d\alpha d\beta.$$

Similarly, define Ω_β as the collection of relays which are switched an odd number of times $(2n_{\alpha\beta}+1)$ by u, and whose last switch was at $u=\beta$ (from +1 to -1). Let $Q_\beta \geq 0$ be the total energy transferred to relays in Ω_β after each has been fully cycled $n_{\alpha\beta}$ times. The energy transfer for the final switch of each relay in Ω_β is q_β, so the total energy transferred by u to relays in Ω_β is

$$Q_\beta + \iint_{\Omega_\beta} q_\beta d\alpha d\beta.$$

The total energy transfer from t_o to t_1 is

$$\int_{t_o}^{t_1} uy dt = Q^e + Q_\alpha + \iint_{\Omega_\alpha} q_\alpha d\alpha d\beta + Q_\beta + \iint_{\Omega_\beta} q_\beta d\alpha d\beta$$

$$\geq \iint_{\Omega_\alpha} q_\alpha d\alpha d\beta + \iint_{\Omega_\beta} q_\beta d\alpha d\beta.$$

In $\mathcal{Q}_2$, both q_α and q_β are non-negative, so

$$\begin{aligned}\int_{t_o}^{t_1} u\dot{y}dt &\geq \iint_{\Omega_\alpha \cap \mathcal{Q}_1} q_\alpha d\alpha d\beta + \iint_{\Omega_\alpha \cap \mathcal{Q}_3} q_\alpha d\alpha d\beta + \iint_{\Omega_\beta \cap \mathcal{Q}_1} q_\beta d\alpha d\beta + \iint_{\Omega_\beta \cap \mathcal{Q}_3} q_\beta d\alpha d\beta \\ &= \iint_{\Omega_\alpha \cap \mathcal{Q}_1} 2\mu(\alpha,\beta)\alpha d\alpha d\beta + \iint_{\Omega_\alpha \cap \mathcal{Q}_3} 2\mu(\alpha,\beta)\alpha d\alpha d\beta \\ &\quad - \iint_{\Omega_\beta \cap \mathcal{Q}_1} 2\mu(\alpha,\beta)\beta d\alpha d\beta - \iint_{\Omega_\beta \cap \mathcal{Q}_3} 2\mu(\alpha,\beta)\beta d\alpha d\beta.\end{aligned}$$

Since $\alpha \geq \beta$, the first and last terms above can be replaced in the inequality:

$$\begin{aligned}\int_{t_o}^{t_1} u\dot{y}dt &\geq \iint_{\Omega_\alpha \cap \mathcal{Q}_1} 2\mu(\alpha,\beta)\beta d\alpha d\beta + \iint_{\Omega_\alpha \cap \mathcal{Q}_3} 2\mu(\alpha,\beta)\alpha d\alpha d\beta \\ &\quad - \iint_{\Omega_\beta \cap \mathcal{Q}_1} 2\mu(\alpha,\beta)\beta d\alpha d\beta - \iint_{\Omega_\beta \cap \mathcal{Q}_3} 2\mu(\alpha,\beta)\alpha d\alpha d\beta.\end{aligned}$$

Introducing the characteristic functions for Ω_α and Ω_β, this can be written

$$\begin{aligned}\int_{t_o}^{t_1} u\dot{y}dt &\geq \iint_{\mathcal{Q}_1} 2\mu(\alpha,\beta)\beta\chi_{\Omega_\alpha} d\alpha d\beta + \iint_{\mathcal{Q}_3} 2\mu(\alpha,\beta)\alpha\chi_{\Omega_\alpha} d\alpha d\beta \\ &\quad - \iint_{\mathcal{Q}_1} 2\mu(\alpha,\beta)\beta\chi_{\Omega_\beta} d\alpha d\beta - \iint_{\mathcal{Q}_3} 2\mu(\alpha,\beta)\alpha\chi_{\Omega_\beta} d\alpha d\beta \\ &= \iint_{\mathcal{Q}_1} 2\mu(\alpha,\beta)\beta\left[\chi_{\Omega_\alpha} - \chi_{\Omega_\beta}\right] d\alpha d\beta - \iint_{\mathcal{Q}_3} 2\mu(\alpha,\beta)\alpha\left[\chi_{\Omega_\beta} - \chi_{\Omega_\alpha}\right] d\alpha d\beta.\end{aligned} \tag{7.4}$$

But Ω_α contains all the relays $\gamma_{\alpha\beta}$ which were in $\mathcal{P}_-$ at t_o and $\mathcal{P}_+$ at t_1. Similarly, Ω_β is exactly all those relays which were switched from $\mathcal{P}_+$ at t_o to $\mathcal{P}_-$ at t_1. Then P_+B_1, the collection of relays which are in the $+1$ state at t_1, can be written as "all relays which started in the $+1$ state, less those which were switched to -1, plus those which were switched from -1 to $+1$":

$$P_+B_1 = [P_+B_o \sim \Omega_\beta] \cup \Omega_\alpha.$$

But $\Omega_\beta \subset P_+B_o$, and $\Omega_\alpha \cap P_+B_o = \emptyset$, so by Lemma 7.3

$$\begin{aligned}\chi_{P_+B_1} &= \chi_{[P_+B_o \sim \Omega_\beta]\cup\Omega_\alpha} \\ &= \chi_{P_+B_o\sim\Omega_\beta} + \chi_{\Omega_\alpha} \\ &= \chi_{P_+B_o} - \chi_{\Omega_\beta} + \chi_{\Omega_\alpha}.\end{aligned}$$

and

$$\chi_{\Omega_\alpha} - \chi_{\Omega_\beta} = \chi_{P_+B_1} - \chi_{P_+B_o}. \tag{7.5}$$

Similarly,

$$P_-B_1 = [P_-B_o \sim \Omega_\alpha] \cup \Omega_\beta,$$

and

$$\chi_{\Omega_\beta} - \chi_{\Omega_\alpha} = \chi_{P_-B_1} - \chi_{P_-B_o}. \tag{7.6}$$

Substituting (7.5) and (7.6) in equation (7.4) gives

$$\begin{aligned}\int_{t_o}^{t_1} uy dt &\geq \iint_{\mathcal{Q}_1} 2\mu(\alpha,\beta)\beta\left[\chi_{P_+B_1} - \chi_{P_+B_o}\right] d\alpha d\beta - \\ &\qquad \iint_{\mathcal{Q}_3} 2\mu(\alpha,\beta)\alpha\left[\chi_{P_-B_1} - \chi_{P_-B_o}\right] d\alpha d\beta \\ &= \iint_{\mathcal{Q}_1} 2\mu(\alpha,\beta)\beta\chi_{P_+B_1} d\alpha d\beta - \iint_{\mathcal{Q}_3} 2\mu(\alpha,\beta)\alpha\chi_{P_-B_1} d\alpha d\beta \\ &\qquad - \left[\iint_{\mathcal{Q}_1} 2\mu(\alpha,\beta)\beta\chi_{P_+B_o} d\alpha d\beta - \iint_{\mathcal{Q}_3} 2\mu(\alpha,\beta)\alpha\chi_{P_-B_o} d\alpha d\beta\right] \\ &= \iint_{\mathcal{Q}_1\cap P_+B_1} 2\mu(\alpha,\beta)\beta d\alpha d\beta - \iint_{\mathcal{Q}_3\cap P_-B_1} 2\mu(\alpha,\beta)\alpha d\alpha d\beta \\ &\qquad - \left[\iint_{\mathcal{Q}_1\cap P_+B_o} 2\mu(\alpha,\beta)\beta d\alpha d\beta - \iint_{\mathcal{Q}_3\cap P_-B_o} 2\mu(\alpha,\beta)\alpha d\alpha d\beta\right] \\ &= Q_r(B_1) - Q_r(B_o).\end{aligned}$$

So the dissipation inequality (7.3) is satisfied.

If $n_{\alpha\beta}$ is infinite for any $\gamma_{\alpha\beta}$, then that relay undergoes an infinite number of full cycles. Since energy is lost in each full cycle, the total energy transfer is positive and infinite. But $Q_r(B)$ is bounded for every B, so the dissipativity inequality (7.3) still holds. The Preisach model is dissipative with respect to the supply rate $w(u, y) = u\dot{y}$. ■

It is important to note the sufficient nature of the dissipativity result of Theorem 7.4. It may be that some physical systems which are in fact dissipative do not have non-negative weighting functions. Indeed, it was seen in Chapter 5 that weighting functions with negative regions resulted in better matches for the SMA actuators. Furthermore, the relationship between magnetic field and strain in a magnetostrictive material displays a so-called "butterfly" hysteresis[9], sketched in Figure 7.5. A decrease in applied field Δf can result in an increase in strain $\Delta\varepsilon$. From Proposition 3.2, a Preisach model for this hysteresis satisfies

$$\Delta\varepsilon = 2\,\mathrm{sgn}[\Delta f] \iint_{\Omega} \mu(\alpha,\beta)\,d\alpha\,d\beta,$$

so that if Δf decreases and $\Delta\varepsilon$ increases,

$$\iint_{\Omega} \mu(\alpha,\beta)\,d\alpha\,d\beta < 0$$

and $\mu \notin \mathcal{M}_P$.

Intuitively, these physical systems also dissipate energy, and it is apparent that the requirement that μ be non-negative is overly restrictive. Understanding the reasons for the conservative nature of this result should be one area of focus for future research.

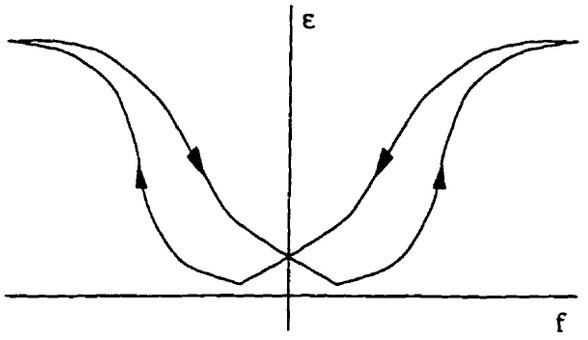

Figure 7.5: Characteristic of Magnetostrictive Hysteresis

7.3 Summary

This chapter examined the energy properties of the Preisach model. In the case of non-negative weighting functions, it was seen that the Preisach plane provides an intuitive framework for analyzing energy storage and loss in the hysteresis. Based on individual relay characteristics, regions in $\mathcal{P}_r$ which are able to store recoverable energy were identified. A formula was then derived which allows the computation of recoverable energy stored as a function of the boundary, and states of minimum energy were identified.

In the second section, it was shown that if $\mu \in \mathcal{M}_P$, the associated Preisach model is dissipative. Although this result is significant, it is nonetheless only sufficient. The example of magnetostrictive materials was cited as a physical system for which a Preisach weighting function would have negative areas.

Dissipativity theory is a powerful tool for the design of stabilizing controllers. It is important to note that, while the dissipativity investigation was guided by energy arguments, the theory is more general. The definitions are not specifically tied to physical energy, and related results hold whether an energy interpretation of the supply rate and storage function exist or not. One use of dissipativity will

be detailed in the next chapter, and another application set out for the future in the final chapter.

Chapter 8

Controller Design

8.1 Background

Figure 8.1 shows a standard single-input single-output feedback interconnection. The system being controlled, H_2, is known as the "plant", and H_1 is the controller. External inputs are labeled r_i, the inputs to the plant and controller are u_i, and the outputs y_i. The input r_2 is typically a disturbance on the control signal. The goal of implementing a controller in a feedback system is to attempt to have the plant output track a desired reference signal r_1. If the reference is time-varying, the controller is referred to as a "tracking controller". If r_1 is constant, the controller is a "regulator".

There are two main aspects to the controller design problem. The first is *stability*: given a plant H_2, what types of controllers will ensure that for "well-behaved" reference signals r, the internal signals u and outputs y will also be "well-behaved". A *robust* stabilizing controller has the ability to maintain stability under small perturbations in plant dynamics. For example, such perturbations may occur as a

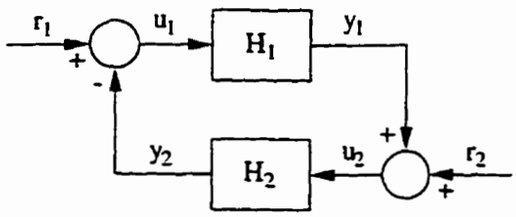

Figure 8.1: Standard Feedback Interconnection

result of system noise or changes in component characteristics due to aging.

The second problem is *performance*, which can be measured in a number of ways. How *closely* does a controller achieve the objective? How *quickly*? How much *energy* is required? The primary result of this chapter is concerned with the stability aspect of controller design. A second preliminary result regarding optimal regulation of Preisach hystereses is also presented.

Before stability can be formally defined, a few mathematical definitions are required.

8.1.1 Mathematical Definitions

This section introduces some of the basic mathematical definitions and notation. The common concepts of L_2 spaces, extended spaces and truncation, as well as signal norms and inner products, are presented. To represent the hysteretic behaviour of the Preisach model, the concept of a relation is defined. $\mathbf{R}$ is the set of all real numbers, and $\mathbf{R}^+ = [0, \infty)$.

Definition 8.1 (Truncation)

Let x be a function mapping $\boldsymbol{R} \mapsto \boldsymbol{R}$, and $T < \infty$. Then the truncation of x

is defined as

$$x_T(t) \triangleq \begin{cases} x(t) & t \leq T \\ 0 & t > T. \end{cases}$$

Definition 8.2 (L_p and L_{pe} Spaces)

The space $L_p(-\infty, \infty; \mathbb{R})$ includes all Lebesgue measurable functions[1] $x : \mathbb{R} \mapsto \mathbb{R}$ *for which*

$$\int_{-\infty}^{\infty} |x(t)|^p \, dt < \infty.$$

The extended space $L_{pe}(-\infty, \infty; \mathbb{R})$ is composed of Lebesgue measurable functions for which

$$\int_{-\infty}^{\infty} |x_T(t)|^p \, dt < \infty,$$

for all $T \geq 0$.

To simplify notation, the spaces $L_p(-\infty, \infty; \mathbf{R})$ and $L_{pe}(-\infty, \infty; \mathbf{R})$ are often referred to as L_p and L_{pe}, respectively. Note that $L_p \subset L_{pe}$.

Central to the notion of stability is the concept of a "well-behaved" signal. A common definition of a "well-behaved" signal is one which does not have unbounded energy; that is, it must be square-integrable. The space L_2 contains all such signals, and will play a key role in the definition of input-output stability. An example of a function which is in L_{2e}, but not in L_2 is $x(t) = t^2$. Functions which are not in L_{2e} have "finite escape time", implying that there exists some finite time t_1 at which it "blows up". An example of such a function is $x(t) = \tan(t)$.

[1] For our purposes, functions which are Lebesgue measurable are essentially those which are bounded except at a countable number of points. A more rigorous definition can be found in [e.g. 52].

Definition 8.3 (p-Norm)

For functions $x \in L_p$, the p-norm ($\|\cdot\|_p : L_p \mapsto \mathbb{R}^+$) of x is defined as

$$\|x\|_p \triangleq \left[\int_{-\infty}^{\infty} |x(t)|^p \, dt\right]^{\frac{1}{p}}.$$

Define the truncated p-norm, $\|\cdot\|_{Tp} : L_{pe} \mapsto \mathbb{R}^+$, as

$$\begin{aligned} \|x\|_{Tp} &\triangleq \|x_T\|_p \\ &= \left[\int_{-\infty}^{\infty} |x_T(t)|^p \, dt\right]^{\frac{1}{p}}. \end{aligned}$$

Where the subscript p is omitted, the 2-norm is implied (ie. $p = 2$).

Definition 8.4 (Inner Product)

Given two scalar functions $x, y \in L_2$, the inner product of these two functions is defined as

$$\langle x, y \rangle \triangleq \int_{-\infty}^{\infty} x(t)y(t)dt,$$

and the truncated inner product, for $x, y \in L_{2e}$, is

$$\begin{aligned} \langle x, y \rangle_T &\triangleq \langle x_T, y_T \rangle \\ &= \int_{-\infty}^{\infty} x_T(t)y_T(t)dt \\ &= \int_{-\infty}^{T} x(t)y(t)dt. \end{aligned}$$

Note that $\langle x, x \rangle = \|x\|^2$, and $\langle x, x \rangle_T = \|x\|_T^2$.

Definition 8.5 (Relation [69])

A relation $\mathcal{R}$ on a space $\mathcal{X}$ defines a set of ordered pairs $(x, y) \in \mathcal{X} \times \mathcal{X}$. The domain and range of a relation can be defined as

$$Do(\mathcal{R}) \triangleq \{x | x \in \mathcal{X} \text{ and } \exists y \in \mathcal{X} \text{ such that } (x, y) \in \mathcal{R}\} \subseteq \mathcal{X}$$

and

$$Ra(\mathcal{R}) \triangleq \{y | y \in \mathcal{X} \text{ and } \exists x \in \mathcal{X} \text{ such that } (x,y) \in \mathcal{R}\} \subseteq \mathcal{X}$$

The nature of a relation is such that a given $x \in Do(\mathcal{R})$ may correspond to more than one $y \in Ra(\mathcal{R})$. As well, there may be more than one $x \in Do(\mathcal{R})$ mapping to the same $y \in Ra(\mathcal{R})$. It is this behaviour which makes relations useful in describing hysteretic systems. The Preisach operator defines a relation Γ whose domain is C^0. As was shown in Chapter 4, if μ is in $\mathcal{M}_P$, $Ra(\Gamma) \subset C^0$ as well.

The notation $(x,y) \in \mathcal{R}$ implies "$x \in Do(\mathcal{R})$ and y in the corresponding set $\mathcal{R}x$". This is different from saying "$x \in Do(\mathcal{R})$ and $y \in Ra(\mathcal{R})$", since there may be some $x \in Do(\mathcal{R})$ and $y \in Ra(\mathcal{R})$ which are unrelated.

Definition 8.6 (Finite Gain)

A relation $\mathcal{R}$, on $\mathcal{X}$, is said to have finite gain if there exists some constant $\gamma \in \mathbb{R}^+$ such that $\|y\| \leq \gamma \|x\|$, for all $(x,y) \in \mathcal{R}$.

The following definition of feedback stability is similar to that found in [12].

Definition 8.7 (Stability)

The feedback system of Figure 8.1, where H_1 and H_2 are relations, will be called stable if, for each $u_1 \in Do(H_1)$ and $u_2 \in Do(H_2)$ there exist finite k_e, k_y independent of T such that $\|e_i\|_T \leq k_e(\|u_1\|_T + \|u_2\|_T)$ and $\|y_i\|_T \leq k_y(\|u_1\|_T + \|u_2\|_T)$, $i = 1,2,\ \forall T \geq 0$.

It has been shown[e.g. 60] that the boundedness of e_i and y_i are equivalent, and only one need be shown to demonstrate system stability.

8.1.2 Previous Work

With the keen interest shown in smart materials in recent years, and the general appeal of the Preisach model, it is not surprising that several works exist on control strategies for this model.

The majority of results pertaining to Preisach model control are concerned with performance improvements. A popular approach is to identify a Preisach model for the plant to be controlled and linearize the hysteresis by cascading an inverse model with the plant. If the identified FOD surface is monotonic in both α and β, then model inversion is possible[43]. This technique has been applied successfully to piezoceramics in [26] and resistance control of SMA in [42]. A similar idea was proposed in [18] for tracking control of a piezoceramic actuator. Recently a new technique, motivated by study of the Preisach model, has been proposed for partial linearization of hysteresis by a linear compensator[8]. The phase shift introduced by the delay in the hysteresis is identified experimentally over a frequency range of interest. A linear compensator called a *phaser*, which has the opposite phase, is placed in front of the hysteresis. Good experimental linearization of a piezoceramic actuator is achieved.

Further developments of note are found in [5], where the existence of optimal controls for a class of hysteresis functionals which include the Preisach model, is shown. In [58], an adaptive control scheme for unknown hystereses of a hybrid play/stop type is presented. Although not directly related to the Preisach model, this last result is exciting given the onerous identification methods used for Preisach models.

All of these works have been concerned with performance or identification aspects. One reference has discussed the issue of stability when an active SMA wire

is used to dampen vibrations in a flexible beam[13]. The authors observe system instability, despite very low bandwidth, and demonstrate that the instability can be removed through the correct choice of feedback variable. A qualitative stability analysis using phase plane techniques is given.

8.2 Velocity Feedback

In some applications, a controller is designed which makes use of velocity measurements to achieve its objective. For example, in [15], the authors discuss the damping of vibrations in a flexible beam using piezoceramic actuators. The actuators are bonded to the beam, and the strain which they generate is measured using strain gauges. Measurements of the rate of change of strain are fed back to a proportional-gain controller, which is able to achieve significant damping of beam vibrations.

In this section, it is shown that the relationship between the Preisach model input and the derivative of its output is *passive*. This allows a whole class of stabilizing controllers for velocity feedback applications to be determined. This result encompasses the application mentioned in [15], and is similar to classical results obtained using passivity theory for position and velocity feedback (PD control) of robot manipulators. It has been shown[e.g. 55] that a PD controller provides robust stability for position control of robot manipulators. The extension of the present results to include position feedback is an area of continuing research.

8.2.1 Passivity

Passivity is a characteristic of a physical system which allows the design of robust stabilizing controllers based on the principle that if both controller and plant are dissipating energy, then a standard negative-feedback configuration should be stable. Robustness is obtained since a plant which dissipates energy generally continues to do so despite small changes in dynamics. It is a common approach in analyzing the stability of robotic and other non-linear systems.

The definition of passivity is a special case of dissipativity, in which the supply rate is $w(u, y) = uy$ and the storage function is zero. Like dissipativity, the theory is motivated by the study of energy storage, where the input-output pair represents instantaneous power. Again, however, the theory and results continue to hold when such an interpretation is not available.

Some examples of such energy pairs are: force and velocity in mechanical systems; current and voltage in electrical systems. In actuator control, the input is generally some form of mechanical or electrical force, and the output is displacement. Hence, to get the force-velocity energy pair, we examine the passivity of $(u, \dot{y})$.

Mathematically, the passivity of a system is expressed as follows:

Definition 8.8 (Passivity[e.g. 12])
A relation $\mathcal{R}$ is said to be passive[2] *if there exists $\delta \geq 0$ and constant β such that, for all $T < \infty$ and $u \in Do(\mathcal{R})$,*

$$\langle u, \mathcal{R}u \rangle_T \geq \delta \|u\|_T^2 + \beta. \tag{8.1}$$

[2]In more recent work, this general definition is referred to as "passive *with bias*", and the more common definition of passivity is given with $\beta = 0$.

$\mathcal{R}$ is said to be strictly passive if (8.1) holds with $\delta > 0$.

If the product $u \cdot \mathcal{R}u$ has units of power, this says that the net energy input over time is positive for every possible input. In other words, the system does not generate any power internally. The underlying assumption in the above definition is that the system starts in a state of minimum stored energy. Otherwise, an input could be generated which recovers any stored energy, causing $\langle u, y \rangle_T$ to be negative.

8.2.2 Preisach Model Passivity

The passivity of the Preisach model with respect to the energy pair $(u, \dot{y})$ has been investigated by Hughes in [28]. It was shown that the model satisfied the inequality $\langle u, \dot{y} \rangle_T \geq -\delta$, for $\delta > 0$. This is a slightly different result from that required by Definition 8.8. The fact that the total energy transferred could be negative results from the lack of a restriction in [28] on the initial state. Essentially, if the system starts out with any stored energy, an input can be constructed to recover that energy, resulting in a negative net energy transfer.

In [19] the idea of minimum energy storage (as defined in Section 7.1.2) was extended to the Preisach model, and it was shown that if the system begins in such a state, then the result from [28] can be improved to the required $\langle u, \dot{y} \rangle_T \geq 0$.

In each of these previous studies, it was first shown that a relay $\gamma_{\alpha\beta}$ is passive if $\mu(\alpha, \beta) \geq 0$. Since a parallel interconnection of passive elements is itself passive[55], then the passivity of the Preisach model follows. Here, a similar result is obtained, but it is obtained more directly, as a special case of the dissipativity result of the previous chapter.

Theorem 8.1 (Preisach Model Passivity)

If $\mu \in \mathcal{M}_P$, the operator $\frac{d}{dt}\Gamma$ is passive.

Proof

From the hypothesis on μ, the Preisach model is dissipative with respect to the supply rate $w(u, y) = u\dot{y}$ (Theorem 7.4). Suppose the system starts in a state of zero energy storage, meaning that $u(t_o) = 0$. Then for any input $u \in Do(\Gamma)$, and all $t_1 > t_o$,

$$S_a(B_o) + \int_{t_o}^{t_1} u \cdot \dot{y} dt \geq S_a(\phi(t_1, t_o, B_o, u)).$$

But since $u(t_o) = 0$, $Q_3 \cap P_- B_o = \emptyset$ and $Q_1 \cap P_+ B_o = \emptyset$, so $S_a(B_o) = 0$ and

$$\int_{t_o}^{t_1} u \cdot \dot{y} dt \geq S_a(\phi(t_1, t_o, B_o, u)) \geq 0.$$

Thus, if the stored energy is zero at $t = -\infty$, then for any $T < \infty$ and $u \in Do(\Gamma)$, we have

$$\langle u, \dot{y} \rangle_T = \int_{-\infty}^{T} u \cdot \dot{y} dt \geq 0,$$

which completes the proof. ∎

8.2.3 Stability Conditions

The velocity feedback configuration is illustrated in Figure 8.2. The input $\dot{r}$ is a reference velocity to be tracked, $\dot{e}$ the velocity tracking error, $\tilde{u}$ the control signal, u the Preisach input, y the actuator position output, and $\dot{y}$ the actuator velocity.

The input u_o can be any function in W_1^2, and may be used to offset any initial conditions on $\tilde{u}$ and any change in ambient conditions which may have occurred

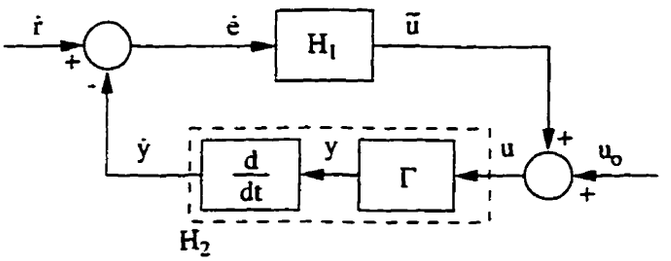

Figure 8.2: Velocity Feedback Configuration

between identification and the current operating conditions. This ensures that the input to the Preisach model is initially zero, so that $u \in Do(H_2)$ and the passivity of H_2 can be exploited. Alternatively, the Preisach model could be "initialized", at least approximately, as was successfully done in the identification procedure for the two-wire SMA actuator (cf. Section 5.2.2).

Well-Posedness

In order to ensure the consistency of internal signals, it is assumed that the system H_1 is a relation with $Do(H_1) = L_2$, that it has some smoothing properties so that $Ra(H_1) \subset W_1^2$, and also $\dot{r} \in L_2$, $u_o \in W_1^2$. Then $u \in W_1^2$ and if $\mu \in \mathcal{M}_P$ then $\Gamma : W_1^2 \mapsto W_1^2$, y is differentiable, and $\dot{y} \in L_2$.

Theorem 8.2 (Stability)

If H_1 is strictly passive with finite gain, and u_o is chosen so that $u(0) = 0$, the feedback system of Figure 8.2 is stable for all $\dot{r} \in L_2$.

Proof

The proof is along the lines of the standard proof of the passivity theorem[e.g. 12]. From the system configuration, and the hypothesis on u_o, we have $u \in Do(H_2)$.

Along with Theorem 8.1 and the hypothesis on H_1, this implies that there exist constants $\delta, \gamma > 0$ such that

$$\begin{aligned} \langle u, \dot{y} \rangle_T &\geq 0, \\ \langle \dot{e}, \tilde{u} \rangle_T &\geq \delta \|\dot{e}\|_T^2, \\ \|\tilde{u}\|_T &\leq \gamma \|\dot{e}\|_T. \end{aligned}$$

Now, choosing any $\dot{r} \in L_2[0, T]$, we have

$$\begin{aligned} \langle \dot{e}, \tilde{u} \rangle_T &= \langle \dot{e}, \tilde{u} \rangle_T + \langle u, \dot{y} \rangle_T - \langle u, \dot{y} \rangle_T \\ &= \langle \dot{r} - \dot{y}, \tilde{u} \rangle_T + \langle \tilde{u} + u_o, \dot{y} \rangle_T - \langle u, \dot{y} \rangle_T \\ &= \langle \dot{r}, \tilde{u} \rangle_T + \langle u_o, \dot{y} \rangle_T - \langle u, \dot{y} \rangle_T \\ &\leq \langle \dot{r}, \tilde{u} \rangle_T + \langle u_o, \dot{y} \rangle_T. \end{aligned}$$

Applying the strict passivity condition on H_1 and the Cauchy-Schwartz inequality $\langle x, y \rangle_T \leq \|x\|_T \|y\|_T$ gives

$$\begin{aligned} \delta \|\dot{e}\|_T^2 &\leq \langle \dot{e}, \tilde{u} \rangle_T \\ &\leq \|\dot{r}\|_T \|\tilde{u}\|_T + \|u_o\|_T \|\dot{y}\|_T \\ &\leq \gamma \|\dot{r}\|_T \|\dot{e}\|_T + \|u_o\|_T \|\dot{y}\|_T \\ &= \gamma \|\dot{r}\|_T \|\dot{e}\|_T + \|u_o\|_T \|\dot{r} - \dot{e}\|_T \\ &\leq (\gamma \|\dot{r}\|_T + \|u_o\|_T) \|\dot{e}\|_T + \|u_o\|_T \|\dot{r}\|_T. \end{aligned}$$

Since $\delta > 0$,

$$\|\dot{e}\|_T^2 \leq \frac{1}{\delta} (\gamma \|\dot{r}\|_T + \|u_o\|_T) \|\dot{e}\|_T + \frac{1}{\delta} \|u_o\|_T \|\dot{r}\|_T,$$

and completing the square in $\|\dot{e}\|_T$ gives

$$\left[\|\dot{e}\|_T - \frac{1}{2\delta} (\gamma \|\dot{r}\|_T + \|u_o\|_T) \right]^2 \leq \frac{1}{4\delta^2} (\gamma \|\dot{r}\|_T + \|u_o\|_T)^2 + \frac{1}{\delta} \|u_o\|_T \|\dot{r}\|_T$$

$$
\begin{aligned}
&= \frac{1}{4\delta^2}\left[\gamma^2 \|\dot{r}\|_T^2 + 2(\gamma+2\delta)\|\dot{r}\|_T \|u_o\|_T + \|u_o\|_T^2\right] \\
&= \frac{1}{4\delta^2}\left[(\gamma+2\delta)\|\dot{r}\|_T + \|u_o\|_T\right]^2 - \frac{\gamma+\delta}{\delta}\|\dot{r}\|_T^2 \\
&\leq \frac{1}{4\delta^2}\left[(\gamma+2\delta)\|\dot{r}\|_T + \|u_o\|_T\right]^2 .
\end{aligned}
$$

Taking the square root of both sides gives

$$
\begin{aligned}
\|\dot{e}\|_T &\leq \frac{1}{2\delta}\left[(\gamma+2\delta)\|\dot{r}\|_T + \|u_o\|_T\right] + \frac{1}{2\delta}\left(\gamma\|\dot{r}\|_T + \|u_o\|_T\right) \\
&= \frac{1}{\delta}\left[(\gamma+\delta)\|\dot{r}\|_T + \|u_o\|_T\right] \\
&\leq k_e\left(\|\dot{r}\|_T + \|u_o\|_T\right).
\end{aligned}
$$

where $k_e = \frac{1}{\delta}\max\{\gamma+\delta, 1\}$. The boundedness of $\tilde{u}$, u and $\dot{y}$ all follow, since $\|\tilde{u}\|_T \leq \gamma\|\dot{e}\|_T$, $\|u\|_T \leq \|\tilde{u}\|_T + \|u_o\|_T$ and $\|\dot{y}\|_T \leq \|\dot{r}\|_T + \|\dot{e}\|_T$.

■

8.3 Comments on Position Regulation

In some applications, the control objective is regulation about a set output value, in the face of some external disturbance. One example of such an application can be found in [68], where piezoceramic actuators bonded to a flexible beam are used to force the beam to maintain a static deformation. Such research has applications in the aerospace industry, where similar schemes could be used to actively tune the flight surfaces of an aircraft[9], or for fine tuning of the transmission surface of large space antennae. An important measure of performance in this case is the maximum output transient caused by disturbances, since this determines the deviation from

the de. e. A control strategy which minimizes this deviation can be said to be "optin. some sense.

The presence an hysteresis nonlinearity complicates the regulation task considerably. Since hysteresis branches are irreversible, even small output perturbations can require very large corrective input swings, leading in turn to undesirably large output transients. Furthermore, for any output value within the hysteretic range of the system, there are an infinite number of corresponding states. In this section, it is assumed that a stabilizing controller has been designed for setpoint regulation, and a strategy is proposed for achieving optimal performance from this controller.

The foundation of the regulation strategy is the choice of state about which to regulate. Given a desired constant reference y_d, there are an infinite number of corresponding states, each reflecting different input histories leading to the same output value. However, if among these the state about which to regulate is chosen in an intelligent manner, output transients during regulation can be minimized.

8.3.1 Preliminaries

First, for any $\ell \in [u_-, u_+]$, define the boundary $B_\ell \triangleq \{(\alpha, \beta) \in \mathcal{P}_r | \alpha = 2\ell - \beta\}$. The form of the boundary B_ℓ is illustrated in Figure 8.3.

Theorem 8.3

Given $\ell \in [u_-, u_+]$, $u_\ell \in \mathcal{U}$ can be constructed so that $B_1 = \phi(t_1, t_o, B_o, u_\ell)$ approximates B_ℓ arbitrarily closely in the metric on $\mathcal{B}$, for any $B_o \in \mathcal{B}$ and $t_1 > t_o$.

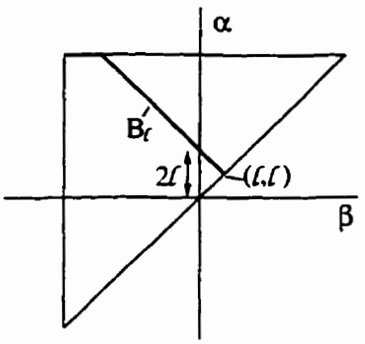

Figure 8.3: Boundary B_ℓ

Proof

Simply define $A \triangleq \max\{u_+ - \ell, \ell - u_-\}$. choose $t_1 > t_o$. and set

$$u_\ell(t) = \frac{t_1 - t}{t_1 - t_o} A \sin(\omega) + \ell. \tag{8.2}$$

The amplitude A is chosen to wipe out the boundary $B(t_o)$. The decaying sinusoid approximates a line parallel to B^*, and the offset ℓ determines the point at which the new state intersects the line $\alpha = \beta$. The approximation error, the distance between B_ℓ and $\phi(t_1, t_o, B_o, u_\ell)$, will be inversely proportional to frequency ω and $t_1 - t_o$. Since the hysteresis is static, these may be chosen arbitrarily, subject to the limits of controller capabilities. ■

Now, define for any $\ell \in [u_-, u_+]$

$$\begin{aligned} \psi(\ell) \triangleq r(B_\ell) &= \iint_{P_+ B_\ell} \mu(\alpha,\beta) d\alpha d\beta - \iint_{P_- B_\ell} \mu(\alpha,\beta) d\alpha d\beta \\ &= 2 \iint_{P_+ B_\ell} \mu(\alpha,\beta) d\alpha d\beta - \iint_{\mathcal{P}_r} \mu(\alpha,\beta) d\alpha d\beta. \end{aligned} \tag{8.3}$$

$\psi(\ell)$ is the output corresponding to the boundary B_ℓ.

Lemma 8.4

If $\mu \in \mathcal{M}_{PC}$, $\psi(\ell)$ is continuous in ℓ.

Proof

The area of integration defined by $P_+ B_\ell$ is continuous in ℓ, and μ is piecewise continuous over $\mathcal{P}_r$. Then from equation (8.3), $\psi(\ell)$ is continuous. ■

Theorem 8.5

For every $y_d \in [y_-, y_+]$, there exists $\ell \in [u_-, u_+]$ such that $r(B_\ell) = y_d$.

Proof

From equation (8.3),

$$\psi(u_-) = -\iint_{\mathcal{P}_r} \mu(\alpha, \beta) d\alpha d\beta = y_-$$

and

$$\psi(u_+) = \iint_{\mathcal{P}_r} \mu(\alpha, \beta) d\alpha d\beta = y_+.$$

So $\psi(\ell)$ connects the endpoints of the major loop. From Lemma 8.4, ψ is continuous, so for any $y_d \in [y_-, y_+]$ there exists (at least one) $\ell \in [u_-, u_+]$ such that $\psi(\ell) = y_d$. ■

8.3.2 Control Configuration

The proposed control configuration is shown in Figure 8.4. ψ^r is defined on $[y_-, y_+]$ as

$$\psi^r(y) \triangleq \min\{\ell \in [u_-, u_+] | \psi(\ell) = y\},$$

which is well-defined by compactness of $[u_-, u_+]$ and Theorem 8.5.[3] The map $\mathcal{D} : \ell \mapsto u_\ell$ generates a decaying sinusoidal input u_ℓ as in equation (8.2). The stabilizing controller C is shown in the standard feedback loop with the Preisach operator. The input to Γ can be switched between the feed-forward input u_ℓ and the control signal u_c, which is subject to a disturbance d.

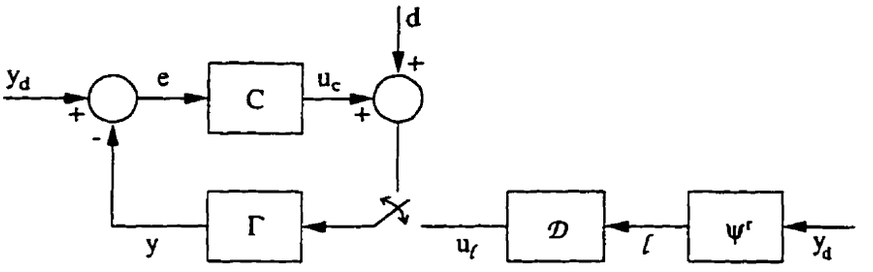

Figure 8.4: Optimal Strategy for Setpoint Regulation

To initialize the system, u_ℓ is used to drive the system to (or close to) the state B_ℓ, such that $y(t_1) \approx r(B_\ell) = y_d$. At this point, the control signal switches to u_c, and regulation begins.

The advantage of this strategy can be seen from the Preisach plane diagram in Figure 8.5. Suppose the boundaries B_ℓ and B_o satisfy $r(B_\ell) = r(B_o) = y_d$. If a small negative disturbance is injected at d, the boundaries assume the shape indicated by the dashed line. The shaded regions show the area which must be swept to recover the initial boundary in each case. Although the input required to recover B_ℓ is more oscillatory, it is much smaller in magnitude, leading to smaller output transients.

Figure 8.6 shows what the input-output behaviour may look like for regulation about the two states B_o and B_ℓ of Figure 8.5. The curves are somewhat exagger-

[3]Note that *any* ℓ satisfying $\psi(\ell) = y_d$ could be used in the regulation strategy; the above map is introduced for the purposes of the block-diagram of Figure 8.4.

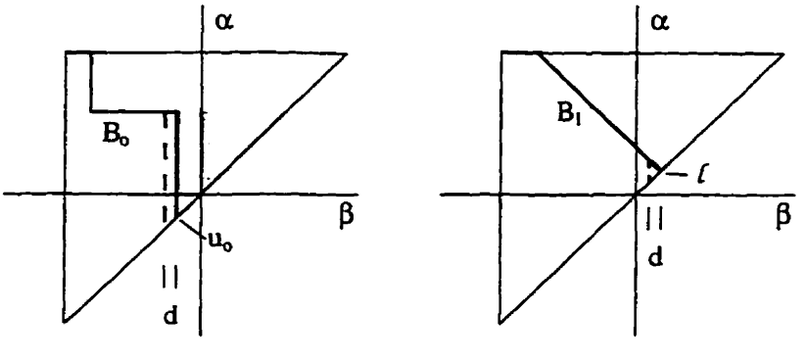

Figure 8.5: Regulation Strategy: Preisach Plane Behaviour

ated for clarity. ψ is the dotted curve which joins the corners of the major loop. Several ascending and descending branches are shown as dashed lines. The paths resulting from each corrective input are solid. In each case, the path begins at the point marked by a dot, representing the deviation from the setpoint caused by the disturbance d.

The particular nature of the locus ψ is that it contains points in the input-output graph which are between two close crossings of the same ascending and descending branches. The point defined by the input and output travels along ascending or descending branches, depending on the sign of the input. If a small negative disturbance d is injected onto the control, a small excursion down a descending branch results. Because branches are irreversible, a different, ascending branch must first be taken to return to the original point. The distance traveled along that ascending branch will determine the maximum output transient during the correction. It can be seen in Figure 8.6 that both the control and output variation resulting from regulation about (u_o, y_d) is much greater than those required for regulation about (ℓ, y_d). Although the output in the second case is oscillatory, the magnitude of output transients is reduced.

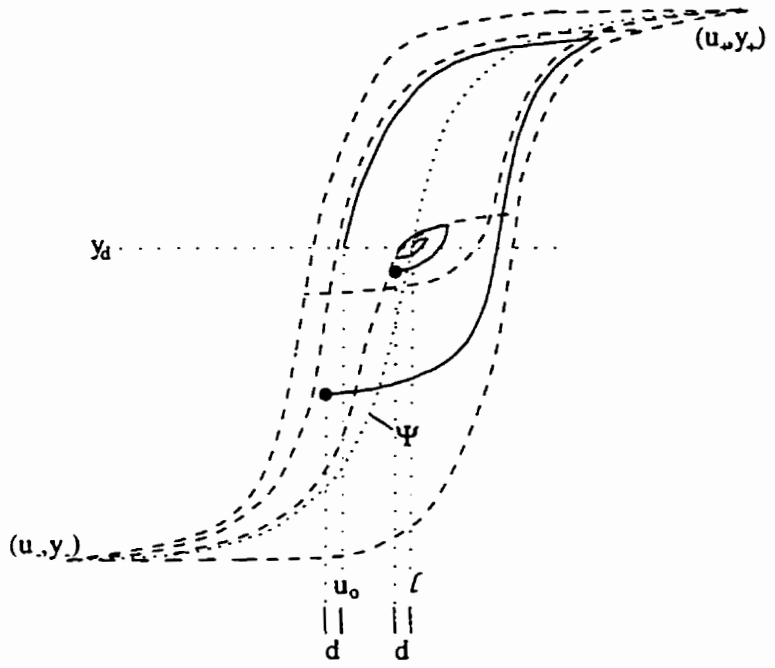

Figure 8.6: Regulation Strategy: Input-Output Behaviour

8.4 Summary

In this chapter, it was shown that, if $\mu \in \mathcal{M}_P$, then the relationship between the input and the output derivative of the Preisach model is passive. The result is used to obtain a class of stabilizing controllers for velocity feedback control of a Preisach hysteresis. A preliminary version of this result has been published in [19]. The SMA models which provided the better match in simulation in Chapter 5 were not in $\mathcal{M}_P$. It is important, therefore, to point out the sufficient nature of both the dissipativity result of Chapter 7 and the Passivity Theorem which was used in this chapter to design the control system. Generalizing these results to broader classes of Preisach weighting functions is a likely course of future research.

A second result was given on the regulation problem. It was shown that, of

the infinite number of states which could be chosen for regulation about a given setpoint, one in particular ensures low transients during regulation. This interesting result arose out of the intuition fostered by the Preisach plane, and would have been difficult to predict from the model input-output form.

Chapter 9

Conclusions and Future Research

The research in this thesis examined some of the properties of the Preisach hysteresis model, as they pertain to controller design. Particular attention was given to the class of Preisach models having non-negative weighting functions μ. For this class, expressions were derived for the energy storage and loss in the model. A state-space representation of the model was introduced, and it was shown that if $\mu \geq 0$, then the state-space model is dissipative with respect to the supply rate uy. The dissipativity of the model led to a stability result for velocity feedback control. A preliminary result on optimal regulation of Preisach systems was also presented. As is typical of non-linear systems, results obtained in this work, although global, were sufficient in nature.

Experimental work involved the identification of Preisach models for two shape memory alloy actuator configurations. Testing confirmed that the Preisach model was suited to represent the relationship between alloy temperature and strain. Three weighting surfaces were identified for each actuator, based on different forms of approximation surfaces. Positive weighting functions were found which provided

a reasonable match to experimental data. This allows the application of the aforementioned control results to shape memory alloy actuators. However, for both actuators a better model match was achieved with other weighting functions which were negative in parts.

9.1 Summary of Contributions

The main contributions of this research are summarized below.

Modelling

- The introduction of an exponential candidate surface in the identification of Preisach model weighting functions. This type of surface is more suited than polynomial-based surfaces to fit the observed behaviour of the SMA identification data.

- The determination of analytical weighting functions for both the one-wire and two-wire SMA actuator configurations.

Control

- The introduction of a state-space representation of the Preisach model. This contribution allows the application of non-linear state-space techniques for controller design to these highly non-linear systems.

- The derivation of sufficient conditions under which the Preisach model is dissipative.

- Associated with the dissipativity of the model, the derivation of sufficient conditions on the controller which guarantee closed-loop stability of velocity feedback control of Preisach hystereses.

9.2 Future Research Directions

This research has opened more doors than it has shut. Ideas for some future projects are outlined below.

- Variations in the characteristics of the different weighting functions identified in Chapter 5 indicate that the identification technique used here may not be very robust. In particular, since the identification surface is differentiated to obtain the weighting function, the surface should match not only the identified data but also its derivatives. Application of recent work by Banks[2, 3] on identification techniques for Preisach-type operators may provide a more robust result.

- The majority of the results obtained in this work relied on the weighting function μ being non-negative. However, it was seen in Chapter 5 that partially negative weighting functions provided a better SMA model match. Furthermore, it was seen that weighting functions for magnetostrictive materials have negative regions. It is thought, therefore, that the condition $\mu \geq 0$ is overly restrictive, notably in the proof of dissipativity. One important area of future research is to fully investigate the requirements for, and implications of, non-negative μ. A proper identification of a weighting surface for a magnetostrictive material may hold the clue to obtaining less stringent conditions

on μ. In particular, a more relaxed condition may prove to be both necessary and sufficient for dissipativity.

- Chapter 6 presented a non-linear, infinite dimensional state-space representation for the Preisach model. Establishing this framework is only the beginning, and opens up new areas for study. Future research will involve further investigation of the state space properties, applications of non-linear state-space techniques for controller design, as well as simply polishing the representation presented here.

- The extension to position control of velocity feedback results from Passivity Theory is a classical result for some non-linear systems such as robotic manipulators[55]. In [45], the authors demonstrate a method for the design of position controllers for dissipative plants, based on matching the controller supply rate to that of the plant. Assuming several conditions are met, it can be shown in the case of the Preisach model that any controller whose state-space is reachable and which is dissipative with respect to the supply rate

$$w_c(u,y) = -a^2 \langle y,y \rangle + (b^2 - c^2) \langle u,u \rangle - \langle \dot{u},y \rangle$$

will provide stable position control. It is not yet clear, however,

  - whether the required assumptions hold in the case of the Preisach model, and
  - what types of controllers satisfy this supply rate.

- The observation that the two-wire actuator can be modeled using the classical form of the Preisach model is surprising, given the time-varying stresses involved. Further research is required in order to fully understand this result.

- Finally, many controllers have been developed in the literature for hysteretic systems which may have associated Preisach models. In particular, the authors of [21] demonstrate excellent results in position control of a two-wire SMA actuator. The control strategy is essentially gain scheduling using constant gains. It would be interesting to attempt to apply the results of this work to a proof of stability for their control system.

Bibliography

[1] J.C. Anderson. *Magnetism and Magnetic Materials*. Chapman and Hall Ltd., London, 1968.

[2] H.T. Banks, A.J. Kurdilla, and G. Webb. Identification of hysteretic control influence operators representing smart actuators: Formulation. Technical Report CRSC-TR96-14, Center for Research in Scientific Computation, North Carolina State University, Raleigh, NC 27695-8205, April 1996.

[3] H.T. Banks, A.J. Kurdilla, and G. Webb. Identification of hysteretic control influence operators representing smart actuators: Convergent approximations. Technical Report CRSC-TR97-7, Center for Research in Scientific Computation, North Carolina State University, Raleigh, NC 27695-8205, April 1997.

[4] M. Bergamasco, F. Salsedo, and P. Dario. Shape memory alloy micromotors for direct-drive actuation of dexterous artificial hands. *Sensors and Actuators*, 17:115–119, 1989.

[5] M. Brokate and J. Sprekels. Existence and optimal control of mechanical processes with hysteresis in viscous solids. *Journal of Applied Mathematics*, 43:219–229, 1989.

[6] M. Brokate and A. Visintin. Properties of the Preisach model for hysteresis. *Journal für die reine und angewandte Mathematik*, 402:1–40, 1989.

[7] W.J. Buehler, J.V. Gilfrich, and R.C. Wiley. Effect of low-temperature phase changes on the mechanical properties of alloys near composition TiNi. *Journal of Applied Physics*, 34(5):1475–1477, May 1963.

[8] J.M. Cruz-Hernández and V. Hayward. On the linear compensation of hysteresis. Technical Report 97-08. Centre for Intelligent Machines, McGill University, Montreal, Canada, May 1997.

[9] B. Culshaw. *Smart Structures and Materials*. Artech House, Boston, London, 1996.

[10] R.F. Curtain and A.J. Pritchard. *Infinite Dimensional Linear Systems Theory*. Number 8 in Lecture notes in Control and Information Sciences. Springer-Verlag, New York, 1978.

[11] G. Dahlquist and A. Björk. *Numerical Methods*. Prentice-Hall, 1974. QA297.D3313.

[12] C. A. Desoer and M. Vidyasagar. *Feedback Systems*. Academic Press, Inc., New York, 1975.

[13] C.A. Dickinson, D. Hughes, and J.T. Wen. Hysteresis in shape memory alloy actuators: the control issues. In V.V. Varandan and J. Chandra, editors, *Proceedings SPIE 2715*, pages 494–506, 1996.

[14] T.W. Duerig and A.R. Pelton. Ti-Ni shape memory alloys. In *Material Properties Handbook: Titanium Alloys*, pages 1035–1048. ASM, 1994. TA480.T54M37.

[15] F. Fariborzi, M.F. Golnaraghi, and G.R. Heppler. Experimental control of free and forced structural vibration using a linear coupling strategy. *Journal of Smart Materials & Structures*, 6:1–9, 1997. preprint.

[16] H. Funakubo. *Shape Memory Alloys*, volume 1 of *Precision Machinery and Robotics*. Gordon and Breach Science Publishers, New York, 1984.

[17] Y. Furuya and H. Shimada. Shape memory actuators for robotic applications. In T.W. Duerig, K.N. Melton, D. Stöckel, and C.M. Wayman, editors, *Engineering Aspects of Shape Memory Alloys*, pages 338–355, Toronto, 1990. Butterworth-Heinemann Ltd.

[18] P. Ge and M. Jouaneh. Tracking control of a piezoceramic actuator. *IEEE Transactions on Control Systems Technology*, 4(3):209–215, 1996.

[19] R.B. Gorbet, K.A. Morris, and D.W.L. Wang. Stability of control for the Preisach hysteresis model. In *Proceedings of the 1997 IEEE International Conference on Robotics and Automation*, volume 1, pages 241–247, April 1997.

[20] R.B. Gorbet and R.A. Russell. A novel differential shape memory alloy actuator for position control. *Robotica*, 13:423–430, 1995.

[21] D. Grant and V. Hayward. Controller for a high strain shape memory alloy actuator: Quenching of limit cycles. In *Proceedings of the 1997 IEEE International Conference on Robotics and Automation*, volume 1, pages 254–259, April 1997.

[22] C.H. Hansen and S.D. Snyder. *Active Control of Noise and Vibration*. Chapman and Hall, New York, 1997. TD892.H357x.

[23] M. Hashimoto, M. Takeda, H. Sagawa, I. Chiba, and K. Satō. Application of shape memory alloy to robotic actuators. *Journal of Robotic Systems*, 2(1):3–25, 1985.

[24] U. Hornung. The mathematics of hysteresis. *Bull. Austral. Math. Soc.*, 30:271–287, 1984.

[25] W. Huang and S. Pellegrino. Shape memory alloy actuators for deployable structures: Phase I. Technical Report CUED/D-STRUCT/TR 163, Department of Electrical Engineering, University of Cambridge, April 1996.

[26] D. Hughes and J.T. Wen. Preisach modeling and compensation for smart material hysteresis. In *Proceedings of the 1994 Symposium on Active Materials and Smart Structures*, College Station, Texas, October 1994.

[27] D. Hughes and J.T. Wen. Preisach modeling of piezoceramic and shape memory alloy hysteresis. In *Proceedings of the 1995 IEEE Control Conference on Applications*, Albany, New York, September 1995.

[28] D.C. Hughes. Piezoceramic and SMA hysteresis modeling and passivity analysis. Doctoral research proposal, Rensselaer Polytechnic Institute, Troy, New York, July 1994.

[29] D.C. Hughes. *Piezoceramic and SMA Hysteresis Modeling and Compensation.* PhD thesis, Rensselaer Polytechnic Institute, 1997.

[30] Y. Huo. A mathematical model for the hysteresis in shape memory alloys. *Continuum Mechanics and Thermodynamics*, 1:283–303, 1989.

[31] K. Ikuta. Micro/miniature shape memory alloy actuator. In *IEEE International Conference on Robotics and Automation*, volume 3, pages 2156–2161. IEEE Computer Society Press, Los Alamitos, California, 1990.

[32] K. Ikuta, M. Tsukamoto, and S. Hirose. Mathematical model and experimental verification of shape memory alloy for designing micro actuators. In *Proceedings of the 1991 IEEE MicroElectroMechanical Systems Conference*, pages 103–108. MEMS '91, 1991.

[33] G. Kadar and E. Della Torre. Hysteresis modeling: I. noncongruency. *IEEE Transactions on Magnetics*, 23(5):2820–2825, September 1987.

[34] M.A. Krasnosel'skiĭ and A.V. Pokrovskii. *Systems with Hysteresis*. Springer Verlag, 1983.

[35] F. Kreith. *Principles of Heat Transfer*. Intext Press, New York, 3 edition, 1973.

[36] E. Kreyszig. *Introductory Functional Analysis With Applications*. John Wiley & Sons, Toronto, 1978.

[37] K. Kuribayashi. Improvement of the response of an SMA actuator using a temperature sensor. *The International Journal of Robotics Research*, 10(1):13–20, February 1991.

[38] L. Kvarnsjö, A. Bergqvist, and G. Engdahl. Application of a stress-dependent magnetic Preisach hysteresis model on a simulation model for Terfenol-D. *IEEE Transactions on Magnetics*, 28(5):2623–2625, September 1992.

[39] A. Lu, D. Grant, and V. Hayward. Design and comparison of high strain shape memory alloy actuators. In *Proceedings of the 1997 IEEE International Conference on Robotics and Automation*, volume 1, pages 260–265, April 1997.

[40] D.R. Madill. Modelling and stability of a shape memory alloy position control system. Master's thesis, University of Waterloo, Waterloo, Canada, 1993.

[41] D.R. Madill and D.W.L. Wang. The modelling and L_2-stability of a shape memory alloy position control system. In *Proceedings of the 1994 IEEE International Conference on Robotics and Automation*, volume 1, pages 293–299. IEEE Computer Society Press, Los Alamitos, California, 1994.

[42] S. Majima, T. Hasegawa, and T. Sasaki. Controller for shape memory alloy actuators to compensate its hysteresis. In *13th IFAC Triennial World Congress*, pages 167–172. IFAC, 1996.

[43] I.D. Mayergoyz. *Mathematical Models of Hysteresis*. Springer-Verlag, New York, 1991.

[44] I.D. Mayergoyz and G. Friedman. Generalized Preisach model of hysteresis. *IEEE Transactions on Magnetics*, 24(1):212–217, January 1988, TK454.4.M3I18.

[45] K.A. Morris and J.N. Juang. Dissipative controller designs for second-order dynamic systems. *IEEE Transactions on Automatic Control*, 39(5):1056–1063, May 1994. TJ212.I48.

[46] Y. Nakano, M. Fujie, and Y. Hosada. Hitachi's robot hand. *Robotics Age*, 6(7):18–20, July 1984.

[47] A.W. Naylor and G.R. Sell. *Linear Operator Theory in Engineering and Science*, volume 40 of *Applied Mathematical Sciences*. Springer-Verlag, 1982. QA1.A647 v40.

[48] J.A. Nelder and R. Mead. A simplex method for function minimization. *Computer Journal*, 7:308–313. 1964.

[49] J. Ortín. Preisach modeling of hysteresis for a pseudoelastic Cu-Zn-Al single crystal. *Journal of Applied Physics*, 71(3):1454–1461, February 1992.

[50] F. Ossart and G. Meunier. Comparison between various hysteresis models and experimental data. *IEEE Transactions on Magnetics*, 26(5):2837–2839, September 1990.

[51] F. Preisach. Uber die magnetische nachwirkung. *Zeitschrift fur Physik*, 94:277–302, 1935.

[52] H.L. Royden. *Real Analysis*. The Macmillan Company, 2nd edition, 1968.

[53] R.A. Russell and R.B. Gorbet. Improving the response of SMA actuators. In *Proceedings of the 1995 IEEE International Conference on Robotics and Automation*, volume 3, pages 2299–2304, May 1995.

[54] L. Schetky. Shape memory effect alloys for robotic devices. *Robotics Age*, 6(7):13–17, July 1984.

[55] J-J.E. Slotine and W. Li. *Applied Nonlinear Control*. Prentice-Hall, Englewood Cliffs, NJ, 1991.

[56] R.C. Smith. Hysteresis modeling in magnetostrictive materials via Preisach operators. Technical Report 97-23, Institute for Computer Applications in Sci-

ence and Engineering, NASA Langley Research Center, Hampton, VA 23665, May 1997.

[57] E.D. Sontag. *Mathematical control theory.* Texts in applied mathematics. Springer-Verlag, New York, 1990.

[58] G. Tao and V. Kokotović. Adaptive control of plants with unknown hystereses. *IEEE Transactions on Automatic Control*, 40(2):200–212, 1995.

[59] F. Vajda and E. Della Torre. Identification of parameters in an accommodation model. *IEEE Transactions on Magnetics*, 30(6):4371–4373, November 1994.

[60] M. Vidyasagar. *Non-Linear Systems Analysis.* Prentice-Hall, Englewood Cliffs, NJ, 2nd edition, 1993.

[61] A. Visintin. Mathematical models of hysteresis. In J.J. Moreau, P.D. Panagiotopoulos, and G. Strang, editors, *Topics in Nonsmooth Mechanics*, chapter VIII, pages 295–326. Birkhauser Verlag, Boston, 1988.

[62] A. Visintin. A collection of references on hysteresis. In *Numerical Analysis and Mathematical Modelling*, volume 24, pages 321–327. Banach Center Publications, Warsaw, 1990.

[63] A. Visintin, editor. *Models of Hysteresis.* Number 286 in Pitman Research Notes in Mathematics Series. Longman Scientific & Technical, 1993.

[64] A. Visintin. *Differential Models of Hysteresis*, volume 111 of *Applied Mathematical Sciences (Yellow-Book).* Springer-Verlag, New York, 1994.

[65] J.C. Willems. Dissipative dynamical systems, Part I: General theory. *Archives for Rational Mechanics & Analysis*, 45:321–351, 1972.

[66] S. Yokota, K. Yoshida, K. Bandoh, and M. Suhara. Response of proportional valve using shape-memory-alloy array actuators. In *13th IFAC Triennial World Congress*, pages 505–510. IFAC, 1996.

[67] C. Youyi, T.Y. Hsu, and T. Ko, editors. *Shape Memory Alloy '86*, Guilin, China, September 6-9 1986. International Symposium on Shape Memory Alloys, China Academic Publishers.

[68] J. Yu. Static shape control of a flexible beam using piezoceramic actuators. Master's thesis, University of Waterloo, Waterloo, Canada, 1997.

[69] G. Zames. On the input-output stability of time-varying nonlinear feedback systems, Part I: Conditions derived using concepts of loop gain, conicity, and positivity. *IEEE Transactions on Automatic Control*, AC-11(2):228–238, April 1966.

[70] Z.Q. Zhao, F.X. Chen, S.Z. Li, and D.Z. Yang. The internal friction associated with martensitic transformation in a CuZnAl shape memory alloy. *Scripta Metallurgica et Materialia*, 25:669-672, 1991.